

**Nondestructive Evaluation of District 08 Bridges  
Using Modal Parameters**

**FINAL REPORT**

Prepared by

N. Stubbs<sup>1</sup>, S. Choi<sup>2</sup>, R.W. Bolton<sup>3</sup>, S. Park<sup>4</sup>  
Texas Engineering Experiment Station  
College Station, Texas 77843

and

C. Sikorsky<sup>5</sup>  
State of California  
Department of Transportation  
Sacramento, CA 95816

Submitted to:

State of California  
Department of Transportation  
Sacramento, CA 95816

TEES PROJECT 32525-58520CE

February 2001

- 
1. A.P. and Florence Wiley Professor
  2. Research Associate
  3. Assistant Professor
  4. Research Associate
  5. Senior Bridge Engineer

DISCLAIMER: The opinions, findings, and conclusions expressed in this publication are those of the authors and not necessarily those of the STATE OF CALIFORNIA

## TABLE OF CONTENTS

	Page
TABLE OF CONTENTS .....	III
LIST OF TABLES .....	VI
LIST OF FIGURES.....	X
 CHAPTER	
1 INTRODUCTION .....	1
2 DESCRIPTION OF STRUCTURES.....	1
2.1. FENNER OVERCROSSING .....	1
2.2. WATSON WASH BRIDGE.....	2
3 SUMMARY OF DATA GATHERING AND ANALYSIS.....	2
4 DESCRIPTION OF THE FINITE ELEMENT MODELS.....	3
4.1. FENNER OVERCROSSING .....	3
4.2. WATSON WASH BRIDGE.....	4
5 RESULTS OF MODAL TESTS FOR STRUCTURES .....	5
5.1. FENNER OVERCROSSING .....	5
5.2. WATSON WASH BRIDGE.....	5
6 RESULTS OF SYSTEMS IDENTIFICATION AND DAMAGE DETECTION .....	6
6.1. RESULTS OF THE SYSTEM IDENTIFICATION .....	6
6.2. DAMAGE DETECTION .....	6
7 FINDINGS.....	7
7.1. FENNER OVERCROSSING .....	7
7.2. WATSON WASH BRIDGE.....	8
REFERENCE .....	9
 APPENDICES	
A. THEORY OF SYSTEMS IDENTIFICATION AND DAMAGE DETECTION .....	A-1
A.1 SYSTEM IDENTIFICATION SCHEME FOR THE BASELINE STRUCTURE.....	A-1

## TABLE OF CONTENTS (continued)

CHAPTER	Page
A.2 DAMAGE LOCALIZATION THEORY (DAMAGE INDEX METHOD).....	A-3
A.3 DAMAGE SEVERITY ESTIMATION .....	A-9
A.4 IDENTIFICATION OF STIFFNESS OF EXISTING STRUCTURE.....	A-10
B. DETAILS OF MODAL TESTING .....	B-1
B.1 INTRODUCTION .....	B-1
B.2 FIELD INSTRUMENTATION .....	B-2
B.3 MODAL TEST INSTRUMENTATION LAYOUT .....	B-3
B.4 MODAL TESTING OF WATSON WASH FRAMES .....	B-3
B.4.1 May 1999 Watson Wash Frame Tests .....	B-4
B.4.2 August 2000 Watson Wash Frame Tests.....	B-4
B.5 MODAL TESTING OF FENNER OVERCROSSING.....	B-5
B.5. SUMMARY .....	B-6
C. SYSTEMS IDENTIFICATION AND DAMAGE DETECTION FOR FENNER OVERHEAD AND WATSON WASH BRIDGES .....	C-1
C.1 FENNER OVERCROSSING .....	C-1
C.1.1 System Identification, September 1999 Field Test.....	C-1
C.1.2 System Identification, December 2000 Field Test.....	C-3
C.1.3 Damage Detection, September 1999 Field Test .....	C-5
C.1.4 Damage Detection, December 2000 Field Test.....	C-8
C.2 WATSON WASH BRIDGE.....	C-10
C.2.1 System Identification, May 1999 Field Test.....	C-10
C.2.1.1 Frame S-1 .....	C-10
C.2.1.2 Frame S-2 .....	C-11
C.2.1.3 Frame S-3 .....	C-12
C.2.1.4 Frame S-4 .....	C-13
C.2.1.5 Frame S-5 .....	C-14
C.2.2 System Identification, August 2000 Field Test .....	C-15
C.2.2.1 Frame S-1 .....	C-15
C.2.2.2 Frame S-2 .....	C-16
C.2.2.3 Frame S-3 .....	C-17
C.2.2.4 Frame S-4 .....	C-18
C.2.2.5 Frame S-5 .....	C-19
C.2.3 Damage Detection, May 1999 Field Test .....	C-20
C.2.3.1 Frame S-1 .....	C-20
C.2.3.2 Frame S-2 .....	C-24
C.2.3.3 Frame S-3 .....	C-28

## TABLE OF CONTENTS (continued)

CHAPTER	Page
C.2.3.4 Frame S-4 .....	C-32
C.2.3.5 Frame S-5 .....	C-36
C.2.4 Damage Detection, December 2000 Field Test .....	C-40
C.2.4.1 Frame S-1 .....	C-40
C.2.4.2 Frame S-2 .....	C-43
C.2.4.3 Frame S-3 .....	C-46
C.2.4.4 Frame S-4 .....	C-49
C.2.4.5 Frame S-5 .....	C-52

## LIST OF TABLES

TABLE		Page
1	Results of Modal Tests: Fenner Overcrossing .....	10
2	Results of Modal Tests: Watson Wash Bridge, Frame S-1 .....	10
3	Results of Modal Tests: Watson Wash Bridge, Frame S-2.....	10
4	Results of Modal Tests: Watson Wash Bridge, Frame S-3 .....	10
5	Results of Modal Tests: Watson Wash Bridge, Frame S-4.....	11
6	Results of Modal Tests: Watson Wash Bridge, Frame S-5.....	11
7	Effective Stiffness Properties: Fenner Overcrossing.....	11
8	Effective Stiffness Properties: Watson Wash Bridge, Frame S-1 .....	11
9	Effective Stiffness Properties: Watson Wash Bridge, Frame S-2 .....	12
10	Effective Stiffness Properties: Watson Wash Bridge, Frame S-3 .....	12
11	Effective Stiffness Properties: Watson Wash Bridge, Frame S-4 .....	12
12	Effective Stiffness Properties: Watson Wash Bridge, Frame S-5.....	13
B.1	PCB 200C20 Piezoelectric Load Cell Specifications.....	B-8
B.2	Kistler 8390A2 Accelerometer Specifications.....	B-8
B.3	SigLab 20-42 Analyzer Specifications.....	B-8
B.4	Modal Test Instrument Settings .....	B-9
B.5	Extracted Frequency and Damping Values Watson Wash Frame S-1, May 1999 Field Test.....	B-9
B.6	Extracted Frequency and Damping Values Watson Wash Frame S-2, May 1999 Field Test.....	B-9
B.7	Extracted Frequency and Damping Values Watson Wash Frame S-3, May 1999 Field Test.....	B-10
B.8	Extracted Frequency and Damping Values Watson Wash Frame S-4, May 1999 Field Test.....	B-10
B.9	Extracted Frequency and Damping Values Watson Wash Frame S-5, May 1999 Field Test.....	B-10
B.10	Extracted Frequency and Damping Values Watson Wash Frame S-1, August 2000 Field Test.....	B-10

**LIST OF TABLES (continued)**

TABLE		Page
B.11	Extracted Frequency and Damping Values Watson Wash Frame S-2, August 2000 Field Test.....	B-11
B.12	Extracted Frequency and Damping Values Watson Wash Frame S-3, August 2000 Field Test.....	B-11
B.13	Extracted Frequency and Damping Values Watson Wash Frame S-4, August 2000 Field Test.....	B-11
B.14	Extracted Frequency and Damping Values Watson Wash Frame S-5, August 2000 Field Test.....	B-11
B.15	Extracted Frequency and Damping Values Fenner Overcrossing, September 1999 Field Test.....	B-12
B.16	Extracted Frequency and Damping Values Fenner Overcrossing, December 2000 Field Test .....	B-12
C.1	Material Properties of the Initial FE Model .....	C-1
C.2	Comparison of Resonant Frequencies of Initial FE Model and Experiment .....	C-1
C.3	MAC Values.....	C-1
C.4	Sensitivity Matrix F for Fenner Overcrossing, September 1999.....	C-2
C.5	System Identification for Fenner Overcrossing, September 1999 .....	C-2
C.6	Identified Material Properties of Fenner Overcrossing, September 1999	C-2
C.7	Material Properties of the Initial FE Model .....	C-3
C.8	Comparison of Resonant Frequencies of Initial FE Model and Experiment .....	C-3
C.9	MAC Values.....	C-3
C.10	Sensitivity Matrix F for Fenner Overcrossing, December 2000 .....	C-4
C.11	System Identification for Fenner Overcrossing, December 2000 .....	C-4
C.12	Identified Material Properties of Fenner Overcrossing, December 2000	C-4
C.13	Initial Values of Material Properties of the Initial FE Model .....	C-10

## LIST OF TABLES (continued)

TABLE		Page
C.14	Sensitivity Matrices F and G for Watson Wash Frame S-1, May 1999..	C-10
C.15	System Identification for Watson Wash Frame S-1, May 1999.....	C-10
C.16	Identified Material Properties of Watson Wash Frame S-1, May 1999..	C-10
C.17	Initial Values of Material Properties of the Initial FE Model .....	C-11
C.18	Sensitivity Matrices F and G for Watson Wash Frame S-2, May 1999..	C-11
C.19	System Identification for Watson Wash Frame S-2, May 1999.....	C-11
C.20	Identified Material Properties of Watson Wash Frame S-2, May 1999..	C-11
C.21	Initial Values of Material Properties of the Initial FE Model .....	C-12
C.22	Sensitivity Matrices F and G for Watson Wash Frame S-3, May 1999..	C-12
C.23	System Identification for Watson Wash Frame S-3, May 1999.....	C-12
C.24	Identified Material Properties of Watson Wash Frame S-3, May 1999..	C-12
C.25	Initial Values of Material Properties of the Initial FE Model .....	C-13
C.26	Sensitivity Matrices F and G for Watson Wash Frame S-4, May 1999..	C-13
C.27	System Identification for Watson Wash Frame S-4, May 1999.....	C-13
C.28	Identified Material Properties of Watson Wash Frame S-4, May 1999..	C-13
C.29	Initial Values of Material Properties of the Initial FE Model .....	C-14
C.30	Sensitivity Matrices F and G for Watson Wash Frame S-5, May 1999..	C-14
C.31	System Identification for Watson Wash Frame S-5, May 1999.....	C-14
C.32	Identified Material Properties of Watson Wash Frame S-5, May 1999..	C-14
C.33	Initial Values of Material Properties of the Initial FE Model .....	C-15
C.34	Sensitivity Matrices F and G for Watson Wash Frame S-1, August 2000 .....	C-15
C.35	System Identification for Watson Wash Frame S-1, August 2000 .....	C-15
C.36	Identified Material Properties of Watson Wash Frame S-1, August 2000 .....	C-15
C.37	Initial Values of Material Properties of the Initial FE Model .....	C-16
C.38	Sensitivity Matrices F and G for Watson Wash Frame S-2, August 2000 .....	C-16

**LIST OF TABLES (continued)**

TABLE		Page
C.39	System Identification for Watson Wash Frame S-2, August 2000 .....	C-16
C.40	Identified Material Properties of Watson Wash Frame S-2, August 2000 .....	C-16
C.41	Initial Values of Material Properties of the Initial FE Model .....	C-17
C.42	Sensitivity Matrices F and G for Watson Wash Frame S-3, August 2000 .....	C-17
C.43	System Identification for Watson Wash Frame S-3, August 2000 .....	C-17
C.44	Identified Material Properties of Watson Wash Frame S-3, August 2000 .....	C-17
C.45	Initial Values of Material Properties of the Initial FE Model .....	C-18
C.46	Sensitivity Matrices F and G for Watson Wash Frame S-4, August 2000 .....	C-18
C.47	System Identification for Watson Wash Frame S-4, August 2000 .....	C-18
C.48	Identified Material Properties of Watson Wash Frame S-4, August 2000 .....	C-18
C.49	Initial Values of Material Properties of the Initial FE Model .....	C-19
C.50	Sensitivity Matrices F and G for Watson Wash Frame S-5, August 2000 .....	C-19
C.51	System Identification for Watson Wash Frame S-5, August 2000 .....	C-19
C.52	Identified Material Properties of Watson Wash Frame S-5, August 2000 .....	C-19

## LIST OF FIGURES

FIGURE		Page
1	As-built Plan View of Fenner Overcrossing .....	14
2	View of Fenner Deck from West Abutment .....	15
3	Profile View of Fenner Structural System .....	15
4	As-built Plan View of Watson Wash Bridge.....	16
5	View of Watson Wash Deck from East Abutment.....	17
6	Side View of Watson Wash Pier and Deck System .....	17
7	View of Typical Watson Wash Pier Girder Connection .....	18
8	Possible Damage Locations in Fenner Overcrossing.....	19
9	Possible Damage Locations in Watson Wash Bridge, Frame S-1 .....	20
10	Possible Damage Locations in Watson Wash Bridge, Frame S-2 .....	21
11	Possible Damage Locations in Watson Wash Bridge, Frame S-3 .....	22
12	Possible Damage Locations in Watson Wash Bridge, Frame S-4 .....	23
13	Possible Damage Locations in Watson Wash Bridge, Frame S-5 .....	24
A.1	Flawed Structure and Estimate of Flawless Structure.....	A-11
B.1	Shoulder Closure during Testing of Watson Wash Bridge .....	B-13
B.2	16-Channel Instrument Setup.....	B-13
B.3	Typical Triaxial Accelerometer Mounting.....	B-14
B.4	Drop-weight Impact Hammer .....	B-14
B.5	Typical Vertical Response.....	B-15
B.5	Typical Time Response of Impact Hammer.....	B-15
B.6	Corresponding Frequency Spectrum of Impact.....	B-15
B.7	Wireframe Model of Response Nodes for Watson Wash Frame S-1, May 1999 Field Test .....	B-16
B.8	Overlay of Vertical FRF Magnitudes for Watson Wash Frame S-1, May 1999 Field Test .....	B-16
B.9	1 <sup>st</sup> Mode Watson Wash Frame S-1, May 1999 Field Test .....	B-17
B.10	2 <sup>nd</sup> Mode Watson Wash Frame S-1, May 1999 Field Test .....	B-17

## LIST OF FIGURES (continued)

FIGURE		Page
B.11	Wireframe Model of Response Nodes for Watson Wash Frame S-2, May 1999 Field Test .....	B-18
B.12	Overlay of Vertical FRF Magnitudes for Watson Wash Frame S-2, May 1999 Field Test .....	B-18
B.13	1 <sup>st</sup> Mode Watson Wash Frame S-2, May 1999 Field Test .....	B-19
B.14	3 <sup>rd</sup> Mode Watson Wash Frame S-2, May 1999 Field Test .....	B-19
B.15	Wireframe Model of Response Nodes for Watson Wash Frame S-3, May 1999 Field Test .....	B-20
B.16	Overlay of Vertical FRF Magnitudes for Watson Wash Frame S-3, May 1999 Field Test .....	B-20
B.17	1 <sup>st</sup> Mode Watson Wash Frame S-3, May 1999 Field Test .....	B-21
B.18	2 <sup>nd</sup> Mode Watson Wash Frame S-3, May 1999 Field Test .....	B-21
B.19	Wireframe Model of Response Nodes for Watson Wash Frame S-4, May 1999 Field Test .....	B-22
B.20	Overlay of Vertical FRF Magnitudes for Watson Wash Frame S-4, May 1999 Field Test .....	B-22
B.21	1 <sup>st</sup> Mode Watson Wash Frame S-4, May 1999 Field Test .....	B-23
B.22	2 <sup>nd</sup> Mode Watson Wash Frame S-4, May 1999 Field Test .....	B-23
B.23	Wireframe Model of Response Nodes for Watson Wash Frame S-5, May 1999 Field Test .....	B-24
B.24	Overlay of Vertical FRF Magnitudes for Watson Wash Frame S-5, May 1999 Field Test .....	B-24
B.25	1 <sup>st</sup> Mode Watson Wash Frame S-5, May 1999 Field Test .....	B-25
B.26	2 <sup>nd</sup> Mode Watson Wash Frame S-5, May 1999 Field Test .....	B-25
B.27	Wireframe Model of Response Nodes for Watson Wash Frame S-1, August 2000 Field Test .....	B-26
B.28	Overlay of Vertical FRF Magnitudes for Watson Wash Frame S-1, August 2000 Field Test .....	B-26
B.29	1 <sup>st</sup> Mode Watson Wash Frame S-1, August 2000 Field Test .....	B-27
B.30	2 <sup>nd</sup> Mode Watson Wash Frame S-1, August 2000 Field Test .....	B-27

## LIST OF FIGURES (continued)

FIGURE		Page
B.31	Wireframe Model of Response Nodes for Watson Wash Frame S-2, August 2000 Field Test .....	B-28
B.32	Overlay of Vertical FRF Magnitudes for Watson Wash Frame S-2, August 2000 Field Test .....	B-28
B.33	1 <sup>st</sup> Mode Watson Wash Frame S-2, August 2000 Field Test .....	B-29
B.34	2 <sup>nd</sup> Mode Watson Wash Frame S-2, August 2000 Field Test .....	B-29
B.35	Wireframe Model of Response Nodes for Watson Wash Frame S-3, August 2000 Field Test .....	B-30
B.36	Overlay of Vertical FRF Magnitudes for Watson Wash Frame S-3, August 2000 Field Test .....	B-30
B.37	1 <sup>st</sup> Mode Watson Wash Frame S-3, August 2000 Field Test .....	B-31
B.38	2 <sup>nd</sup> Mode Watson Wash Frame S-3, August 2000 Field Test .....	B-31
B.39	Wireframe Model of Response Nodes for Watson Wash Frame S-4, August 2000 Field Test .....	B-32
B.40	Overlay of Vertical FRF Magnitudes for Watson Wash Frame S-4, August 2000 Field Test .....	B-32
B.41	1 <sup>st</sup> Mode Watson Wash Frame S-4, August 2000 Field Test .....	B-33
B.42	2 <sup>nd</sup> Mode Watson Wash Frame S-4, August 2000 Field Test .....	B-33
B.43	Wireframe Model of Response Nodes for Watson Wash Frame S-5, August 2000 Field Test .....	B-34
B.44	Overlay of Vertical FRF Magnitudes for Watson Wash Frame S-5, August 2000 Field Test .....	B-34
B.45	1 <sup>st</sup> Mode Watson Wash Frame S-5, August 2000 Field Test .....	B-35
B.46	2 <sup>nd</sup> Mode Watson Wash Frame S-5, August 2000 Field Test .....	B-35
B.47	Wireframe Model of Response Nodes for Fenner Overcrossing, September 1999 Field Test.....	B-36
B.48	Overlay of Vertical FRF Magnitudes for Fenner Overcrossing, September 1999 Field Test.....	B-36
B.49	1 <sup>st</sup> Mode Fenner Overcrossing, September 1999 Field Test .....	B-37
B.50	2 <sup>nd</sup> Mode Fenner Overcrossing, September 1999 Field Test .....	B-37

## LIST OF FIGURES (continued)

FIGURE	Page
B.51	3 <sup>rd</sup> Mode Fenner Overcrossing, September 1999 Field Test..... B-38
B.52	Wireframe Model of Response Nodes for Fenner Overcrossing, December 2000 Field Test ..... B-39
B.53	Overlay of Vertical FRF Magnitudes for Fenner Overcrossing, December 2000 Field Test ..... B-39
B.54	1 <sup>st</sup> Mode Fenner Overcrossing, December 2000 Field Test..... B-40
B.55	2 <sup>nd</sup> Mode Fenner Overcrossing, December 2000 Field Test..... B-40
B.56	3 <sup>rd</sup> Mode Fenner Overcrossing, December 2000 Field Test ..... B-41
C.1	Damage Detection Model..... C-5
C.2	Sensor Locations ..... C-5
C.3	Damage Detection Results Using the First Experiment Mode and First Bending Mode of Baseline Model: (a) Result Using the Measurement along the Sensors A1-A9; (b) Result Using the Measurement along the Sensors B1-B9; (c) Result Using the Measurement along the Sensors C1-C9; (d) Result Using the Measurement along the Sensors D1-D9..... C-6
C.4	Damage Detection Results Using First Torsional Mode of Experimental Data and Baseline Model..... C-7
C.5	Damage Detection Results Using the First Experiment Mode and First Bending Mode of Baseline Model: (a) Result Using the Measurement along the Sensors A1-A9; (b) Result Using the Measurement along the Sensors D1-D9..... C-8
C.6	Damage Detection Results Using First Torsional Mode of Experimental Data and Baseline Model..... C-9
C.7	Damage Detection Model for Watson Wash Frame S-1, May 1999..... C-20
C.8	Sensor Locations for Watson Wash Frame S-1, May 1999 ..... C-20
C.9	Damage Detection Results Using the First Bending Mode: (a) Result Using the Measurement along the Sensors A1-A8; (b) Result Using the Measurement along the Sensors B1-B8 ..... C-21
C.10	Damage Detection Results Using the First Bending Mode: (a) Result Using the Measurement along the Sensors C1-C8; (b) Result Using the Measurement along the Sensors D1-D8..... C-22

## LIST OF FIGURES (continued)

FIGURE		Page
C.11	Damage Detection Results Using First Torsional Mode.....	C-23
C.12	Damage Detection Model for Watson Wash Frame S-2, May 1999.....	C-24
C.13	Sensor Locations for Watson Wash Frame S-2, May 1999 .....	C-24
C.14	Damage Detection Results Using the First Bending Mode: (a) Result Using the Measurement along the Sensors A1-A9; (b) Result Using the Measurement along the Sensors B1-B9 .....	C-25
C.15	Damage Detection Results Using the First Bending Mode: (a) Result Using the Measurement along the Sensors C1-C9; (b) Result Using the Measurement along the Sensors D1-D9.....	C-26
C.16	Damage Detection Results Using First Torsional Mode.....	C-27
C.17	Damage Detection Model for Watson Wash Frame S-3, May 1999.....	C-28
C.18	Sensor Locations for Watson Wash Frame S-3, May 1999 .....	C-28
C.19	Damage Detection Results Using the First Bending Mode: (a) Result Using the Measurement along the Sensors A1-A11; (b) Result Using the Measurement along the Sensors B1-B11 .....	C-29
C.20	Damage Detection Results Using the First Bending Mode: (a) Result Using the Measurement along the Sensors C1-C11; (b) Result Using the Measurement along the Sensors D1-D11 .....	C-30
C.21	Damage Detection Results Using First Torsional Mode.....	C-31
C.22	Damage Detection Model for Watson Wash Frame S-4, May 1999.....	C-32
C.23	Sensor Locations for Watson Wash Frame S-4, May 1999 .....	C-32
C.24	Damage Detection Results Using the First Bending Mode: (a) Result Using the Measurement along the Sensors A1-A9; (b) Result Using the Measurement along the Sensors B1-B9 .....	C-33
C.25	Damage Detection Results Using the First Bending Mode: (a) Result Using the Measurement along the Sensors C1-C9; (b) Result Using the Measurement along the Sensors D1-D9.....	C-34
C.26	Damage Detection Results Using First Torsional Mode.....	C-35
C.27	Damage Detection Model for Watson Wash Frame S-5, May 1999.....	C-36
C.28	Sensor Locations for Watson Wash Frame S-5, May 1999 .....	C-36

## LIST OF FIGURES (continued)

FIGURE		Page
C.29	Damage Detection Results Using the First Bending Mode: (a) Result Using the Measurement along the Sensors A1-A8; (b) Result Using the Measurement along the Sensors B1-B8 .....	C-37
C.30	Damage Detection Results Using the First Bending Mode: (a) Result Using the Measurement along the Sensors C1-C8; (b) Result Using the Measurement along the Sensors D1-D8 .....	C-38
C.31	Damage Detection Results Using First Torsional Mode.....	C-39
C.32	Damage Detection Model for Watson Wash Frame S-1, August 2000 ..	C-40
C.33	Sensor Locations for Watson Wash Frame S-1, August 2000 .....	C-40
C.34	Damage Detection Results Using the First Bending Mode: (a) Result Using the Measurement along the Sensors A1-A8; (b) Result Using the Measurement along the Sensors D1-D8 .....	C-41
C.35	Damage Detection Results Using First Torsional Mode.....	C-42
C.36	Damage Detection Model for Watson Wash Frame S-2, August 2000 ..	C-43
C.37	Sensor Locations for Watson Wash Frame S-2, August 2000 .....	C-43
C.38	Damage Detection Results Using the First Bending Mode: (a) Result Using the Measurement along the Sensors A1-A9; (b) Result Using the Measurement along the Sensors D1-D9 .....	C-44
C.39	Damage Detection Results Using First Torsional Mode.....	C-45
C.40	Damage Detection Model for Watson Wash Frame S-3, August 2000 ..	C-46
C.41	Sensor Locations for Watson Wash Frame S-3, August 2000 .....	C-46
C.42	Damage Detection Results Using the First Bending Mode: (a) Result Using the Measurement along the Sensors A1-A11; (b) Result Using the Measurement along the Sensors D1-D11 .....	C-47
C.43	Damage Detection Results Using First Torsional Mode.....	C-48
C.44	Damage Detection Model for Watson Wash Frame S-4, August 2000 ..	C-49
C.45	Sensor Locations for Watson Wash Frame S-4, August 2000 .....	C-49
C.46	Damage Detection Results Using the First Bending Mode: (a) Result Using the Measurement along the Sensors A1-A9; (b) Result Using the Measurement along the Sensors D1-D9 .....	C-50
C.47	Damage Detection Results Using First Torsional Mode.....	C-51

**LIST OF FIGURES (continued)**

FIGURE		Page
C.48	Damage Detection Model for Watson Wash Frame S-5, August 2000 ..	C-52
C.49	Sensor Locations for Watson Wash Frame S-5, August 2000 .....	C-52
C.50	Damage Detection Results Using the First Bending Mode: (a) Result Using the Measurement along the Sensors A1-A8; (b) Result Using the Measurement along the Sensors D1-D8.....	C-53
C.51	Damage Detection Results Using First Torsional Mode.....	C-54

## **1. INTRODUCTION**

Using the systems identification and damage localization techniques developed to date (Stubbs et al., 1997), the objective of the proposed work was to evaluate the effectiveness of the repair methods proposed by the Office of Structure Maintenance and Investigations (OSM&I) on two structures along the I-40 corridor in San Bernardino County. The two structures selected were the right (eastbound) structure of the Fenner Overcrossing (Bridge #54-0800) and the right (eastbound) structure of the Watson Wash Bridge (Bridge #54-0805). A modal test was performed on each bridge before repair work was accomplished. The structures were then tested after the repairs were performed. After each test the modal parameters were extracted and the bridge superstructure evaluated. The modal analysis provided changes in frequencies and mode shapes; the systems identification and the damage localization provided changes in both material and structural properties of the superstructure. Details of the repair work were not part of this investigation and were handled by others. The results of the project are summarized in this report.

## **2. DESCRIPTION OF STRUCTURES**

### **2.1 Fenner Overcrossing**

The Fenner Overcrossing is located on Interstate 40 approximately 35 miles west of Needles, San Bernadino County, California. The Fenner Overcrossing is a three-span, skewed, two-lane interstate bridge 207 ft. long. The bridge was constructed in 1968. The structure consists of prestressed-concrete girders with a cast-in-place deck structural system. The girders are simply supported at the abutments and piers while the deck is continuous. The three span lengths going from west to east are, respectively, 52.5 ft., 93.5 ft., and 55.5 ft. The 7-in. thick deck is 48 ft. wide with integral longitudinal barrier rails. Seven longitudinal 4.5-ft deep, prestressed-concrete girders support each span. The girder spacing is 8.0 ft center to center with 4.0 ft overhangs beyond the outside girders. The right outside girder is skewed in order to accommodate the geometry of the ramp

merging lane. Figure 1 is a reproduction of the as-built overall plan and cross-sectional view of the structure. Figure 2 depicts a view of the deck and barrier rail from the west abutment. Figure 3 shows a typical profile view of the structural system.

## **2.2 Watson Wash Bridge**

The Watson Wash Bridge is located on Interstate 40 approximately 38 miles west of Needles, San Bernadino County, California. The Watson Wash Bridge is a skewed two-lane interstate bridge 741 ft. long and was constructed in 1968. The structure is a cast-in-place reinforced-concrete deck and girder structural system with sixteen 42-ft central spans and two shorter 34.5 ft spans at each abutment. The structure is composed of five frames (here denoted Frame S-1 to Frame S-5) connected with shear transfer hinges. The multi-span Watson Wash Bridge was treated as five separate interconnected frames numbered sequentially from the west abutment. Watson Wash Frames S-1 and S-5, and S-2 and S-4 were similar with respect to the length and number of spans and the location of hinges. Frame S-3 was a symmetrical structure spanning Bent 8 to Bent 12. Each frame consisted of the following elements: (1) a 7-in. thick deck, 41 ft wide with integral longitudinal barrier rails; (2) six cast in place 12-in. wide by 24-in. deep longitudinal girders support the deck seventeen 42-ft wide continuous skewed bents; and (3) girders with spacing 7.0-ft center to center and 3.0-ft overhangs beyond the outside girders. Figure 4 is a reproduction of the as-built overall plan view of the structure. Figure 5 presents a view of the deck and barrier rail from the east abutment. Figure 6 shows a typical profile view of the structural system. Figure 7 shows a detailed view of a girder pier connection.

## **3. SUMMARY OF DATA GATHERING AND ANALYSIS**

A modal test was performed on the right structure of the Fenner Overcrossing (Bridge #54-0800) on 17 May 1999 and the Watson Wash Bridge (Bridge #54-0805) on 18 - 19 May 1999 prior to the commencement of deck repair work. The modal tests required an excitation device as well as the accelerometers to be placed on the

superstructure. While there was no need to close the bridge for testing, some traffic control was required. District # 08 provided traffic control for both structures.

In order to resolve certain modeling issues, the Fenner Overcrossing Bridge was retested in June 1999, prior to any repair work. Repair work was completed on the Watson Wash Bridge in July 2000 and a second modal test was performed on the structure on 15-16 August 2000. Repair work was completed on the Fenner Overcrossing Bridge in November 2000 and the bridge was retested on 13 December 2000. Details of the testing of both structures are provided in Appendix B of this report.

The modal parameters for these structures were extracted from the time data collected using the commercially available modal package ME'Scope. The first 2-3 frequencies and mode shapes for each structure were extracted. Additional frequencies and mode shapes were extracted depending upon the quality of the time data. Simultaneously, theoretical modal parameters from finite element models of the structures were developed to guide the interpretation of the data.

Using the nondestructive damage detection method developed at Texas A&M University (Stubbs et al., 1997), the parameters of a model of the bridges were identified and changes in material and structural properties, including boundary conditions, of that model were determined. Note that the number of parameters in the model to be identified was consistent with the quality and quantity of modal data to be provided from the modal analysis. As a minimum, this analysis provided values for the effective concrete modulus of elasticity and the stiffness of the superstructure.

## **4. DESCRIPTION OF THE FINITE ELEMENT MODELS**

### **4.1 Fenner Overcrossing**

The concrete deck was modeled using 4-node shell elements. A total of 689 nodes and 624 elements were used. The prestressed concrete girders were modeled using

the combination of beam and shell elements. The upper and lower flanges were modeled using beam elements while the webs were modeled using shell elements. The intermediate diaphragms were also modeled using shell elements. The bents and abutments were modeled using 8-node brick elements. The soil around the foundations of bents were modeled using linear spring elements. A typical value of 800 kcf, dense sand (Bowles, 1996), was used as the modulus of subgrade reaction of the soil. Also, the soil surrounding the abutments were modeled using linear spring elements.

#### **4.2 Watson Wash Bridge**

A finite element (FE) model for the Watson Wash bridge was developed to define a baseline model. The concrete decks of Frames S-1 through S-5 were modeled using 4-node plate elements, the decks of Frames S-1 and S-5 were modeled using 420 elements each, the deck of Frames S-2 and S-4 were modeled using 532 elements each, and the deck of Frame S-3 was modeled using 644 elements. The concrete girders and diaphragms were also modeled using plate elements. Each bent was modeled with the combination of 55 plate elements for the column and 10 brick elements for the footings. The two abutments were modeled using 7 plate elements. The soil-structure interaction between the abutments and bents were modeled using linear elastic spring elements.

The initial material properties for the FE model were generated as follows: (1) reinforced concrete was assumed to have a mass density of  $\rho = 4.7 \text{ lb-s}^2/\text{ft}^4$ , Poisson's ratio of  $\nu = 0.15$ , and the elastic modulus (E) of 3,133 ksi; and (2) the soil was assumed to have a typical modulus of subgrade reaction of 600 kcf. Note that the assumed modulus of subgrade reaction was based on a review of the log of test borings included in the as-built plans. Note also that the spring stiffness of the soil-structure interaction between the footing of the bents and the soil was obtained from the modulus of subgrade reaction by multiplying by the appropriate area. Similarly, the spring stiffness representing the soil around the abutment system was also estimated by multiplying the modulus of subgrade reaction by the appropriate area.

## **5. RESULTS OF MODAL TESTS FOR STRUCTURES**

The details of the modal testing are presented in Appendix B of this report. That Appendix contains a detailed discussion on the instrumentation, the instrumentation layout, the testing procedures, the modal analysis, and the results of the modal analysis. In this section only the results relevant to the evaluation of the effectiveness of the repair are presented.

### **5.1 Fenner Overcrossing**

Two modes were used in the systems identification and damage localization of the Fenner Overcrossing: the first bending mode and the first torsional mode. These modes are depicted in Figures B.49 and B.50 for the 1999 test and Figures B.54 and B.55 for the 2000 test (See Appendix B). The frequencies associated with Fenner Overcrossing tests are listed in Table 1. Note that Test 1 and Test 2 were performed before the repair and Test 3 was performed after the repair. The results indicate that before and after the repair there was a 2.48 percent decrease in the first bending frequency and an increase of less than one percent in the first torsional frequency.

### **5.2 Watson Wash Bridge**

Typically, two of the extracted modes were used in the analysis of the Watson Wash Bridge. These modes, denoted Mode 1 and Mode 2, are depicted in Appendix B. For example, Mode 1 and Mode 2 for Frame S-1 are depicted in Figure B.9 and B.10. The results of the modal analysis for the Watson Wash Bridge are summarized in Tables 2-6. Except for Frame S-4 (Table 5), in which the 2<sup>nd</sup> mode apparently increased 1.01 percent after the repair, the effect of the repair on the modal response was to decrease the frequency of the measured modes. The decrease in frequency was greatest in Frame S-1 (Table 2) and least in Frame S-5 (Table 6).

## **6. RESULTS OF THE SYSTEMS IDENTIFICATION AND DAMAGE DETECTION**

### **6.1 Results of the Systems Identification**

The structural model of the Fenner Overcrossing selected to be identified in this study consisted of a bridge with uniform deck modulus, deck mass density, bent modulus, bent mass density, and uniform stiffness for the springs that modeled the soil-structure interaction. The results of the systems identification for the Fenner Overcrossing are listed in Table 7. The parameters to be identified consisted of the effective value of the modulus of the girders, the moduli of the deck and bent, the stiffness of the springs modeling the soil-structure interaction, and the effective mass density of the concrete comprising the structure. By “effective” modulus or mass density we mean the values assigned to the appropriate parameters in the model to be identified. The results of the systems identification indicate that the impact of the repair was a small increase in the effective stiffness of the superstructure (2.75 percent) and an insignificant change in the mass density. Details of the system identification procedures are provided in Appendix A and Appendix C.

For each of the substructures of the Watson Wash Bridge, the structural model to be identified consisted of a structure with uniform modulus for the deck and the bents, and mass density of the deck and the bents. The quality of information provided from the modal analysis dictated the complexity of the model to be identified. The results of the systems identification for the Watson Wash Bridge are listed in Table 8 to Table 12. The parameters to be identified were the effective modulus of the deck and bents, and the mass density of the deck concrete. The results indicate that for all five frames comprising the structure, the impact of the repair was increased (7 to 15 percent) in the effective mass density of the deck. Except for Frame S-4, no significant increase in the identified stiffness of the deck occurred, according to the analysis.

### **6.2 Damage Detection**

The damage detection algorithm summarized in Appendix A permits the identification of possible damage locations in the structure from a knowledge of changes

in the mode shapes of the structure. In this study the pristine (undamaged) structure is taken to be the pre-repair identified model. Note that the identified models have uniform densities and moduli. Note also that the extracted modal parameters associated with the post-repair structures are associated with the potentially defective structure.

The damage localization results for the Fenner Overcrossing are presented in Figure 8. Note that the possible damage locations are concentrated near Bent 2 and Bent 3. Since the deck was recently resurfaced and the testing team had no access to the bridge underside, corroborating evidence for the existence of damage was not provided.

The damage localization results for the Watson Wash Bridge are presented in Figure 9 to Figure 13. According to the present methodology, all five frames have incurred some level of damage. Since the test team had access to the underside of the Watson Wash Bridge, a visual inspection of the deck was performed from below and the predicted locations of damage and observed locations of damage were compared. It was noted that the predicted damage locations corroborated with locations where major repairs were made or where there was evidence of sealant leaking.

## **7. FINDINGS**

The objective of this project was to use existing tools from systems identification and damage detection to evaluate nondestructively the impact of a repair program on the Fenner Overcrossing and the Watson Wash Bridge. On the basis of the testing and analysis, we present the following findings.

### **7.1 Fenner Overcrossing**

1. The superstructure experienced a 2.75 percent increase in modulus.
2. No change in the effective mass density of the superstructure was identified.
3. Potential damage locations are in the deck and in the neighborhood of Bent 2 and Bent 3.

## REFERENCE

Stubbs, N., Park, S., and Sikorsky, C. (1997). "A General Methodology to Non-destructively Evaluate Bridge Structural Safety", *Technical Report Submitted to State of California Department of Transportation, Sacramento, California*, Texas Engineering Experiment Station, Texas A&M Univeristy, College Station, TX.

Bowles, J.E. (1996). *Foundation Analysis and Design*, McGraw-Hill, New York, NY.

## 7.2 Watson Wash Bridge

1. For Frame S-1, Frame S-2, Frame S-3, and Frame S-5, the impact of the repair was to significantly increase the effective mass density of the deck (7 – 15 percent) and not change the effective modulus of the deck.
2. For Frame S-4, the impact of the repair was to significantly increase the effective mass density of the deck (7.71 percent) and increase the effective modulus of the deck by 3.67 percent. Note that the effect of introducing 1-inch asphaltic concrete overlay on the frames is equivalent to increasing the mass of the deck while not modifying the stiffness of the deck.
3. All five frames of the Watson Wash Bridge have potential damage.

**Table 1. Results of Modal Tests: Fenner Overcrossing**

Mode Description	Frequency (Hz)			Relative Change (%)	
	Test 1	Test 2	Test 3	$\frac{\omega_{\text{Test 2}} - \omega_{\text{Test 1}}}{\omega_{\text{Test 1}}}$	$\frac{\omega_{\text{Test 3}} - \omega_{\text{Test 2}}}{\omega_{\text{Test 2}}}$
	(May 15, 1999)	(Sep. 23, 1999)	(Dec. 15, 2000)		
First Bending	4.29	4.44	4.33	3.50	-2.48
First Torsion	5.27	5.49	5.54	4.17	0.91

**Table 2. Results of Modal Tests: Watson Wash Bridge, Frame S-1**

Mode Description	Frequency (Hz)		Relative Change (%)
	Test 1	Test 2	$\frac{\omega_{2000} - \omega_{1999}}{\omega_{1999}}$
	(May 17, 1999)	(Sep. 15, 2000)	
Mode 1	5.88	5.50	-6.46
Mode 2	6.87	6.25	-9.02
Mode 3	N/A	8.13	

**Table 3. Results of Modal Tests: Watson Wash Bridge, Frame S-2**

Mode Description	Frequency (Hz)		Relative Change (%)
	Test 1	Test 2	$\frac{\omega_{2000} - \omega_{1999}}{\omega_{1999}}$
	(May 17, 1999)	(Sep. 15, 2000)	
Mode 1	5.98	5.50	-8.03
Mode 2	7.15	6.75	-5.59

**Table 4. Results of Modal Tests: Watson Wash Bridge, Frame S-3**

Mode Description	Frequency (Hz)		Relative Change (%)
	Test 1	Test 2	$\frac{\omega_{2000} - \omega_{1999}}{\omega_{1999}}$
	(May 17, 1999)	(Sep. 15, 2000)	
Mode 1	5.59	5.44	-2.68
Mode 2	6.97	6.31	-9.47

**Table 5. Results of Modal Tests: Watson Wash Bridge, Frame S-4**

Mode Description	Frequency (Hz)		Relative Change (%) $\frac{\omega_{2000} - \omega_{1999}}{\omega_{1999}}$
	Test 1 (May 17, 1999)	Test 2 (Sep. 15, 2000)	
Mode 1	5.98	5.63	-5.85
Mode 2	6.93	7.00	1.01

**Table 6. Results of Modal Tests: Watson Wash Bridge, Frame S-5**

Mode Description	Frequency (Hz)		Relative Change (%) $\frac{\omega_{2000} - \omega_{1999}}{\omega_{1999}}$
	Test 1 (May 17, 1999)	Test 2 (Sep. 15, 2000)	
Mode 1	5.93	5.44	-5.06
Mode 2	7.02	6.88	-2.03

**Table 7. Effective Stiffness Properties: Fenner Overcrossing**

	Girder Modulus, E (ksi)	Deck and Bent Modulus E (ksi)	Stiffness Soil-Structure Interaction (kcf)	Mass Density (lb-s <sup>2</sup> /ft <sup>4</sup> )
Before Repair (1999)	2,430	2,254	12,174	4.7
After Repair (2000)	2,497	2,316	12,174	4.7
$(x_{2000} - x_{1999})/x_{1999}, \%$	2.76	2.75	0	0

**Table 8. Effective Stiffness Properties: Watson Wash Bridge, Frame S-1**

	Girder Modulus, E (ksi)	Deck and Bent Modulus E (ksi)	Stiffness Soil-Structure Interaction (kcf)	Mass Density (lb-s <sup>2</sup> /ft <sup>4</sup> )
Before Repair (1999)	2,515	2,515	-	4.71
After Repair (2000)	2,520	2,520	-	5.04
$(x_{2000} - x_{1999})/x_{1999}, \%$	0.20	0.20		7.01

**Table 9. Effective Stiffness Properties: Watson Wash Bridge, Frame S-2**

	Girder Modulus, E (ksi)	Deck and Bent Modulus E (ksi)	Stiffness Soil- Structure Interaction (kcf)	Mass Density (lb-s <sup>2</sup> /ft <sup>4</sup> )
Before Repair (1999)	2,630	2,630	-	4.67
After Repair (2000)	2,655	2,655	-	5.38
$(x_{2000} - x_{1999})/x_{1999}, \%$	0.95	0.95		15.2

**Table 10. Effective Stiffness Properties: Watson Wash Bridge, Frame S-3**

	Girder Modulus, E (ksi)	Deck and Bent Modulus E (ksi)	Stiffness Soil- Structure Interaction (kcf)	Mass Density (lb-s <sup>2</sup> /ft <sup>4</sup> )
Before Repair (1999)	2,583	2,583	-	4.70
After Repair (2000)	2,586	2,586	-	5.26
$(x_{2000} - x_{1999})/x_{1999}, \%$	0.12	0.12		11.9

**Table 11. Effective Stiffness Properties: Watson Wash Bridge, Frame S-4**

	Girder Modulus, E (ksi)	Deck and Bent Modulus E (ksi)	Stiffness Soil- Structure Interaction (kcf)	Mass Density (lb-s <sup>2</sup> /ft <sup>4</sup> )
Before Repair (1999)	2,535	2,535	-	4.67
After Repair (2000)	2,628	2,628	-	5.03
$(x_{2000} - x_{1999})/x_{1999}, \%$	3.67	3.67		7.71

**Table 12. Effective Stiffness Properties: Watson Wash Bridge, Frame S-5**

	Girder Modulus, E (ksi)	Deck and Bent Modulus E (ksi)	Stiffness Soil- Structure Interaction (kcf)	Mass Density (lb-s <sup>2</sup> /ft <sup>4</sup> )
Before Repair (1999)	2,595	2,595	-	4.71
After Repair (2000)	2,582	2,582	-	4.56
$(x_{2000} - x_{1999})/x_{1999}, \%$	0.19	0.19		13.4





**Figure 2. View of Fenner Deck from West Abutment**

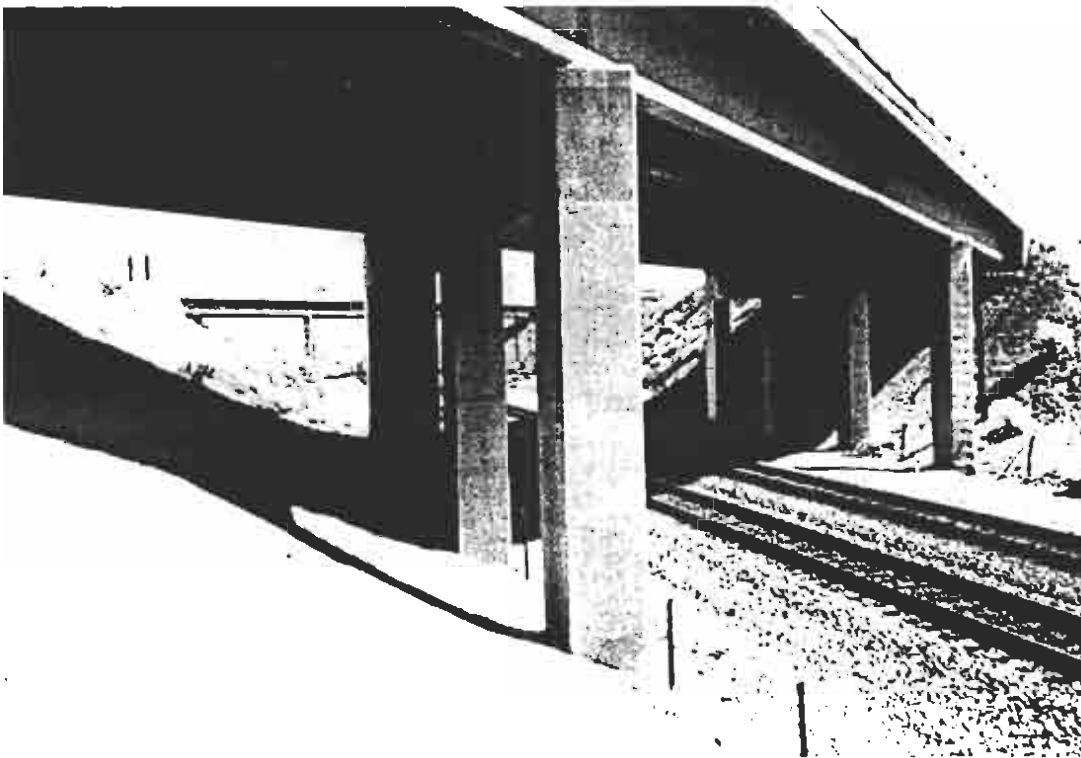


**Figure 3. Profile View of Fenner Structural System**

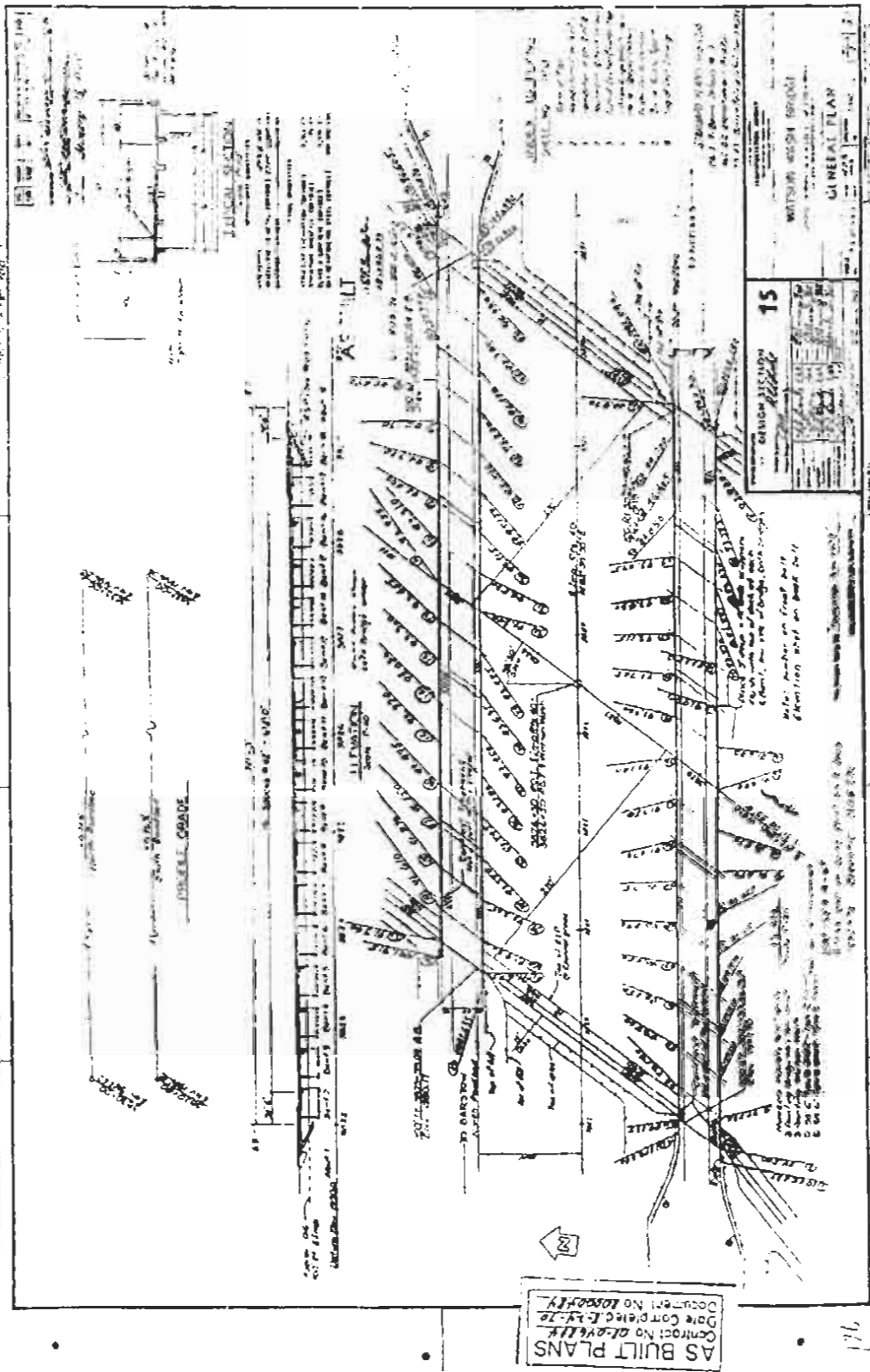
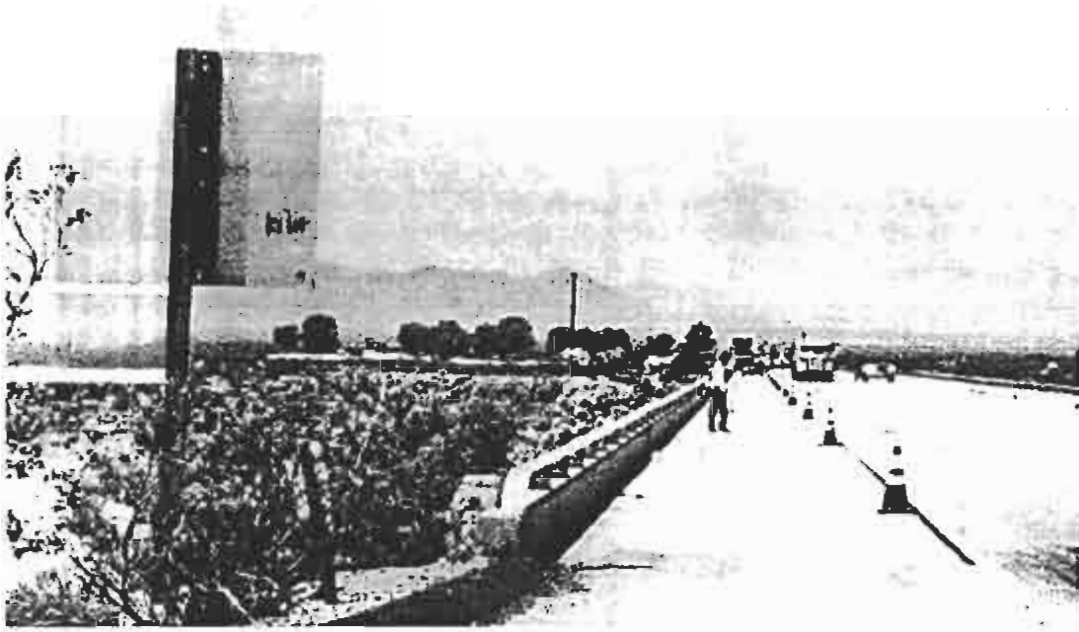
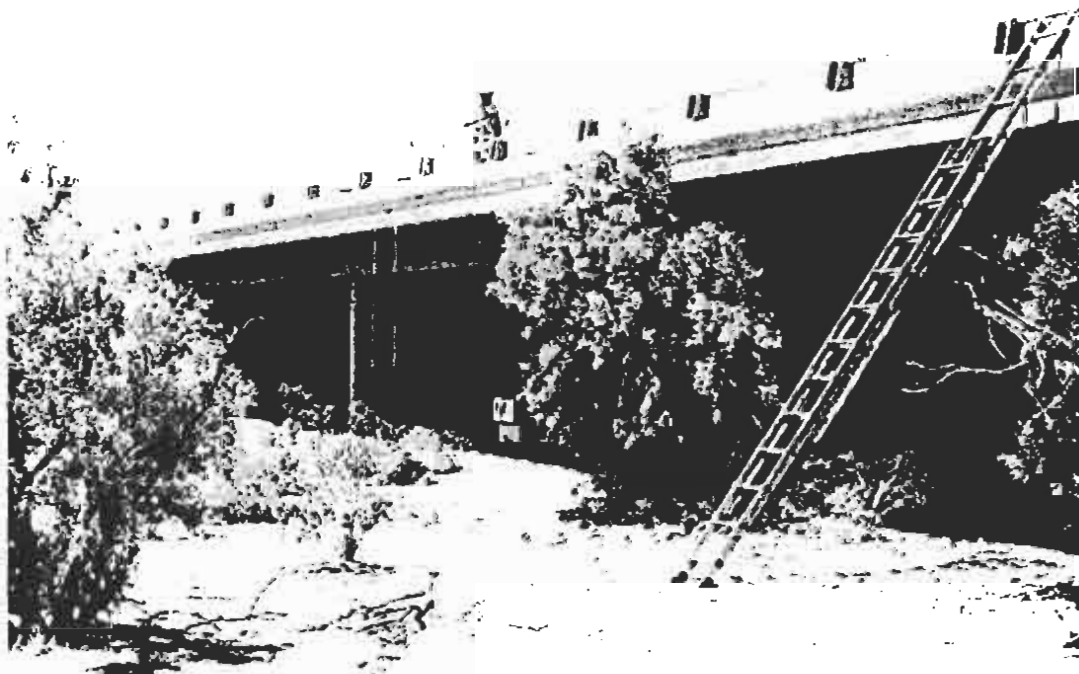


Figure 4. As-built Plan View of Watson Wash Bridge



**Figure 5. View of Watson Wash Deck from East Abutment**



**Figure 6. Side View of Watson Wash Pier and Deck System**

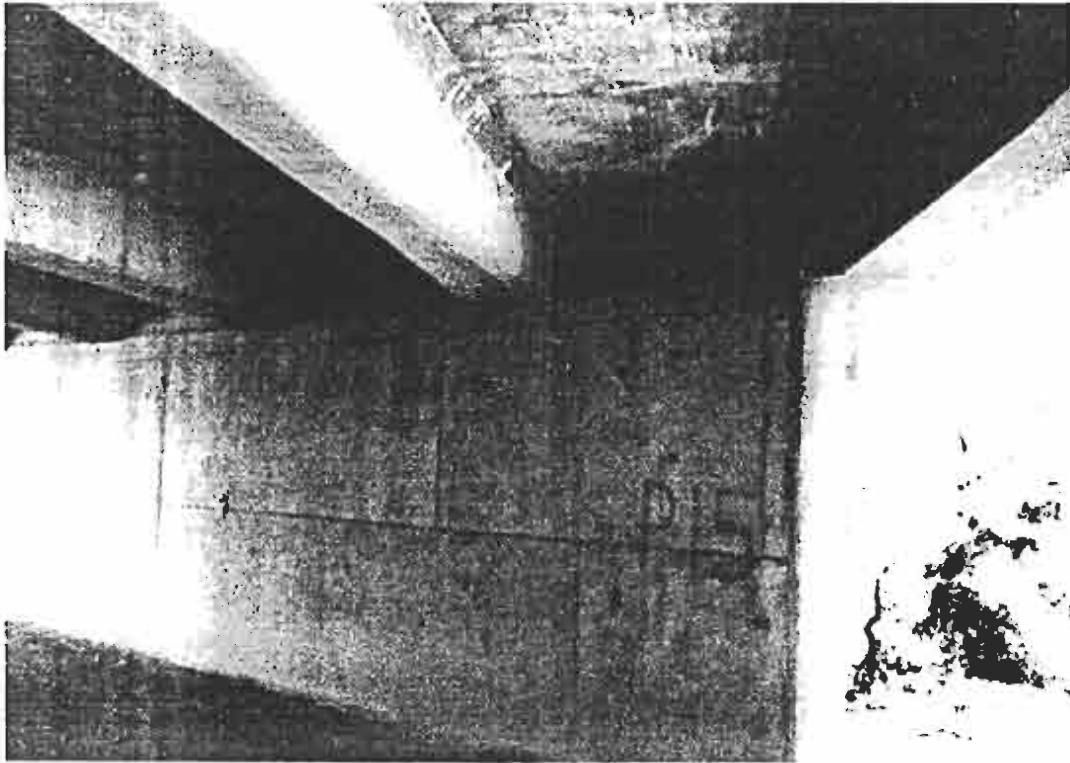


**Figure 7. View of Typical Watson Wash Pier Girder Connection**

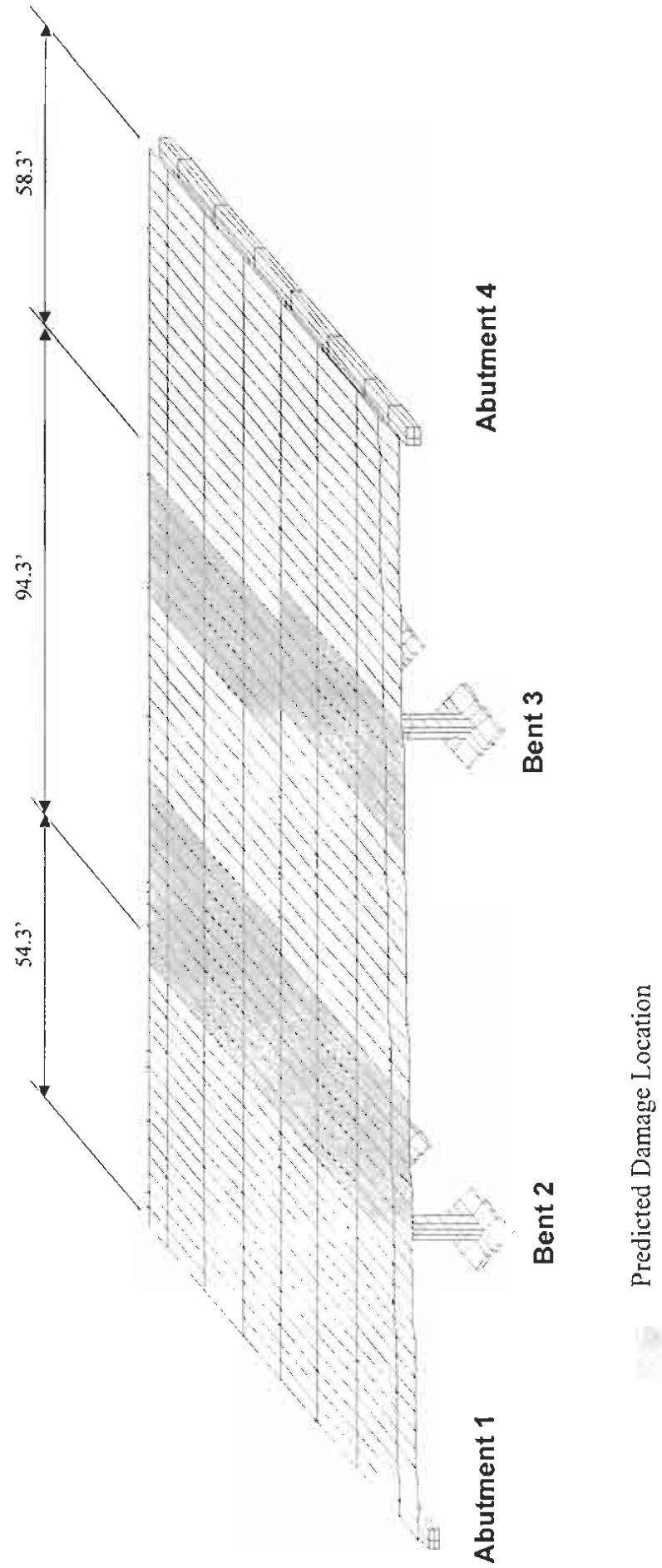


**Figure 8. Possible Damage Locations in Fenner Overcrossing**

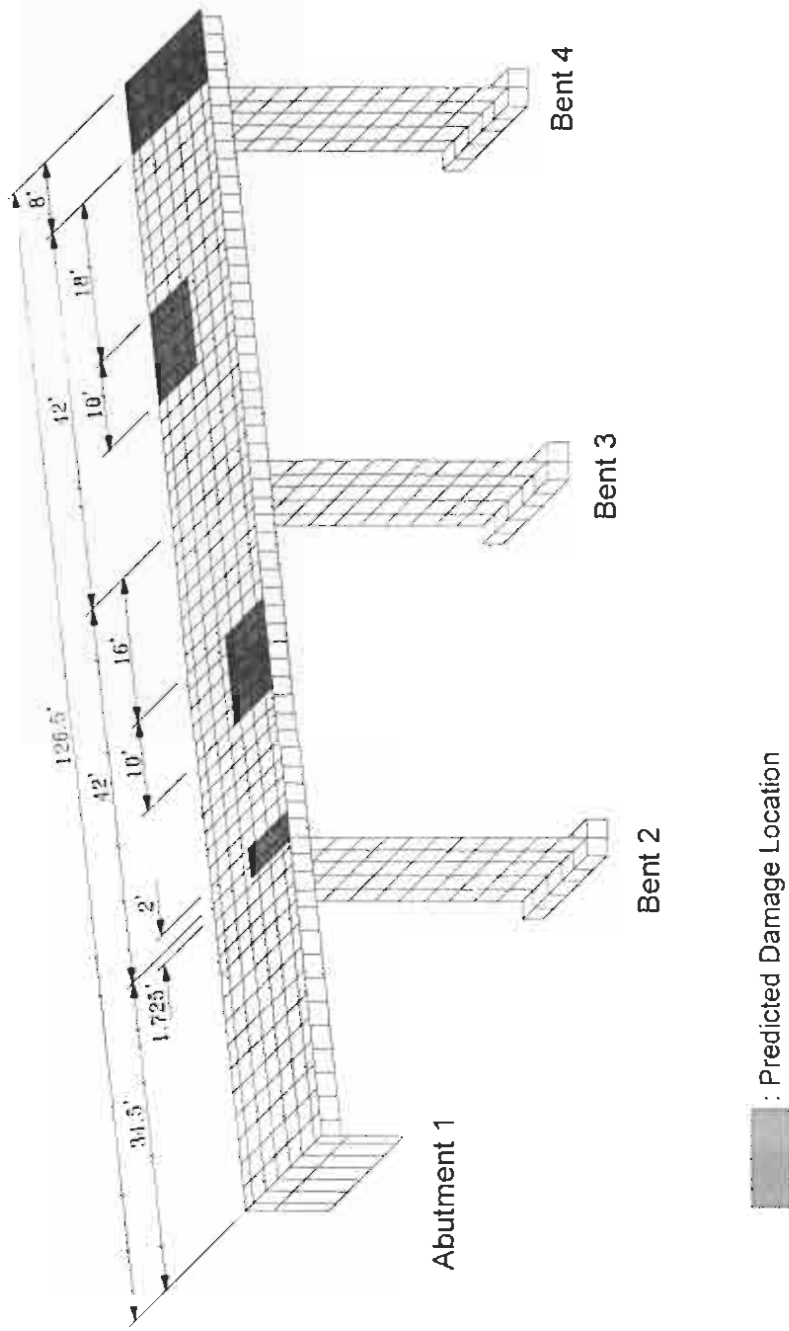


Figure 9. Possible Damage Locations in Watson Wash Bridge, Frame S-1

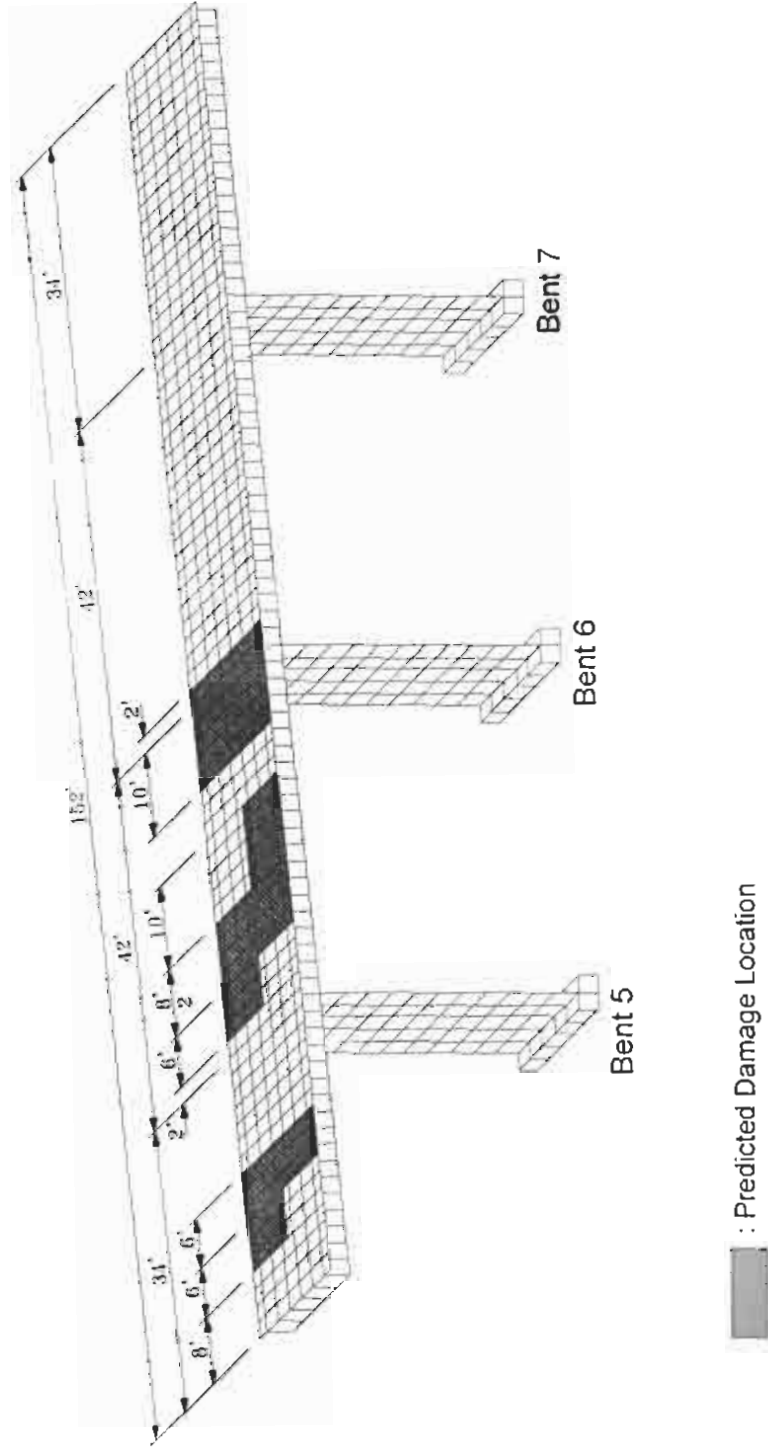


Figure 10. Possible Damage Locations in Watson Wash Bridge, Frame S-2

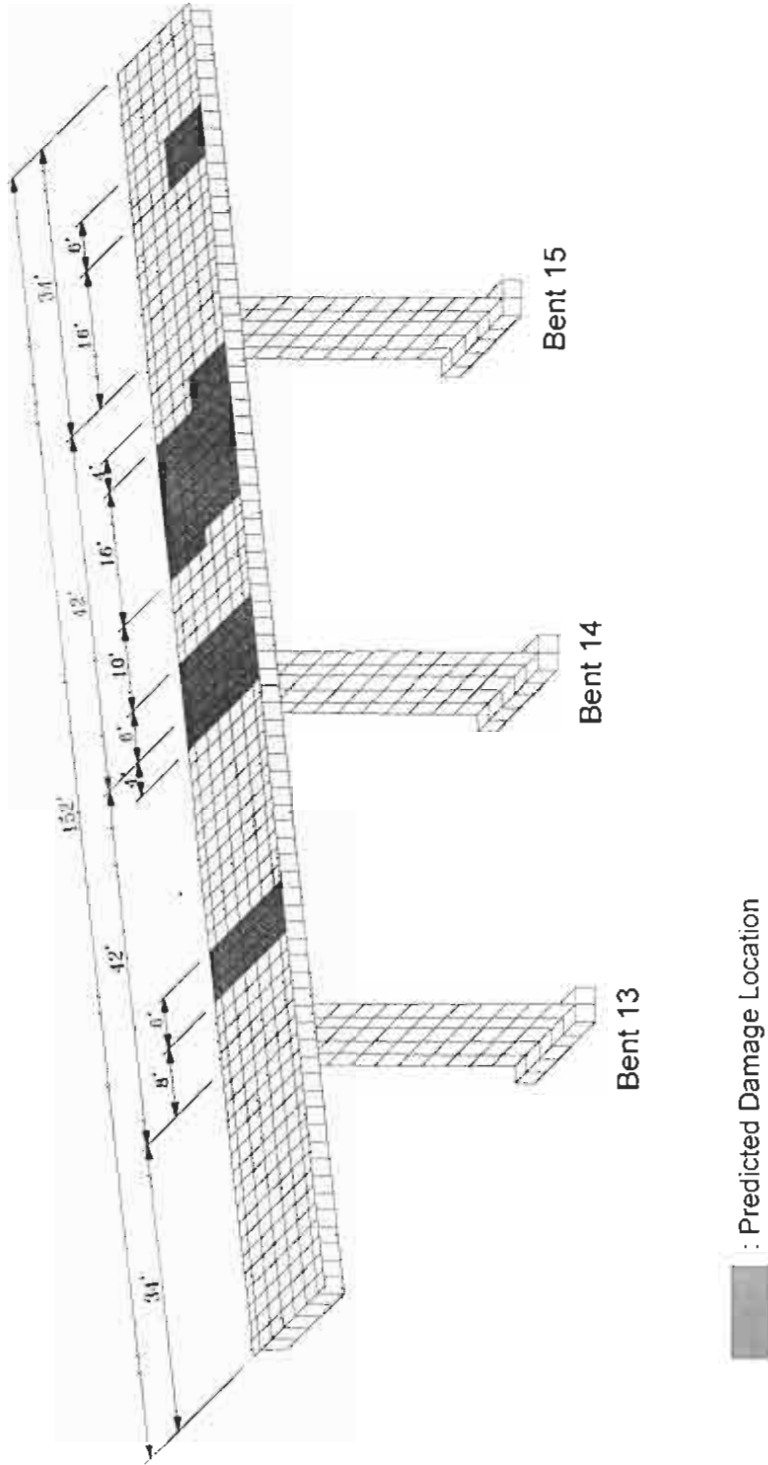


Figure 12. Possible Damage Locations in Watson Wash Bridge, Frame S-4

## APPENDIX A

### THEORY OF SYSTEMS IDENTIFICATION AND DAMAGE DETECTION

#### A.1 SYSTEM IDENTIFICATION SCHEME FOR THE BASELINE STRUCTURE

The rationale behind the development of the baseline model can be explained with the aid of Figure A.1. Suppose a flawed (i.e., damaged) structure (Refer to Figure A.1(a)) is given with field-measured mode shapes  $\Phi_i^*$  and eigenfrequencies  $\omega_i^*$ . Assume that the magnitude of the flaw is small in comparison to a flawless (i.e., baseline) structure. Suppose that an estimate of the flawless structure can be identified, shown in Figure A.1(b), using only the frequency information from the flawed structure. Then the identified baseline model (Refer to Figure A.1(b)) will have the same eigenfrequencies  $\omega_i^*$  (in the least square sense) of the flawed model (Refer to Figure A.1(a)) but the mode shapes of the two structures will be different in the neighborhood of the flaw. This difference in the mode shapes of the identified baseline structure and the measured mode shapes of the existing structure may then be exploited to localize the flaw.

Here, a system identification methodology to identify baseline modal responses of a structure is outlined (Stubbs and Kim, 1996). Consider a linear skeletal structure with  $NE$  members and  $N$  nodes. Suppose  $k_j^*$  is the unknown stiffness of the  $j^{\text{th}}$  member of the structure for which  $M$  eigenvalues are known. Also, suppose  $k_j$  is a known stiffness of the  $j^{\text{th}}$  member of a FE model for which the corresponding set of  $M$  eigenvalues are known. Then, relative to the FE model, the fractional stiffness change of the  $j^{\text{th}}$  member of the structure,  $\alpha_j$ , and the stiffnesses are related according to the following equation:

$$k_j^* = k_j (1 + \alpha_j) \quad (\text{A.1})$$

The fractional stiffness change of  $NE$  members may be obtained using the following equation (Stubbs and Osegueda, 1990):

$$\mathbf{Z} = \mathbf{F}\alpha \quad (\text{A.2})$$

where  $\alpha$  is a  $NE \times 1$  matrix containing the fractional changes in stiffness between the FE model and the structure,  $\mathbf{Z}$  is a  $M \times 1$  matrix containing the fractional changes in eigenvalues between the two systems, and  $\mathbf{F}$  is a  $M \times NE$  stiffness sensitivity matrix relating the fractional changes in stiffnesses to the fractional changes in eigenvalues.

The  $M \times NE$ ,  $\mathbf{F}$  matrix can be determined as follows: first,  $M$  eigenvalues are numerically generated from the initial FE model; second, the stiffness of the first member of the FE model is modified by a known amount; third, the corresponding set of  $M$  eigenvalues are numerically generated for the modified FE model; fourth, the fractional changes between the  $M$  initial eigenvalues and  $M$  eigenvalues of the modified structure are computed; fifth, each component of the first column of the  $\mathbf{F}$  matrix (i.e., the  $M \times 1$ ,  $\mathbf{F}$  matrix) is computed by dividing the fractional changes in each eigenvalue by the magnitude of the modification at member one; and finally, the  $M \times NE$ ,  $\mathbf{F}$  matrix is generated by repeating the entire procedures for all  $NE$  members.

Using the above rationale as a basis, the following 6-step algorithm is proposed to identify a given structure:

1. Select a target structure (e.g., a post-damage state of the structure) for which sufficient eigenfrequencies that can be used to identify the baseline structure are available. (Note that the mode shapes of the damaged structure in defining the target structure are ignored.)
2. Select an initial FE model of the structure, utilizing all possible knowledge about the design and construction of the structure.
3. As outlined above, compute the sensitivity matrix of the FE model.
4. As outlined above, compute the fractional changes in eigenvalues between the FE model and the target structure.
5. Fine-tune the FE model by first solving Equation (A.2) to estimate stiffness changes (i.e., to compute the  $NE \times 1$ ,  $\alpha$  matrix) and next solving Equation (A.1) to update

the stiffness parameters of the FE model.

6. Repeat steps 1~5 until  $Z \cong 0$  or  $\alpha \cong 0$  (i.e., as they approach zero) when the parameters of the FE model are identified.

The converged FE model is the baseline model. It has the frequencies of the damaged (i.e., target) structure but none of its members are damaged. Furthermore, the mode shapes of the baseline model differ from those of the damaged structure. Once the baseline model is identified, its modal parameters can be numerically generated (e.g., using commercial software ABAQUS (1994)).

## **A.2 DAMAGE LOCALIZATION THEORY (DAMAGE INDEX METHOD)**

In the field of Nondestructive Damage Detection (NDD) using modal parameters, one of the more difficult problems is that of making a statement regarding the integrity of a relatively small portion of a structure when very few modal parameters are available. In such cases, inverse methods using systems of equations usually result in unsolvable systems with few equations but many unknowns. The discipline of pattern recognition provides a way to deal with such heavily underdetermined systems (Nadler and Smith, 1993).

In pattern recognition, physical world data are transduced into the so-called pattern space. Using techniques of dimensionality reduction, the pattern space is reduced to a smaller dimension known as the feature space. Data in the feature space are introduced to a decision algorithm and the elements of the feature space are classified into a finite number of clusters. In the problem at hand, the dynamic response of the structure in the time domain represents the physical world data and the modal parameters represent the pattern space. The feature space is represented by indicators that are a function of measurable pre-damage and post-damage modal parameters. These indicators can be selected in such a manner that they reflect internal structure in the data. The decision algorithm is a means by which the data space is partitioned into  $D_n$  clusters (decision

spaces). In this study,  $n = 2$  and the decision spaces correspond to the cases: (a) a structure is not damaged at a given location, and (b) a structure is damaged at a given location. For each instance the indicator of damage will fall into one of the two categories.

The damage index method utilizes the change in mode shapes of the pre-damage and post-damage structure to detect and locate damage in a structure (Stubbs et al., 1992). Consider a linear, undamaged, skeletal structure with  $NE$  elements and  $N$  nodes. After writing the equations of motion for the structure and solving the eigenvalue problem, the  $i^{\text{th}}$  modal stiffness,  $K_i$ , of the arbitrary structure is given by (Craig, 1981)

$$K_i = \Phi_i^T C \Phi_i \quad (\text{A.3})$$

where  $\Phi_i$  is the  $i^{\text{th}}$  modal vector and  $C$  is the system stiffness matrix. From matrix structural analysis, the contribution of the  $j^{\text{th}}$  member to the  $i^{\text{th}}$  modal stiffness,  $K_{ij}$ , is given by

$$K_{ij} = \Phi_i^T C_j \Phi_i \quad (\text{A.4})$$

where  $C_j$  is the contribution of the  $j^{\text{th}}$  member to the system stiffness matrix. The fraction of modal energy for the  $i^{\text{th}}$  mode that is concentrated in the  $j^{\text{th}}$  member (i.e., the element sensitivity of the  $j^{\text{th}}$  member to the  $i^{\text{th}}$  mode) is given by

$$F_{ij} = K_{ij}/K_i \quad (\text{A.5})$$

Let the corresponding modal parameters in Equations (A.3) to (A.5) associated with a subsequently damaged structure be characterized by asterisks. Then for the damaged structure,

$$F_{ij}^* = K_{ij}^* / K_i^* \quad (\text{A.6})$$

where  $K_{ij}^*$  and  $K_i^*$  are given by, respectively

$$K_{ij}^* = \Phi_i^{*T} C_j^* \Phi_i^* \quad (A.7)$$

and

$$K_i^* = \Phi_i^{*T} C^* \Phi_i^* \quad (A.8)$$

Again, from matrix structural analysis, the stiffness matrices  $C_j$  and  $C_j^*$  in Equations (A.4) and (A.7) may be written as follows:

$$C_j = k_j C_{j0} \quad (A.9)$$

and

$$C_j^* = k_j^* C_{j0} \quad (A.10)$$

where the scalars  $k_j$  and  $k_j^*$ , respectively, are parameters representing the material stiffness properties of the undamaged and damaged  $j^{\text{th}}$  member of the structure, and the matrix  $C_{j0}$  involves only geometric quantities (and possibly terms containing Poisson's ratio). The quantities  $F_{ij}$  and  $F_{ij}^*$  are related by the equation:

$$F_{ij}^* = F_{ij} + dF_{ij} \quad (A.11)$$

where  $dF_{ij}$  is related to the change in the fraction of modal energy of the  $j^{\text{th}}$  member in the  $i^{\text{th}}$  mode. The quantity  $dF_{ij}$  can be obtained from the expression:

$$dF_{ij} = \frac{K_{ij}}{K_i} \left[ \frac{dK_{ij}}{K_{ij}} - \frac{dK_i}{K_i} \right] \quad (A.12)$$

Assuming that the structure is damaged at a single location  $j$  and the resulting change in  $F_{ij}$  is only a function of  $k_j$ , a first order approximation of  $dK_{ij}$  can be obtained

from the expression:

$$dK_{ij} \cong \frac{\partial K_{ij}}{\partial k_j} dk_j + \frac{\partial K_{ij}}{\partial u_{ij}} \frac{\partial u_{ij}}{\partial k_j} dk_j \quad (\text{A.13})$$

where

$$u_{ij} = \Phi_i^T C_{j0} \Phi_i \quad (\text{A.14})$$

Using Equations (A.4) and (A.9), it can be shown that

$$\frac{\partial K_{ij}}{\partial k_j} = u_{ij} \quad (\text{A.15})$$

and

$$\frac{\partial K_{ij}}{\partial u_{ij}} = k_j \quad (\text{A.16})$$

Next, introducing the modal force vector associated with the  $j^{\text{th}}$  member and the  $i^{\text{th}}$  mode,  $A_{ij}$ , given by

$$A_{ij} = C_j \Phi_i \quad (\text{A.17})$$

it can be shown that by using Equations (A.9), (A.14), and (A.17),

$$u_{ij} = \frac{1}{k_j} A_{ij}^T C_{j0}^{-1} A_{ij} \quad (\text{A.18})$$

Therefore, if it is assumed that the modal force  $A_{ij}$  remains constant while  $k_j$  changes (note that the assumption is true in the case of a statically determinant system), then

$$\frac{\partial u_{ij}}{\partial k_j} = -\frac{2u_{ij}}{k_j} \quad (\text{A.19})$$

Since it has been assumed that the structure is damaged in only one location, it follows readily that  $dK_{ij} = dK_i$ . Also, since  $K_i \gg K_{ij}$ , from Equation (A.12)

$$dF_{ij} \cong \frac{dK_{ij}}{K_i} = -\frac{u_{ij}}{K_i} dk_j = -F_{ij} \alpha_j \quad (\text{A.20})$$

where  $\alpha_j = dk_j/k_j$ , the fractional change in the stiffness of Element  $j$ . Substituting the result of Equation (A.20) into Equation (A.11), and substituting for  $F_{ij}^*$  using Equations (A.6) to (A.11), it can be shown that

$$\frac{k_j^*}{K_i^*} = k_j \frac{u_{ij}}{K_i} (1 - \alpha_j) \quad (\text{A.21})$$

Substituting for  $\alpha_j = (k_j^* - k_j)/k_j$  in Equation (A.21), and rearranging, one obtains:

$$\frac{k_j}{k_j^*} = \left( \frac{u_{ij}^*}{K_i^*} + \frac{u_{ij}}{K_i} \right) / 2 \frac{u_{ij}}{K_i} \quad (\text{A.22})$$

Setting  $f_{ij}^* = u_{ij}^*/K_i^*$  and  $f_{ij} = u_{ij}/K_i$ , Equation (A.22) reduces to

$$DI_{ij} = \frac{k_j}{k_j^*} = \frac{f_{ij}^*/f_{ij} + 1}{2} \quad (\text{A.23})$$

where  $DI_{ij}$  is the indicator of damage in the  $j^{\text{th}}$  member using the  $i^{\text{th}}$  mode. If  $DI_{ij} > 1$ , damage may exist. From Equation (A.23), the fundamental indicator of damage is the quotient  $f_{ij}^*/f_{ij}$ . Note that the one in the numerator is, essentially, a shifting factor while the two in the denominator is a scaling factor. Equation (A.23) becomes singular when  $f_{ij} \rightarrow 0$ : a condition which will occur when, simultaneously, the element size approaches zero and the element is located at a node of a mode. Here the division-by-zero difficulty can be overcome by

simply shifting the axis of reference for the sensitivities. For example, if the origin is shifted from  $f_{ij} = 0$  to  $f_{ij} = -1$ , then

$$f_{ij}' \rightarrow 1 + f_{ij} \quad (\text{A.24})$$

and

$$f_{ij}^* \rightarrow 1 + f_{ij}^* \quad (\text{A.25})$$

So the new indicator function,  $DI_{ij}$ , which will also form the basis of feature space (in the pattern recognition sense), becomes

$$DI_{ij} = \frac{f_{ij}^* + 1}{f_{ij}' + 1} \approx \left[ \frac{\Phi_i^{*T} C_{j_0} \Phi_i^* + \Phi_i^{*T} C \Phi_i^*}{\Phi_i^T C_{j_0} \Phi_i + \Phi_i^T C \Phi_i} \right] \frac{\Phi_i^T C \Phi_i}{\Phi_i^{*T} C \Phi_i^*} \quad (\text{A.26})$$

There are two important characteristics of the indicator  $DI_{ij}$  given by Equation (A.26): first, the expression attempts to express the changes in stiffness at a specific location in terms of measurable pre-damage and post-damage mode shapes ( $\Phi_i$  and  $\Phi_i^*$ ); and second, the term  $C_{j_0}$  on the right hand side of Equation (A.26) can be determined from a knowledge of the geometry of the structure. Thus for each damage location  $j$ , there are as many  $DI_{ij}$ 's available as there are mode shapes. As noted above, in the context of pattern recognition, the latter values of  $DI_{ij}$  define the feature space. The following expression will be the convenient form of damage index  $DI_j$  for a single location if several modes (NM) are used

$$DI_j = \frac{\sum_{i=1}^{NM} (\Phi_i^{*T} C_{j_0} \Phi_i^* + \Phi_i^{*T} C \Phi_i^*) \Phi_i^T C \Phi_i}{\sum_{i=1}^{NM} (\Phi_i^T C_{j_0} \Phi_i + \Phi_i^T C \Phi_i) \Phi_i^{*T} C \Phi_i^*} \quad (\text{A.27})$$

The final step in damage localization is classification. Classification analysis addresses itself to the problem of assigning an object to one of a number of possible

groups on the basis of observations made on the objects. In this study, the objects are the members of the structure. There are two groups: undamaged elements and damaged elements. Finally, the observations made on the objects are the  $DI_j$ 's. Many techniques are available to accomplish the end. Examples of these methods include classification on the basis of: (1) Bayes' rule (from which the well known Linear Discriminant Analysis and Quadratic Discriminant Analysis are derived), (2) nearest distance, and (3) hypothesis testing (Gibson and Melsa 1975). While other approaches are available (García 1996), the authors currently have utilized primarily techniques from hypothesis testing. The criteria for damage localization is established based on statistical reasoning. The values,  $DI_1, DI_2, DI_3, \dots, DI_{NE}$  for each element, are considered as realization of a random variable. The normalized damage indicator is given by

$$z_j = \frac{DI_j - \mu_{DI}}{\sigma_{DI}} \quad (A.28)$$

where  $\mu_{DI}$  and  $\sigma_{DI}$  represent mean and standard deviation of the damage index,  $DI_j$ , respectively. Let  $H_0$  be the hypothesis that the structure is not damaged at member  $j$ , and let  $H_1$  be the hypothesis that the structure is damaged at member  $j$ . The following decision rules may be used to assign damage to member  $j$ : (1) choose  $H_1$  if  $z_j \geq \lambda$  and (2) choose  $H_0$  if  $z_j < \lambda$  where  $\lambda$  is a threshold which assigns a level of significance.

### A.3 DAMAGE SEVERITY ESTIMATION

Note that in Equation (A.23) the indicator of damage is the ratio of the undamaged stiffness to the damaged stiffness. Such a number exists for each potentially damaged member. For example, in the case of a truss there is a  $DI_j$  associated with every member  $j$ . Here the damage is expressed as the fractional change in stiffness of an element:

$$\alpha_j = \frac{k_j^* - k_j}{k_j} = \frac{1}{DI_j} - 1 \quad (\text{A.29})$$

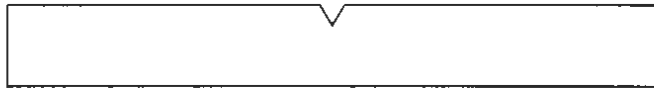
Thus if there is no damage,  $\alpha_j = 0$ ; if there is damage,  $\alpha_j < 0$ . Note that if  $\alpha_j = -1$ , all stiffness capacity is completely lost.

#### A.4 IDENTIFICATION OF STIFFNESS OF EXISTING STRUCTURE

Having stiffness parameters for the baseline structure, location of damage, and the severity of damage, the stiffness properties of the existing structure can be obtained from the equation:

$$k_j^{(\text{existing})} = k_j^{(\text{baseline})} [1 + \alpha_j] \quad (\text{A.30})$$

Note that if there is no damage at location  $j$ , the stiffness properties of the baseline and the existing structures are the same.



(a) Flawed Structure:  $\Phi_i^*, \omega_i^*$



(b) Estimate of Flawless Structure:  $\Phi_i, \omega_i$

**Figure A.1 Flawed Structure and Estimate of Flawless Structure**

## APPENDIX B

### DESCRIPTION OF FIELD TESTS AND MODAL PROPERTY EXTRACTION

#### B.1 INTRODUCTION

Results of the field modal tests performed on the multi-frame Watson Wash Bridge and the Fenner Overcrossing are documented in this appendix. The goal of these tests was to determine the pre and post rehabilitation modal properties of the structures in order to establish the impact of the rehabilitation process on both structures. Selected modal data were used in subsequent systems identification and damage detection analyses to establish additional changes in structural characteristics.

Experimental field data were collected from the Watson Wash Bridge located on Interstate 40, 38 miles west of Needles, San Bernardino County, California during the period of 18 May 1999 to 19 May 1999 and fifteen months later during the period 15 August 2000 to 16 August 2000. The right I40 eastbound structure was the subject of both tests. Similar data were collected from the Fenner Overcrossing located on Interstate 40, 36 miles west of Needles, San Bernardino County, California on 17 May 1999, 24 September 1999, and 14.5 months later on 13 December 2000. Again the right I40 eastbound structure was tested. The multi-span Watson Wash Bridge was treated as five separate interconnected frames numbered sequentially from the west abutment. Watson Wash Frames S-1 and S-5, and S-2 and S-4 were similar in regard to the length and number of spans and the location of hinges. Frame S-3 was unique. The Fenner Overcrossing was treated as a single three span structure.

Field data collection and measurement techniques used in these field tests were designed to provide high resolution spatial modal data while minimizing the impact of the measurement process on usability of the structures. The investigated structures were in-service bridges that remained open to traffic during tests. Obstruction of traffic was limited to shoulder closures and limited lane closures, Figure B.1 shows a typical closure in place during testing of Watson Wash. The global damage detection algorithm applied to these structures required that two or more low-frequency global modes be measured

with sufficient resolution to accurately extract irregularities in mode shape curvatures. A typical field data set consisted of up to ninety measured structural response accelerations measured at thirty nodal points distributed throughout the each frame or structure. Data were collected with several instrumentation setups utilizing five triaxial accelerometers per setup. A common impact point was used to excite each frame or structure for all setups. A large aggregate data set derived from the individual instrument setups was used to perform a structural modal analysis for each of the five multi-span Watson Wash frames and the three-span Fenner Overcrossing.

The discussion of these tests is divided into five sections. The first section describes and summarizes the settings of the field instrumentation. Section Two outlines the modal analysis and extraction process. Section Three discusses the modal properties of the multi-frame Watson Wash Structure. The fourth section presents the modal properties of the Fenner Overcrossing. The last section is devoted to summary and conclusions pertaining to the field modal tests.

## **B.2 FIELD INSTRUMENTATION**

The lightweight mobile field equipment shown in Figure B.2 allowed quick movement through sequential instrument setups. The goal during field tests was to acquire all modal response data for a single structure in a four hour time period. It typically took fifteen minutes to move accelerometers and reset instrumentation for each setup and ten minutes to acquire data. Field response data was acquired using five triaxial accelerometers, which measured structural response along orthogonal global axes. Figure B.3 shown a typical accelerometer installation on the bottom of a Watson Wash longitudinal girder. The drop-weight impact hammer shown in Figure B.4 was used to impact each structure. Time data acquired in these tests were processed on a 16-channel digital signal analyzer shown in Figure B.2.

The drop weight impact hammer was instrumented with a 20,000 lb., PCB 200C20 piezoelectric load cell. Lead ballast was used to increase impact head

weight to 120 lb. Table B.1 summarizes the specifications of this instrument. Kistler 8390A2 triaxial accelerometers were used for all acceleration measurements. Specifications for the accelerometer are summarized in Table B.2. Data from the accelerometers and impact hammer were acquired and processed on a 16-channel SigLab 20-42 DSP analyzer manufactured by DSP Technologies. Time data were transferred to a laptop computer for further analysis. Table B.3 presents selected specification data for the SigLab 20-42. A typical vertical accelerometer time response is shown in Figure B.5. Typical acceleration ranges were on the order of  $\pm 0.025$  g. Instrument sensitivities were adequate to record these low g (acceleration) levels. Figure B.6 is a time trace of a typical hammer impact. The magnitude of the frequency spectrum for the hammer is shown in Figure B.7. The hammer was designed to provide sufficient energy content in the DC to 100 Hz frequency range to increase the response above background noise levels.

### **B.3 MODAL TEST INSTRUMENTATION LAYOUT**

Frequency response functions (FRFs), auto-spectrums, cross-spectrums, coherence functions, and time data were collected using acquisition/analysis software provided by the DSP vendor. FRFs were transferred to MESScope Version 2.0 and natural frequencies, modal damping, and mode shapes were extracted. Fifteen analyzer instrument channels were assigned to the five triaxial accelerometers. Their corresponding directional inputs and the relationships were maintained during all modal testing. The system was calibrated using a linear calibration factor for each accelerometer axis. Common modal test instrument settings are summarized in Table B.4. Spectral resolution of the resulting FRFs was 0.0625 Hz. All response data were saved as time traces and FRFs extracted off-line.

### **B.4 MODAL TESTING OF WATSON WASH FRAMES**

Experimental field data were collected from the Watson Wash Bridge during the period of 18 May 1999 to 21 May 1999 and fifteen months later during the period 15 August 2000 to 16 August 2000. The right I40 eastbound structure was the subject of

both tests. The multi-span Watson Wash Bridge was treated as five separate interconnected frames numbered sequentially from the west abutment. Instrumentation and cabling were confined to areas under the structure and accelerometers were mounted on the bottom of longitudinal girders. Response nodes were located at mid-span, pier, and hinge points along both outside longitudinal girders. During the May 1999 test period mid-span and hinge points of two interior longitudinal girders were also recorded. The impact hammer was the only instrument located on the bridge deck and was positioned over an outside girder on shoulder beyond the outside pavement stripe. Traffic was not stopped and flow impeded only by a shoulder closure protecting the impact hammer and operator. Review of the results of the two modal tests indicated that the average frequencies of the first and second extracted modes dropped 0.33 Hz and 0.43 Hz respectively. Average damping levels increased from 3.3% to over 4.0%. Both changes are attributed primarily to installation of the asphaltic concrete overlay which varied from 1 to 4 inches.

#### **B.4.1 May 1999 Watson Wash Frame Tests**

Extracted modal frequencies and damping for May 1999 tests are presented in Tables B.5 through B.9. The identified modes are associated with the first vertical bending and first torsional modes of each frame. Figures B.7, B.11, B.15, B.19, and B.23 identify the response nodes measured in May 1999 testing. Overlays of the vertical acceleration FRF magnitudes for each frame are presented in Figures B.8, B.12, B.16, B.20, and B.24. All of the FRFs display numerous closely spaced modes in the 5 to 10 Hz range. Generally the extracted modes in Tables B.5 through B.9 were the first two major lower modes in the range. Average frequency of the first mode for all frames was 5.87 Hz. The second mode average frequency was 6.98 Hz. Average indicated percent critical damping levels for these two modes were 3.4 % and 3.2 %. Mode shapes for the first extracted lower mode are presented in Figures B.9, B.13, B.17, B.21, and B.25. Mode shapes for the second modes are presented in Figures B.10, B.14, B.18, B.22, and B.26. A review of these shapes indicates that the first modes are complex global bending modes and the second modes are torsional modes.

#### **B.4.2 August 2000 Watson Wash Frame Tests**

Extracted modal frequencies and damping for August 2000 tests are presented in Tables B.10 through B.15. These modes correspond to the same modes identified in May 1999 testing and are again associated with the first vertical bending and first torsional modes of each frame. Figures B.27, B.31, B.35, B.39, and B.43 identify the response nodes measured in August 2000 testing. Only the response of outside girder nodes was measured. Overlays of the vertical acceleration FRF magnitudes for each frame are presented in Figures B.28, B.32, B.36, B.40, and B.44. All of the FRFs again displayed numerous closely spaced modes in the 5 to 10 Hz range. Average frequency of the first and second mode for all frames was 5.54 Hz and 6.55 Hz, respectively. Damping values were not computed for these modes. A review other FRF computations indicated that damping levels increased to slightly over 4.0%. Mode shapes for the first extracted lower mode are presented in Figures B.29, B.33, B.37, B.41, and B.45. Mode shapes for the second modes are presented in Figures B.30, B.34, B.38, B.42, and B.46. A review of these shapes indicates that the first modes are complex global bending modes and the second modes are global torsional modes.

#### **B.5 MODAL TESTING OF FENNER OVERCROSSING**

Field data were collected from the Fenner Overcrossing located on Interstate 40, 36 miles west of Needles, San Bernardino County, California on 17 May 1999, 24 September 1999, and 14.5 months later on 14 December 2000. Note that due to sensor malfunctions in the 17 May 1999 test, the 24 September 1999 test was a repeat of the May test. The right I40 eastbound structure was tested. The Fenner Overcrossing was treated as a single three span structure. Instrumentation and cabling were confined to the overcrossing shoulder beyond the outside pavement stripe during testing except for measurements on interior girders. All testing was done on the deck. Traffic was not stopped and overcrossing flow impeded only to the extent needed to protect the instrumentation placed on shoulder stripping with traffic cones. A Lane 2 closure was used during testing of the outside girder along the median and a Lane 1 closure was used during measurements of nodes on interior girders. Measurement locations on the

structure were over the outside longitudinal girders at abutments, piers, and mid-span for all spans and also at quarter points for the main center span. Interior girders were also measured at similar points. No measurements were taken on pier columns.

The same three lower global modes were identified in each test. These modes correspond to the first vertical bending, first torsional, and first plate mode of the structure. The first bending and torsional modes were very closely spaced which lead to some difficulty in identifying and extracting these modes. Table B.15 and B.16 present extracted modal frequencies and damping for the September 1999 and December 2000 testing respectively. No change was noted in the frequencies of the first two modes. The third mode frequency increased 0.09 Hz. Average damping levels increased from 3.1% to 3.8% and is attributed to the asphalt concrete overlay applied to the bridge between tests. Figures B.47 and B.52 identify the response nodes measured in September 1999 and December 2000 testing, respectively. Two interior girder lines were measured in the 1999 testing to evaluate affect of a deck closure pour between the girders. Only select interior girder points were measured in the 2000 testing as aids in identifying the first three modes. Overlays of the vertical acceleration FRF magnitudes for test are presented in Figures B.48 and B.53. In both FRFs the first two modes overlap and are not easily separable. The first plate modes is more easily identified. Mode shapes for the three extracted lower modes are presented in Figures B.49 through B.51 for the September 1999 tests and in Figures B.53 through B.56 for the December 2000 test. A review of these shapes indicates that the modes are global bending, torsional, and plate modes for the whole structure and have not changed in shape.

## **B.6 SUMMARY**

Result of two modal tests on the eastbound Watson Wash Bridge and and two modal tests on the eastbound Fenner Overcrossing were presented. These tests were conducted to recorded changes in modal properties of the structures resulting from rehabilitation processes applied to the structures between the tests. A review of the resulting extracted modes indicates that the average frequency of the first bending and

first torsional modes of the five frames comprising the Watson Wash Bridge dropped 0.33 Hz and 0.43 Hz respectively. Average damping increased 0.7%. Both of these changes are attributed primarily to a 1-inch to 4-inch asphaltic concrete overlay applied between the tests. Three lower global modes were identified in both tests of the Fenner Overcrossing. The frequencies of these modes exhibited very little change other than an increase in average damping levels of 0.7% between tests. This observation is attributed to a 1-inch to 4-inch asphaltic overlay applied to the structure between the tests.

**Table B.1 PCB 200C20 Piezoelectric Load Cell Specifications**

Characteristics	Specifications	Units
Sensitivity	.256	mV/lbf
Rise time	< 15	micro-seconds
Amplitude range	0 - 20000	lbf
Discharge time constant	>2000	Sec
Linearity	<1	%full-scale

**Table B.2 Kistler 8390A2 Accelerometer Specifications**

Characteristics	Specifications	Units
Sensitivity	500	mV/g
Frequency range (+/- 5%)	DC – 150	Hz
Amplitude range	+/-2	g peak
Resolution (broadband)	1.5	Mg
Linearity	+/-1	%FS
Transverse sensitivity	< 5	%
Weight	210(7.4)	gram (oz)

**Table B.3 SigLab 20-42 Analyzer Specifications**

Characteristics	Specifications	Units
Channels	16	
Frequency range	20	kHz/channel
Channel match:		
Amplitude	+/- 1	dB
Phase	+/- 1	Degree
Dynamic range	> 84	dB
A/D resolution	20	bit sigma delta
Anti-alias filters	>90	dB rejection

**Table B.4 Modal Test Instrument Settings**

Characteristics	Specifications	Notes/Units
Accelerometer channels	2-16 each accelerometer connected in sequence	Siglab channels
Load cell channel	1	Siglab channel
Sample frequency	512	Hz
Sample length	8192	Samples per channel
Spectral Resolution	0.0625	Hz
Number of repetitions	5	Linear average
Channel gain	Varied	Adjusted for overloading
Trigger method	+ 25% Load cell full scale	Pretrigger save all channels
Accelerometer window	Boxcar	
Load cell window	Boxcar	

**Table B.5 Extracted Frequency and Damping Values  
Watson Wash Frame S-1, May 1999 Field Test**

Mode	Frequency Hz	Damping %
1	5.88	3.9
2	6.87	3.8

**Table B.6 Extracted Frequency and Damping Values  
Watson Wash Frame S-2, May 1999 Field Test**

Mode	Frequency Hz	Damping %
1	5.98	3.6
2	7.15	2.8

**Table B.7 Extracted Frequency and Damping Values  
Watson Wash Frame S-3, May 1999 Field Test**

Mode	Frequency Hz	Damping %
1	5.59	3.1
2	6.97	3.5

**Table B.8 Extracted Frequency and Damping Values  
Watson Wash Frame 4, May 1999 Field Test**

Mode	Frequency Hz	Damping %
1	5.98	3.9
2	6.93	3.3

**Table B.9 Extracted Frequency and Damping Values  
Watson Wash Frame S-5, May 1999 Field Test**

Mode	Frequency Hz	Damping %
1	5.94	2.5
2	7.02	2.8

**Table B.10 Extracted Frequency and Damping Values  
Watson Wash Frame S-1, August 2000 Field Test**

Mode	Frequency Hz	Damping %
1	5.50	N/A
2	6.25	N/A

**Table B.11 Extracted Frequency and Damping Values  
Watson Wash Frame S-2, August 2000 Field Test**

Mode	Frequency Hz	Damping %
1	5.50	N/A
2	6.75	N/A

**Table B.12 Extracted Frequency and Damping Values  
Watson Wash Frame S-3, August 2000 Field Test**

Mode	Frequency Hz	Damping %
1	5.44	N/A
2	6.31	N/A

**Table B.13 Extracted Frequency and Damping Values  
Watson Wash Frame S-4, August 2000 Field Test**

Mode	Frequency Hz	Damping %
1	5.63	N/A
2	7.00	N/A

**Table B.14 Extracted Frequency and Damping Values  
Watson Wash Frame S-5, August 2000 Field Test**

Mode	Frequency Hz	Damping %
1	5.63	N/A
2	6.44	N/A

**Table B.15 Extracted Frequency and Damping Values  
Fenner Overcrossing, September 1999 Field Test**

Mode	Frequency Hz	Damping %
1	4.35	3.9
2	4.47	2.7

**Table B.16 Extracted Frequency and Damping Values  
Fenner Overcrossing, December 2000 Field Test**

Mode	Frequency Hz	Damping %
1	4.33	4.3
2	4.47	3.6
3	5.54	3.6



**Figure B.1 Shoulder Closure during Testing of Watson Wash Bridge**

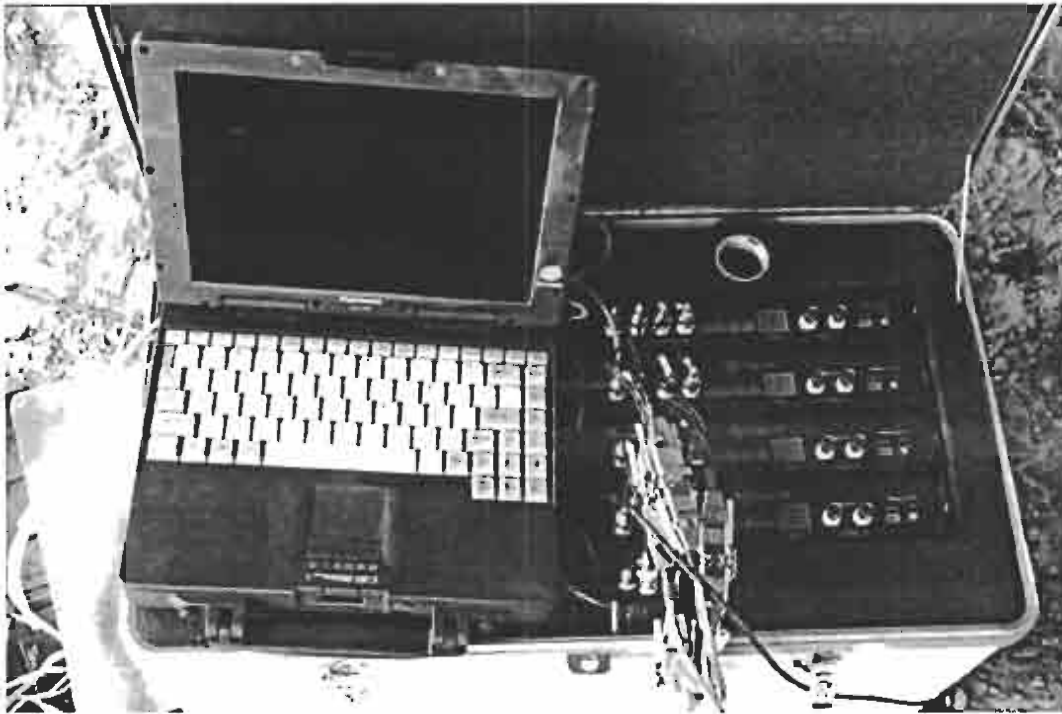


**Figure B.2 16-Channel Instrument Setup**



**Figure B.3 Typical Triaxial Accelerometer Mounting**

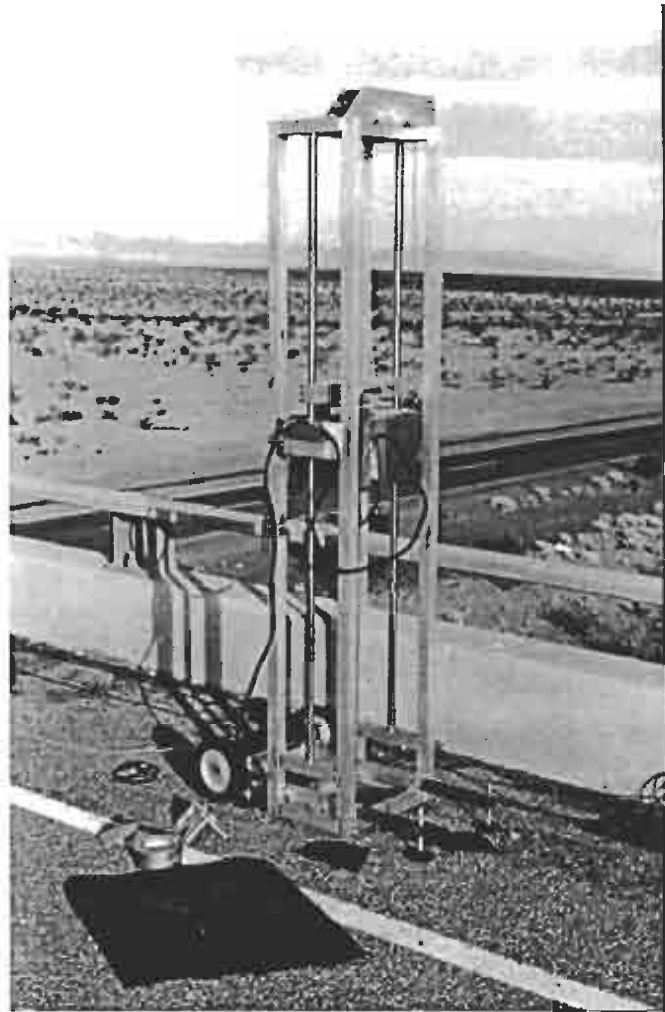


**Figure B.4 Drop-Weight Impact Hammer**

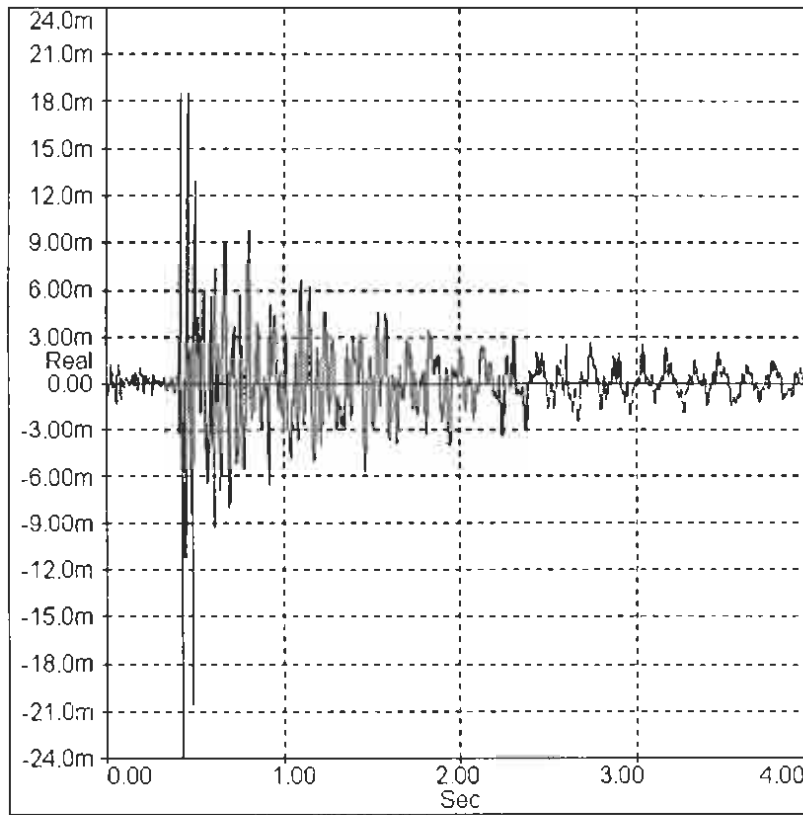


**Figure B.5 Typical Vertical Response (g)**

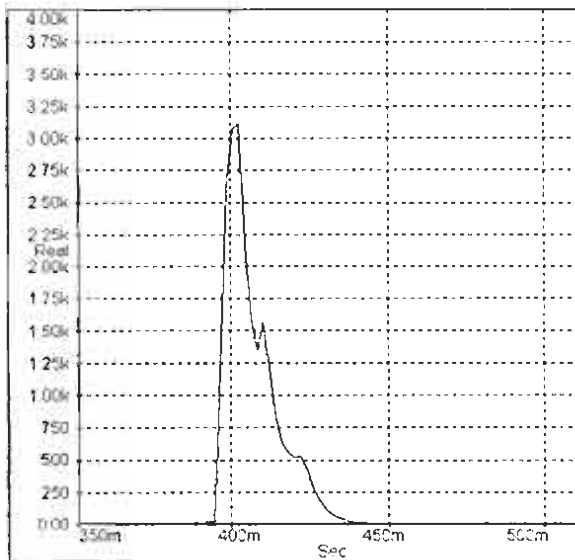


**Figure B.6 Typical Time Response of Impact Hammer**

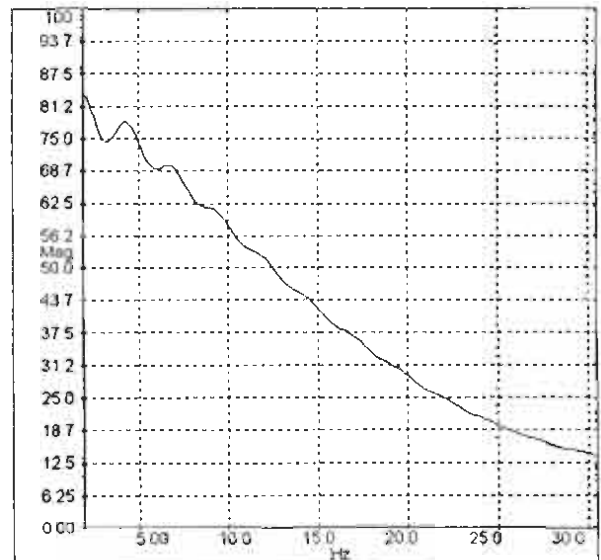


**Figure B.7 Corresponding Frequency Spectrum of Impact**

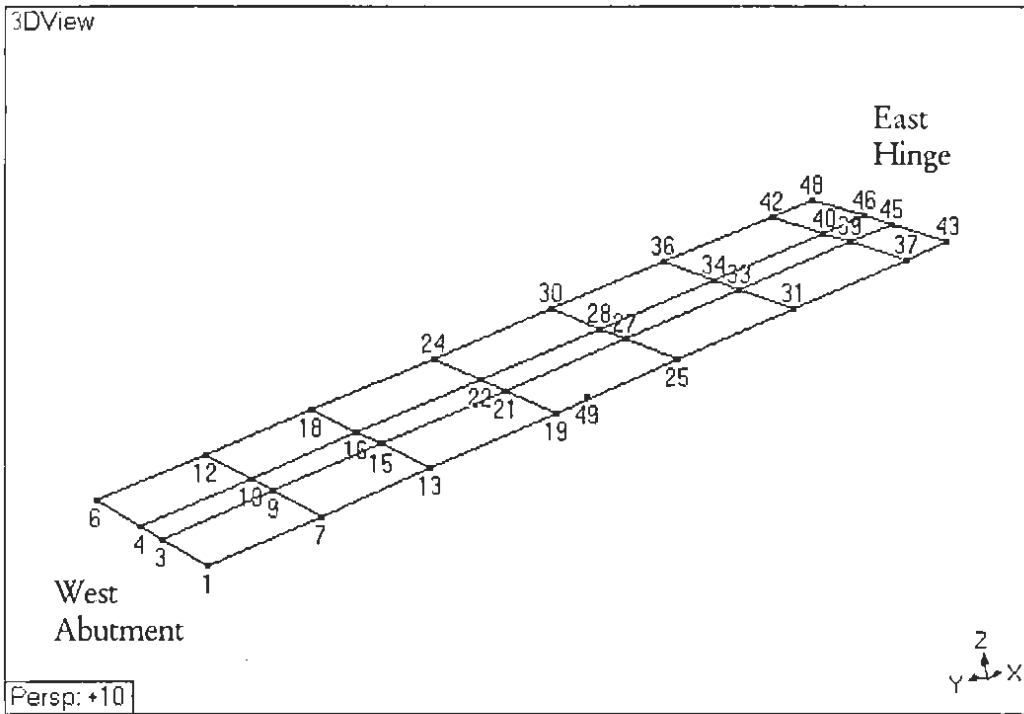


**Figure B.7 Wireframe Model of Response Nodes for Watson Wash Frame S-1, May 1999 Field Test**

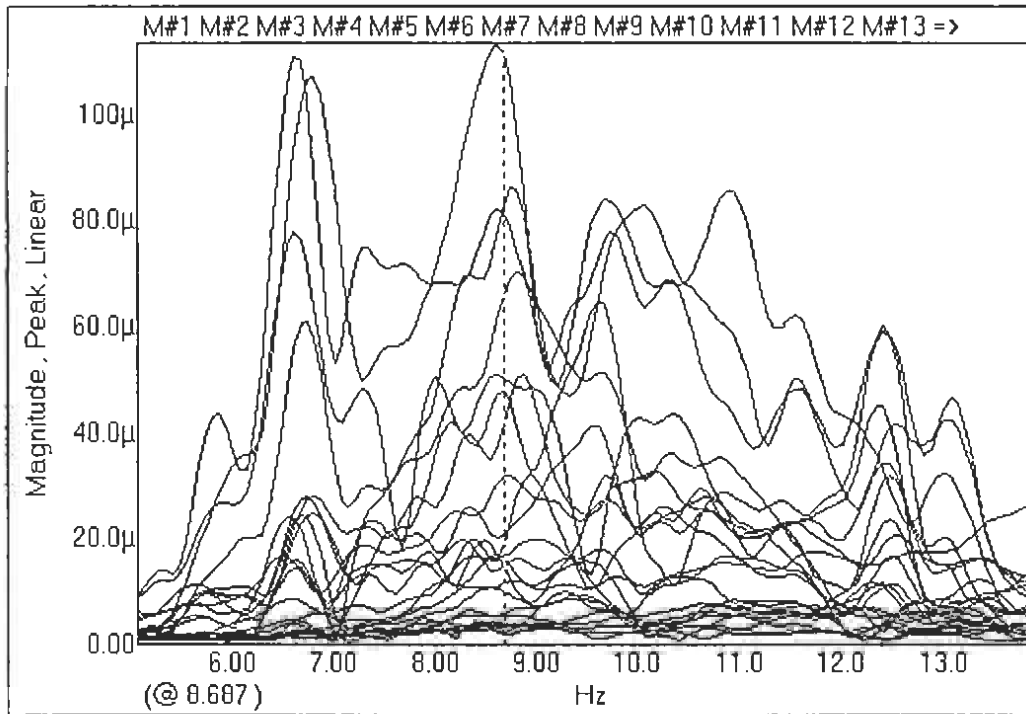


**Figure B.8 Overlay of Vertical FRF Magnitudes for Watson Wash Frame S-1, May 1999 Field Test**

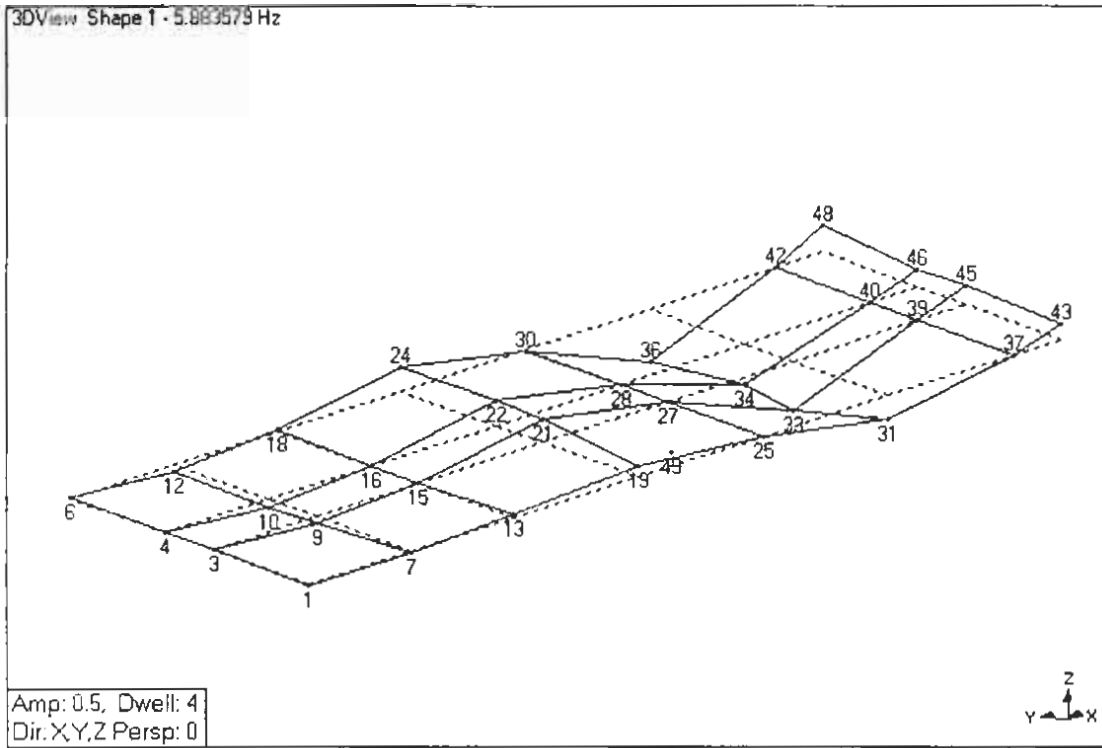


Figure B.9 1<sup>st</sup> Mode Watson Wash Frame S-1, May 1999 Field Test

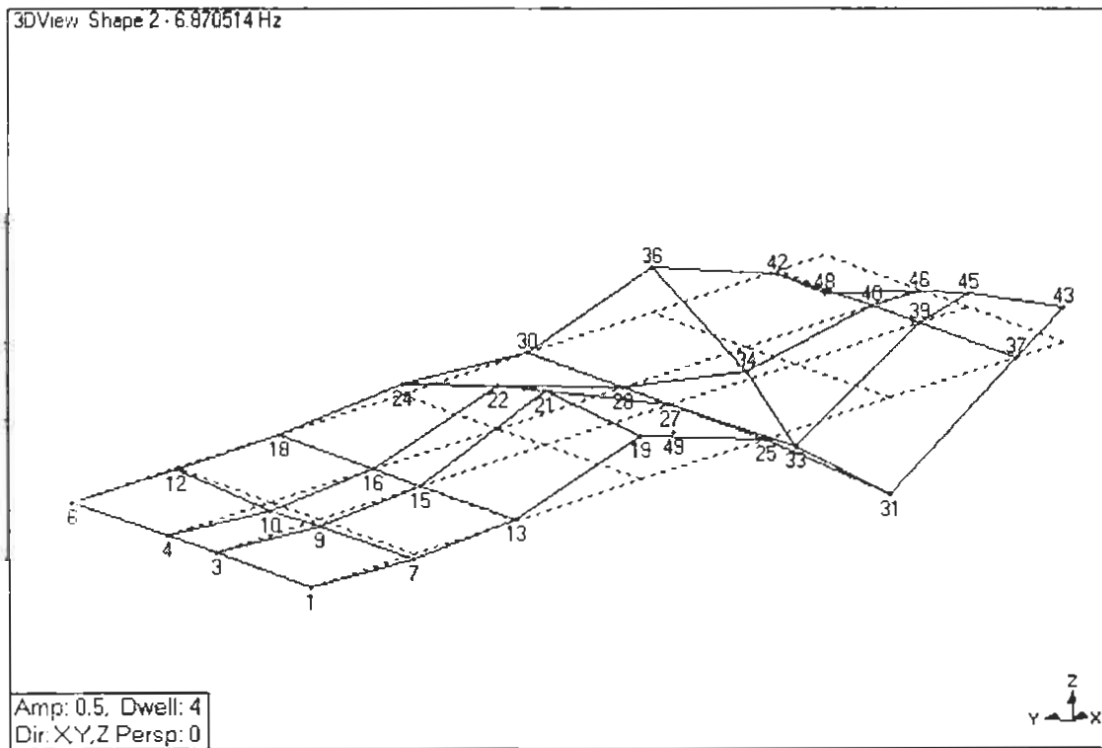
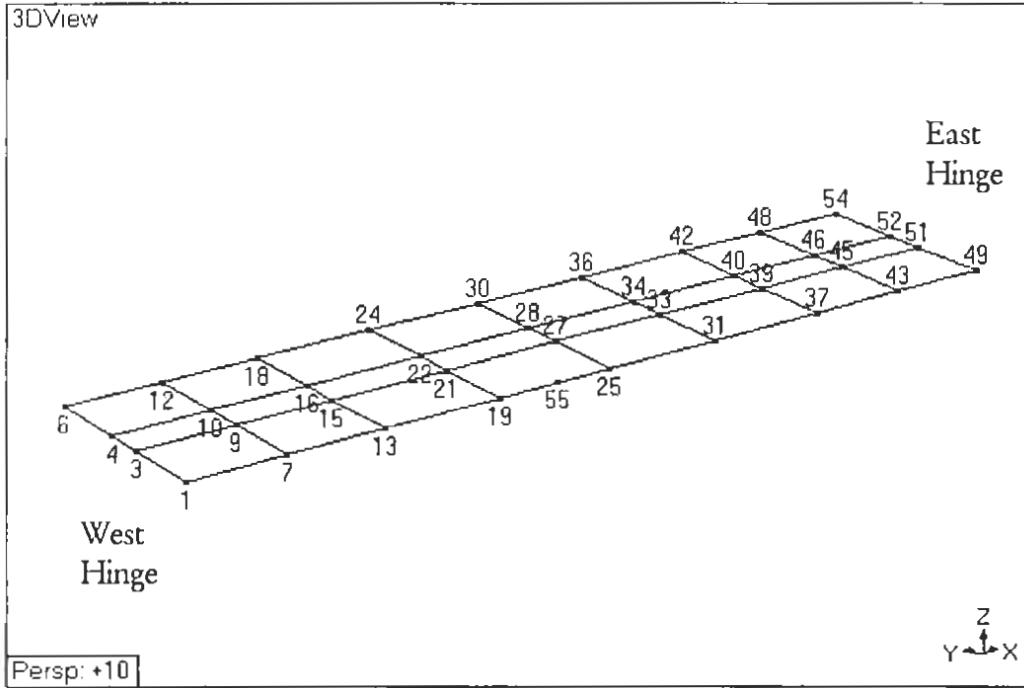
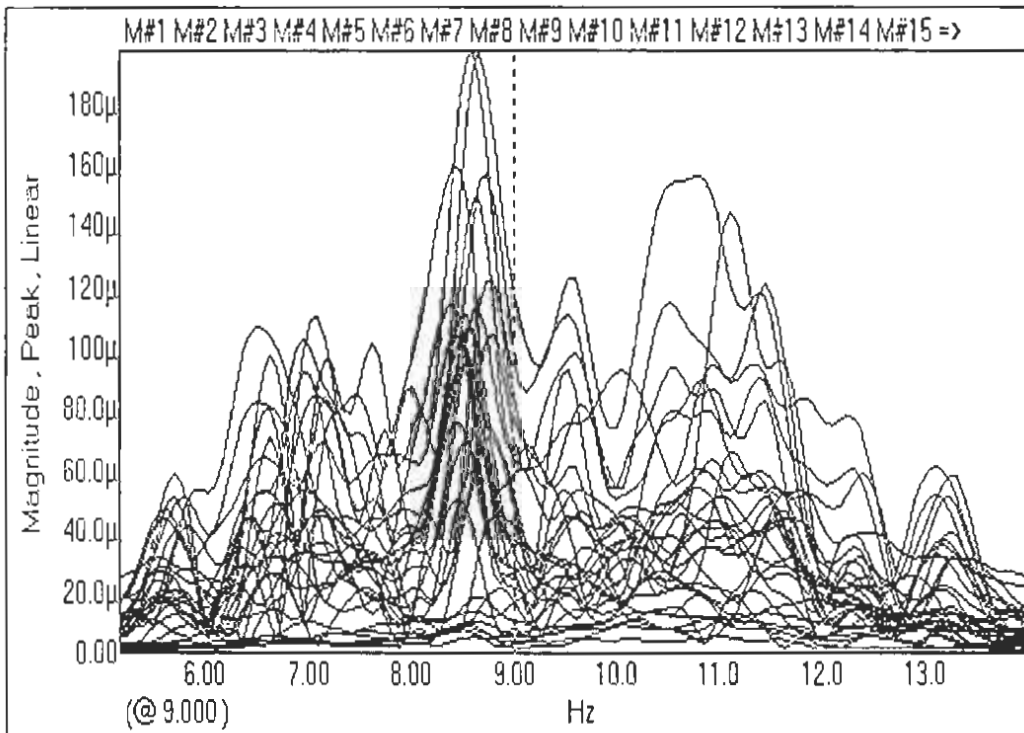


Figure B.10 2<sup>nd</sup> Mode Watson Wash Frame S-1, May 1999 Field Test



**Figure B.11 Wireframe Model of Response Nodes for  
Watson Wash Frame S-2, May 1999 Field Test**



**Figure B.12 Overlay of Vertical FRF Magnitudes for  
Watson Wash Frame S-2, May 1999 Field Test**

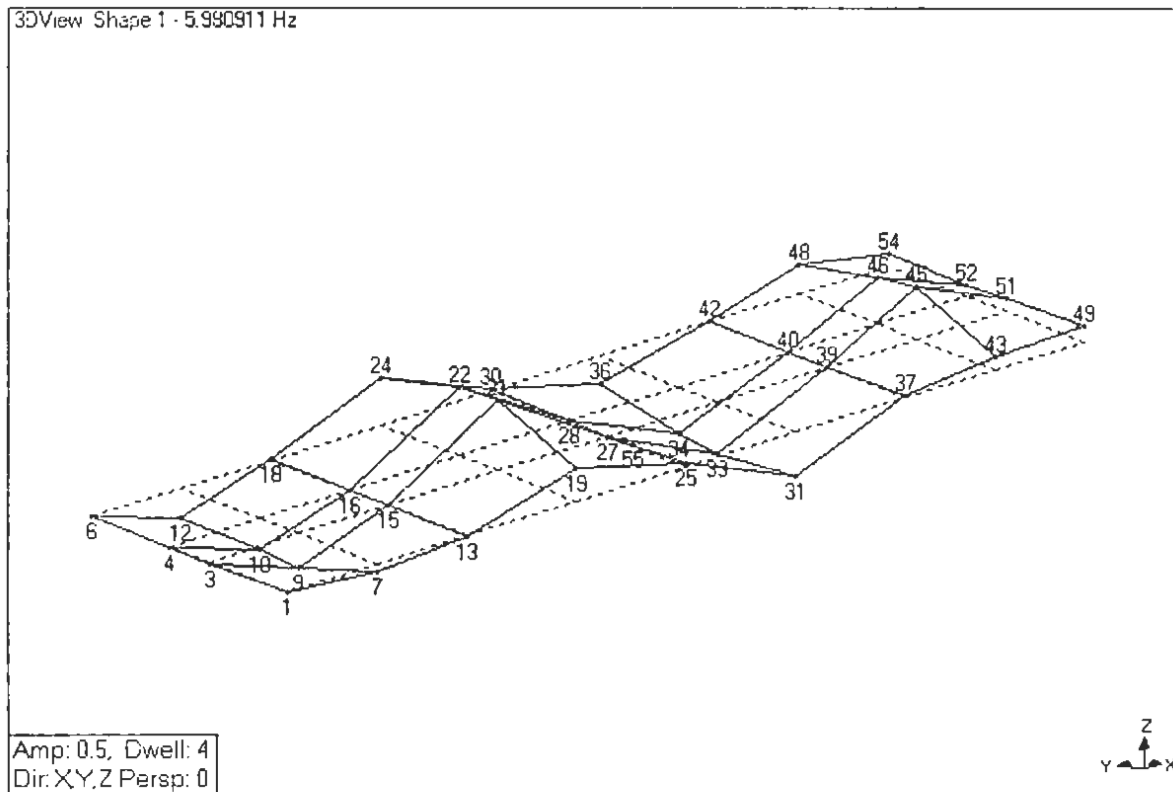


**Figure B.13 1<sup>st</sup> Mode Watson Wash Frame S-2, August 2000 Field Test**

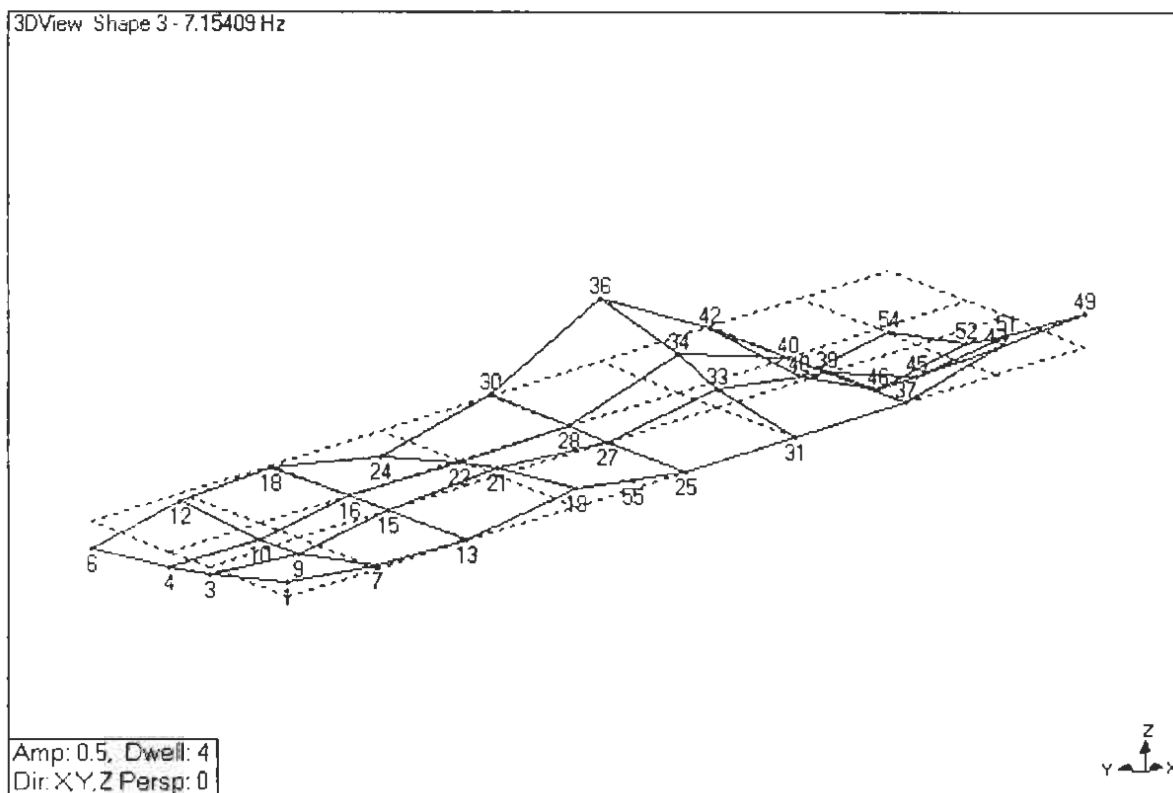


**Figure B.14 3<sup>rd</sup> Mode Watson Wash Frame S-2, May 1999 Field Test**

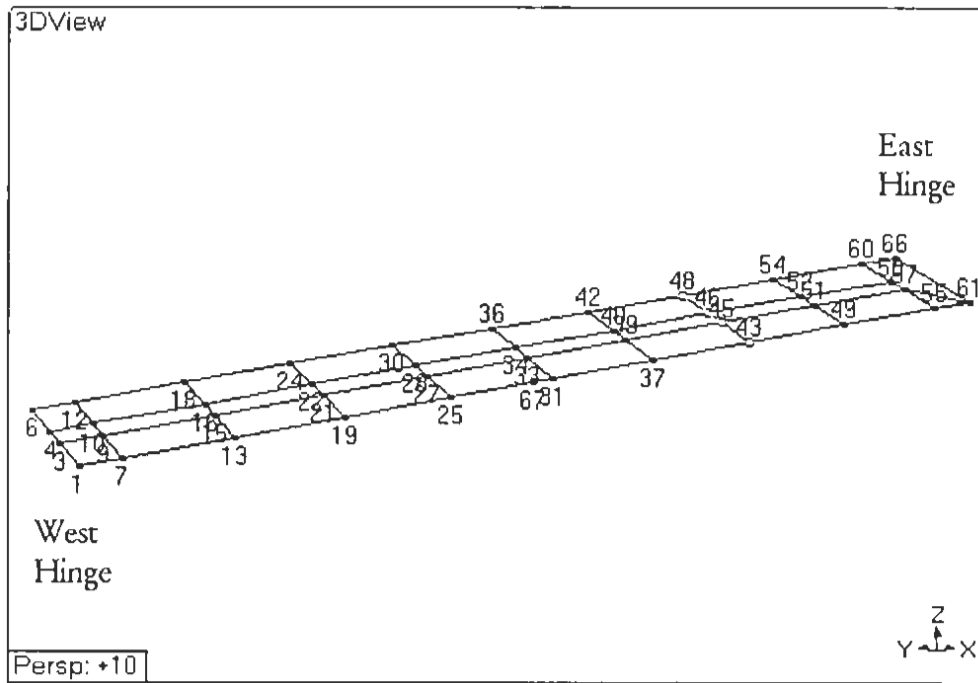


**Figure B.15 Wireframe Model of Response Nodes for  
Watson Wash Frame S-3, May 1999 Field Test**

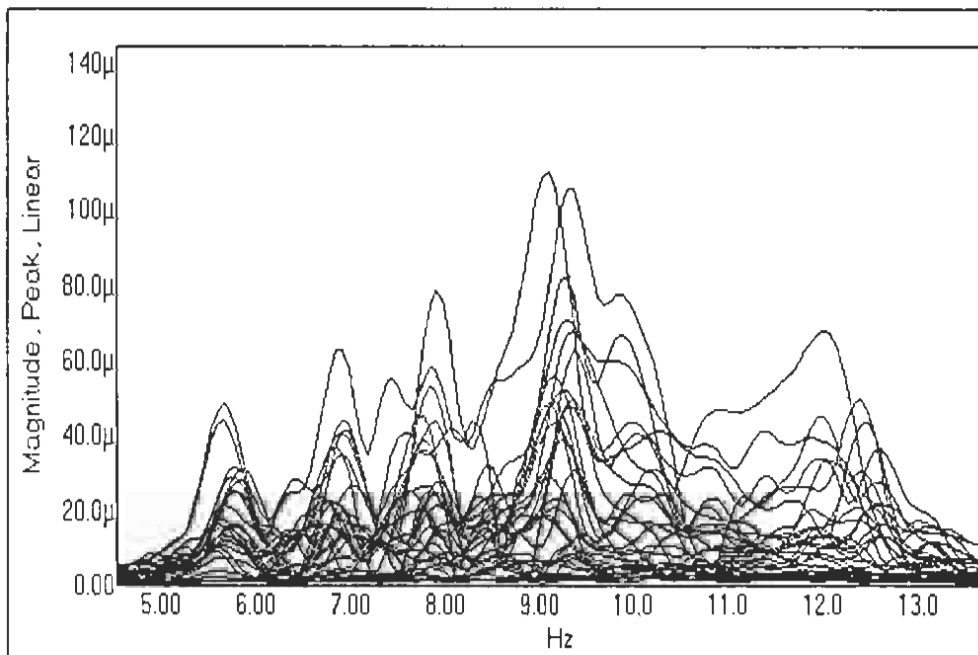


**Figure B.16 Overlay of Vertical FRF Magnitudes for  
Watson Wash Frame S-3, May 1999 Field Test**

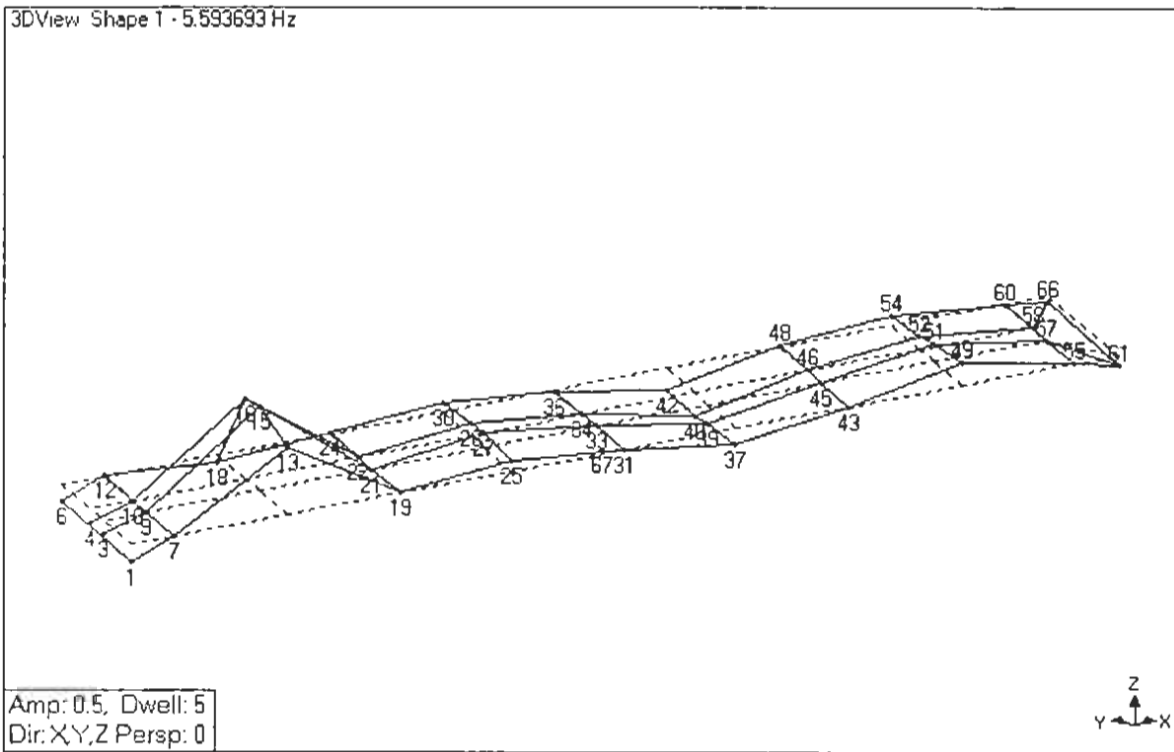


Figure B.17 1<sup>st</sup> Mode Watson Wash Frame S-3, May 1999 Field Test

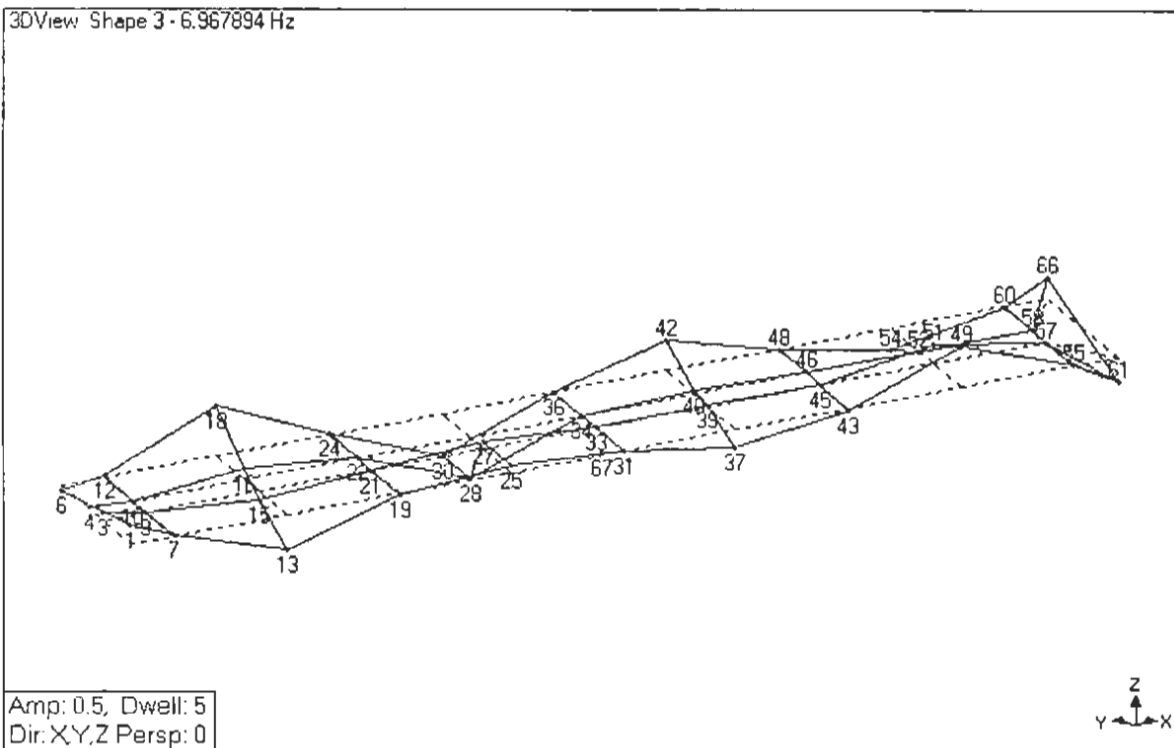
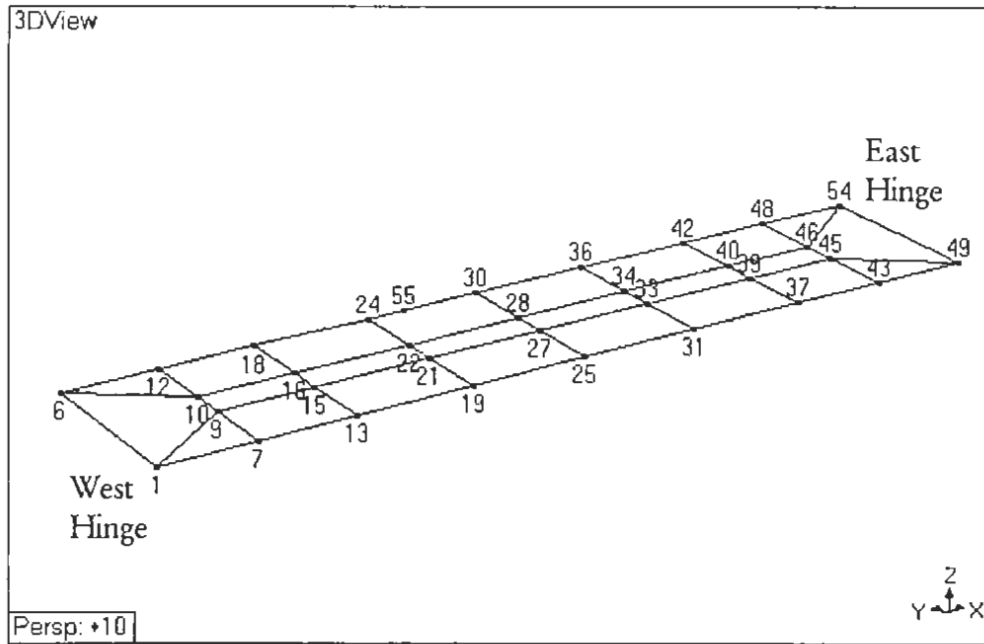
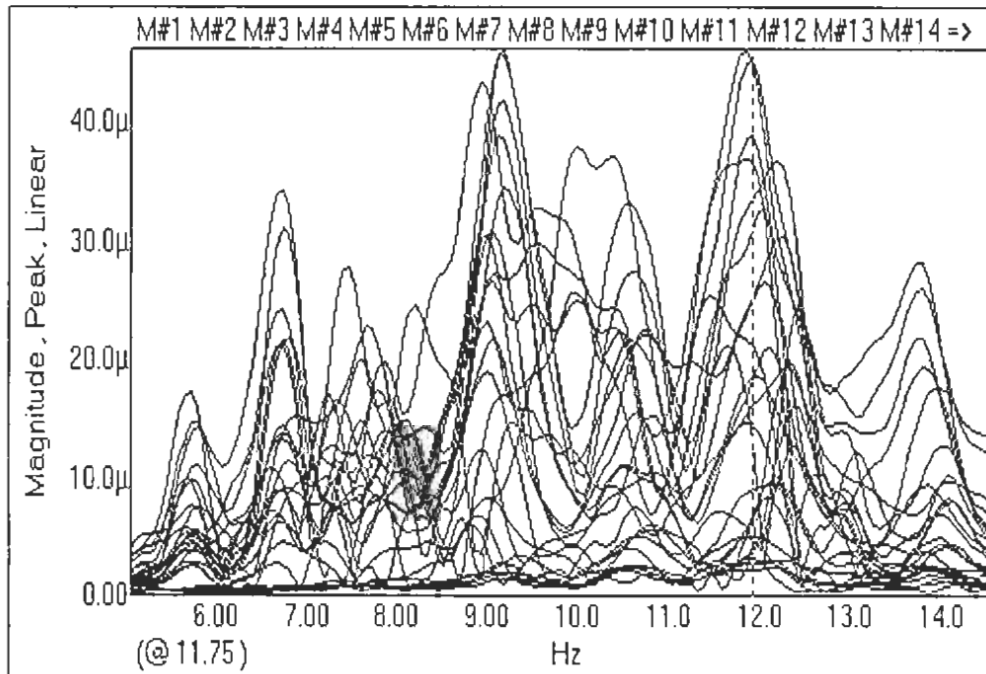


Figure B.18 2<sup>nd</sup> Mode Watson Wash Frame S-3, May 1999 Field Test



**Figure B.19 Wireframe Model of Response Nodes for Watson Wash Frame S-4, May 1999 Field Test**



**Figure B.20 Overlay of Vertical FRF Magnitudes for Watson Wash Frame S-4, May 1999 Field Test**

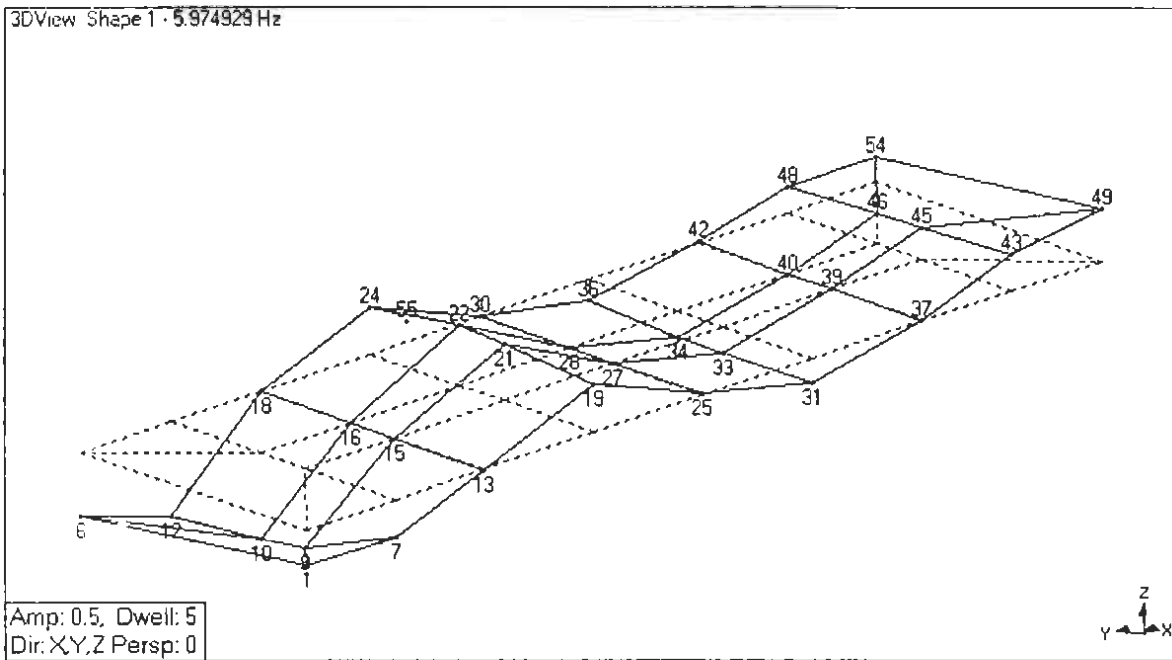


Figure B.21 1<sup>st</sup> Mode Watson Wash Frame S-4, May 1999 Field Test

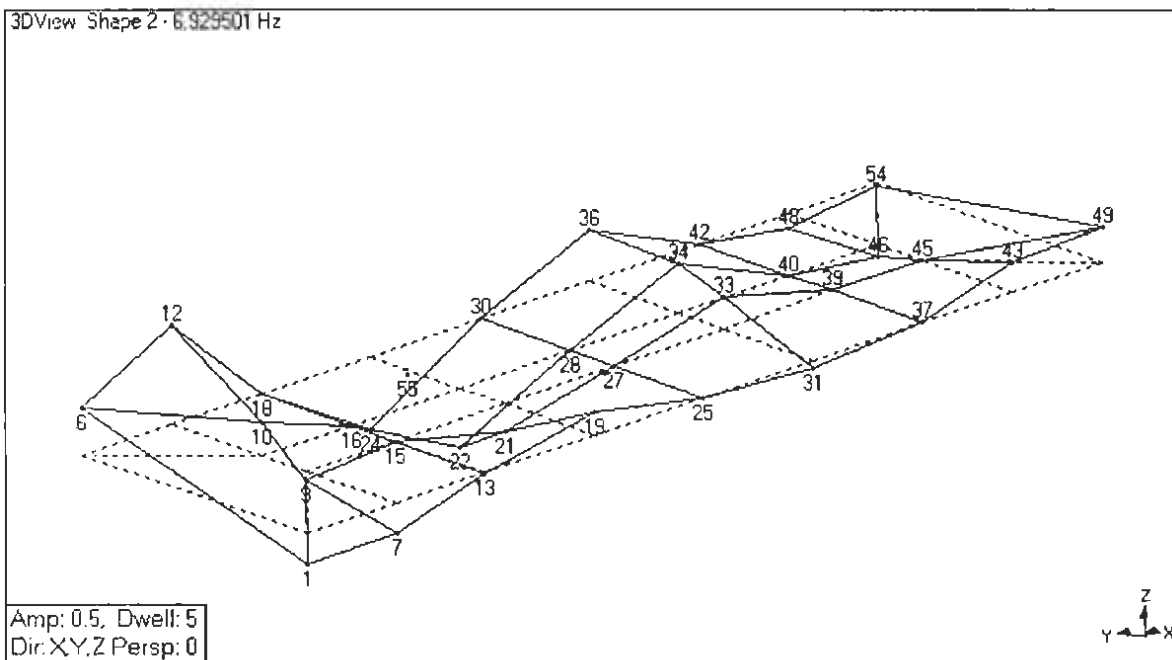
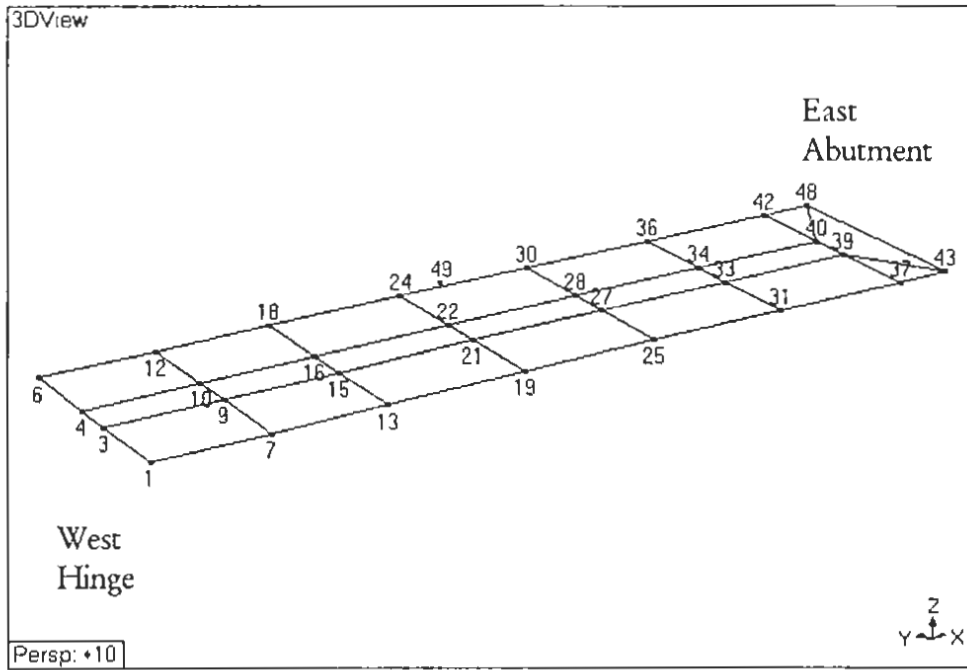
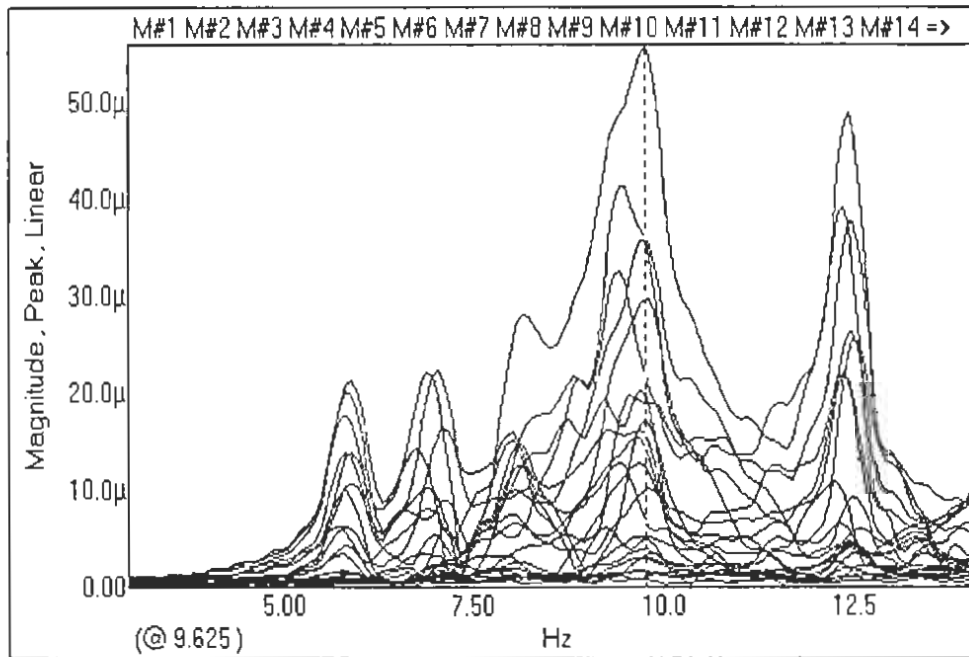


Figure B.22 2<sup>nd</sup> Mode Watson Wash Frame S-4, May 1999 Field Test



**Figure B.23 Wireframe Model of Response Nodes for Watson Wash Frame S-5, May 1999 Field Test**



**Figure B.24 Overlay of Vertical FRF Magnitudes for Watson Wash Frame S-5, May 1999 Field Test**

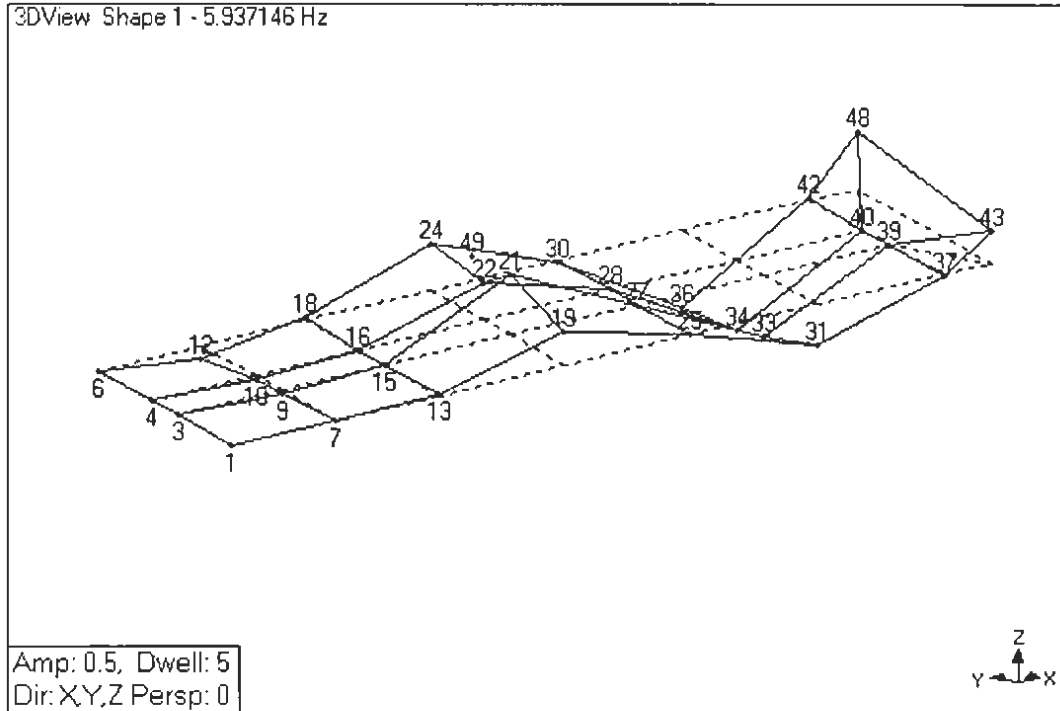


Figure B.25 1<sup>st</sup> Mode Watson Wash Frame S-5, May 1999 Field Test

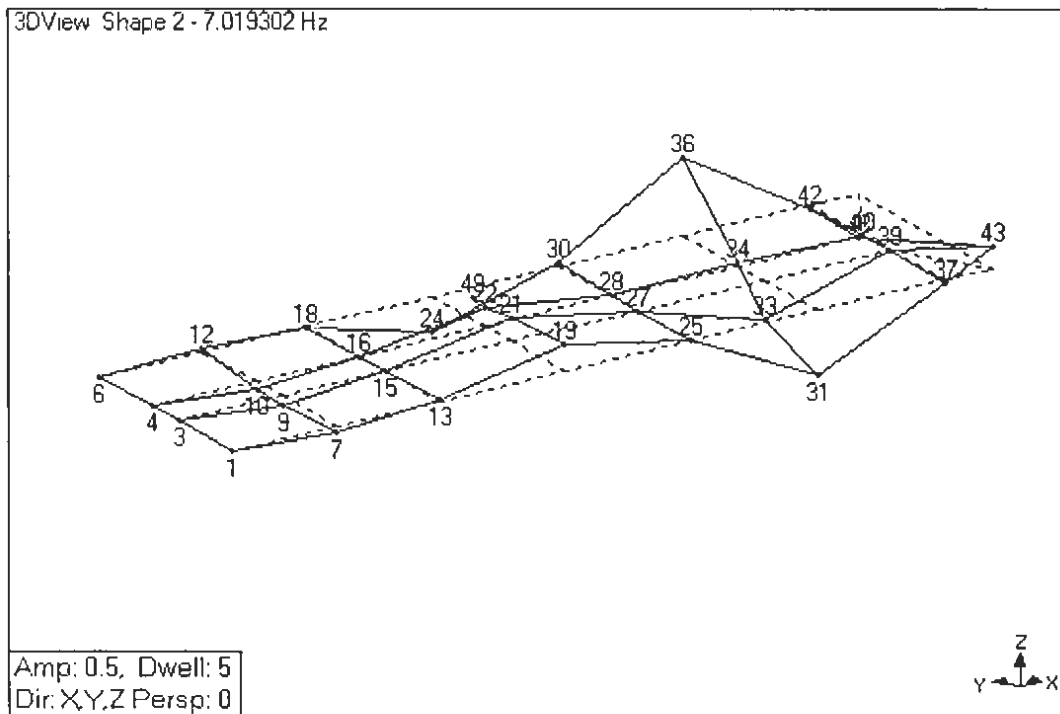
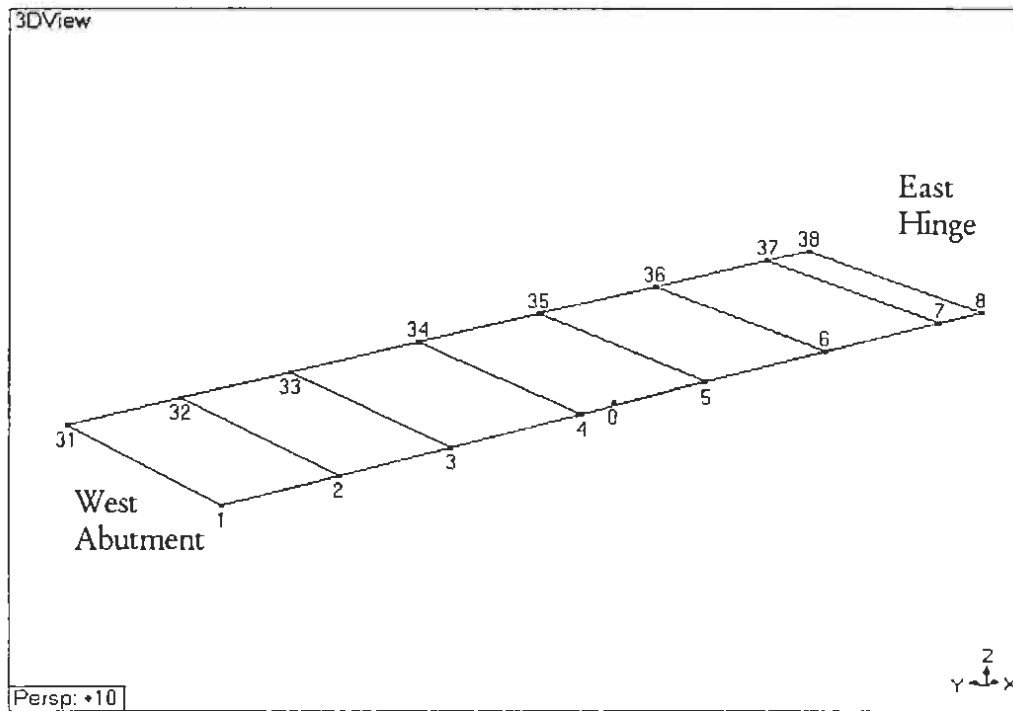
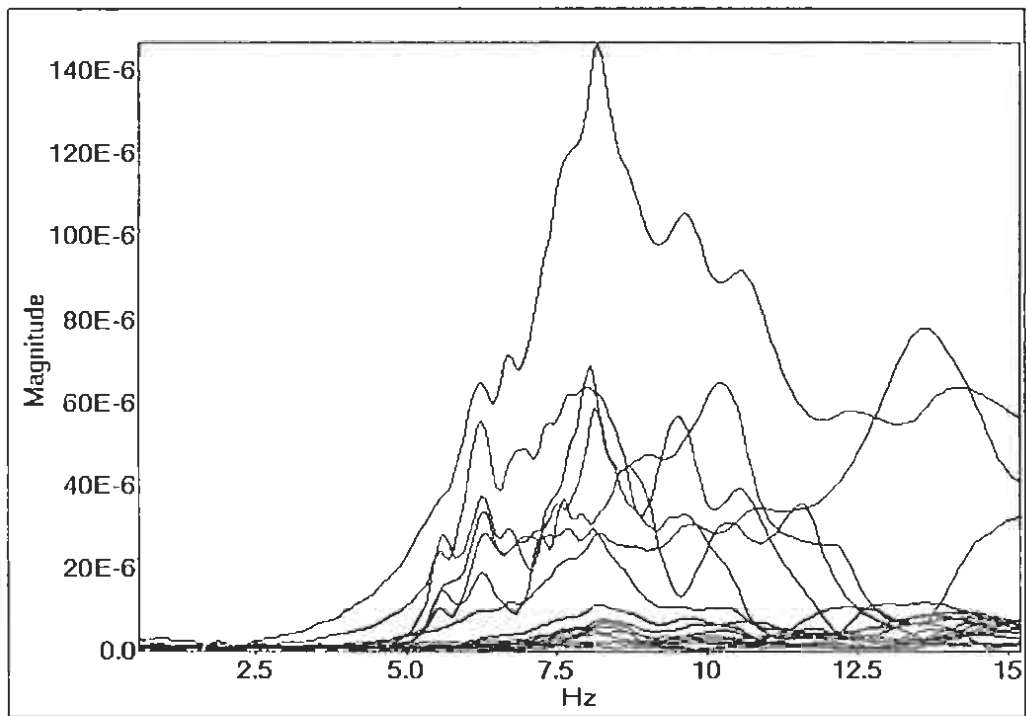


Figure B.26 2<sup>nd</sup> Mode Watson Wash Frame S-5, May 1999 Field Test



**Figure B.27 Wireframe model of Response Nodes for Watson Wash Frame S-1, August 2000 Field Test**



**Figure B.28 Overlay of Vertical FRF Magnitudes for Watson Wash Frame S-1, August 2000 Field Test**

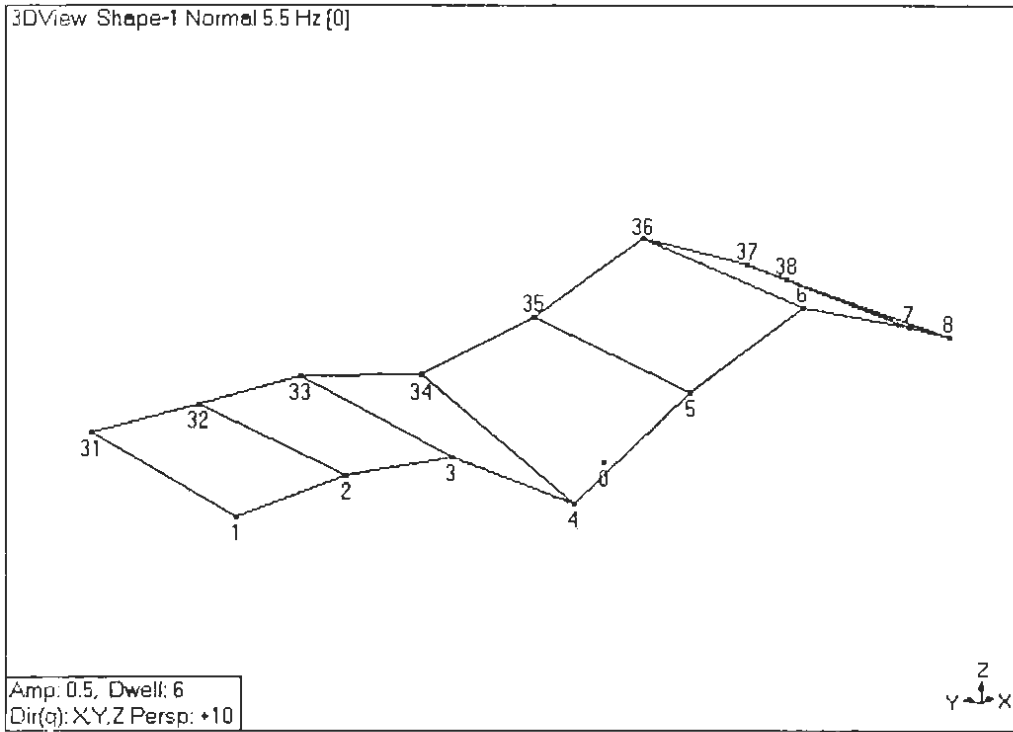


**Figure B.29 1<sup>st</sup> Mode Watson Wash Frame S-1, August 2000 Field Test**

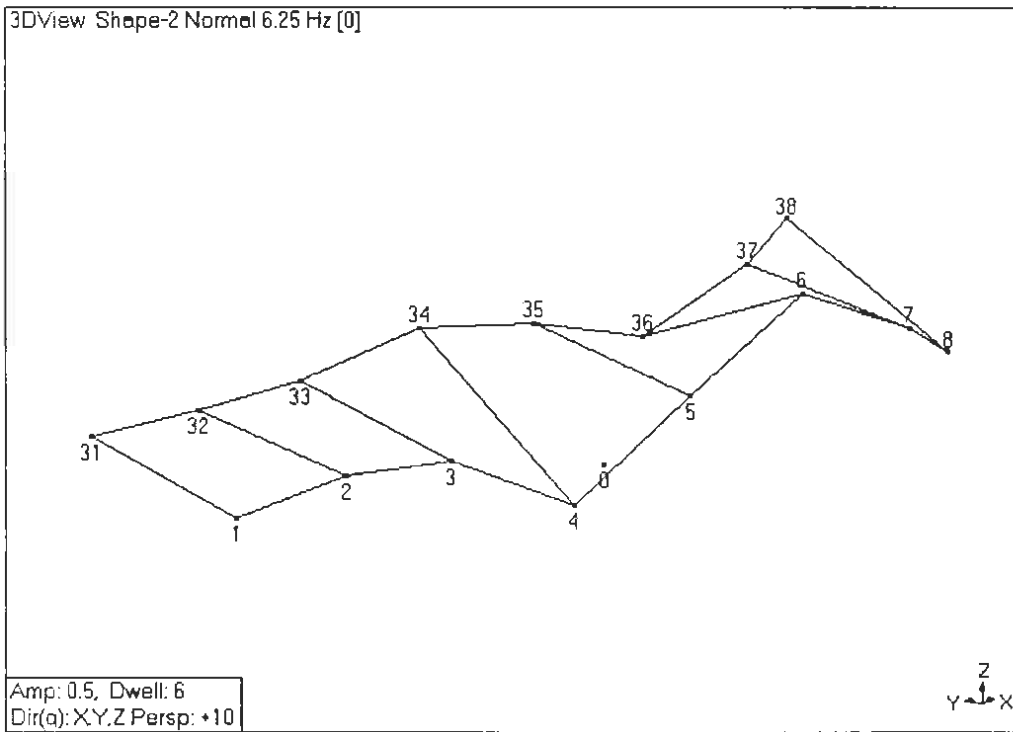


**Figure B.30 2<sup>nd</sup> Mode Watson Wash Frame S-1, August 2000 Field Test**

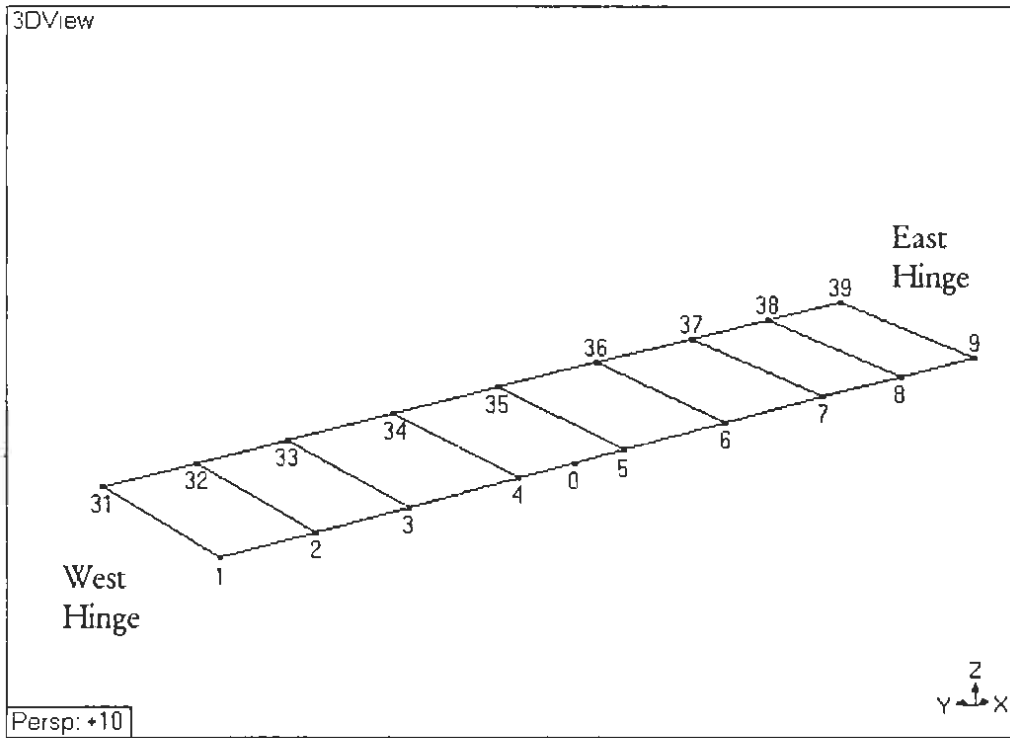


**Figure B.31 Wireframe Model of Response Nodes for  
Watson Wash Frame S-2, August 2000 Field Test**

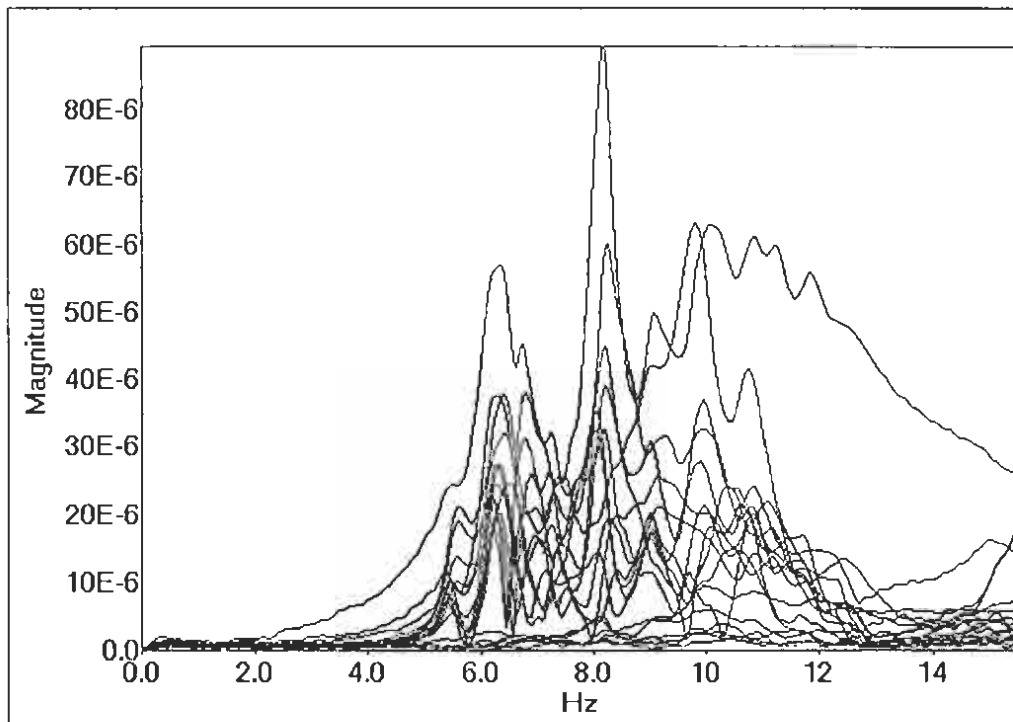


**Figure B.32 Overlay of Vertical FRF Magnitudes for  
Watson Wash Frame S-2, August 2000 Field Test**

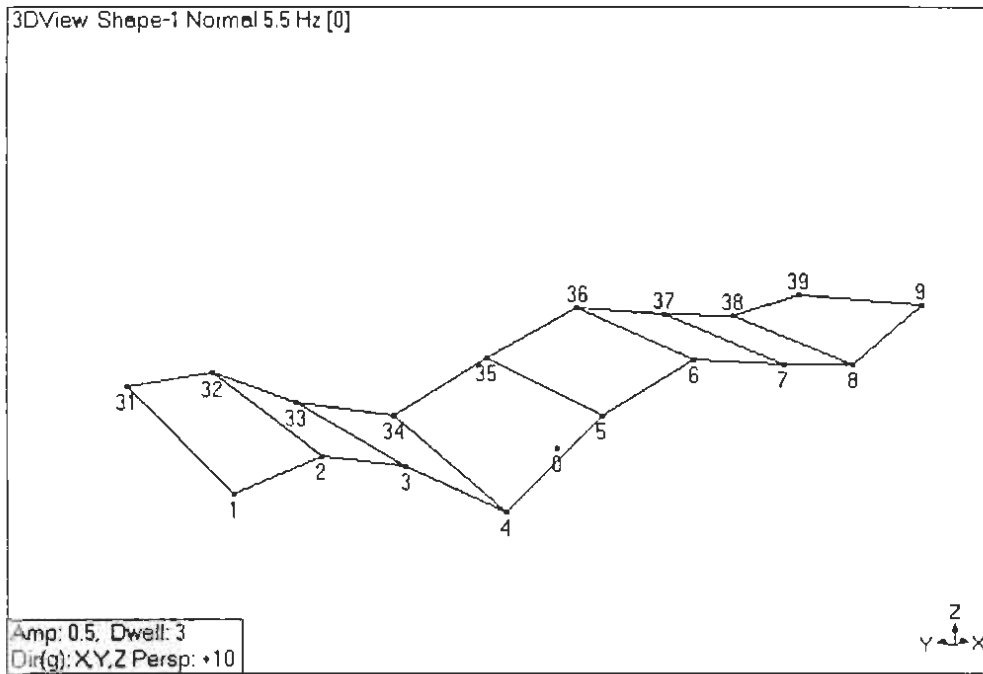


Figure B.33 1<sup>st</sup> Mode Watson Wash Frame S-2, August 2000 Field Test

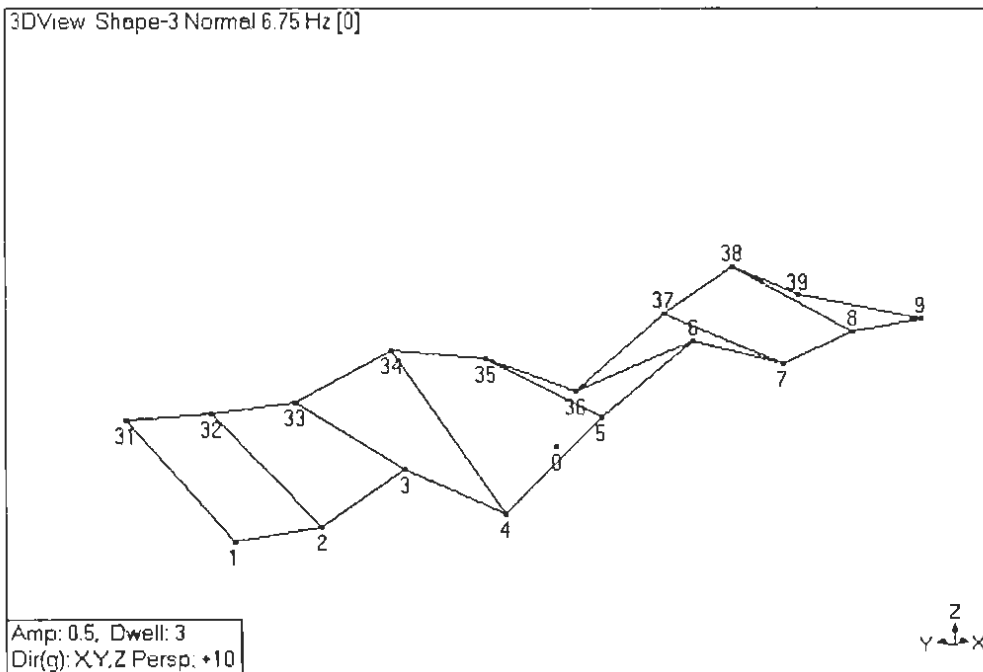
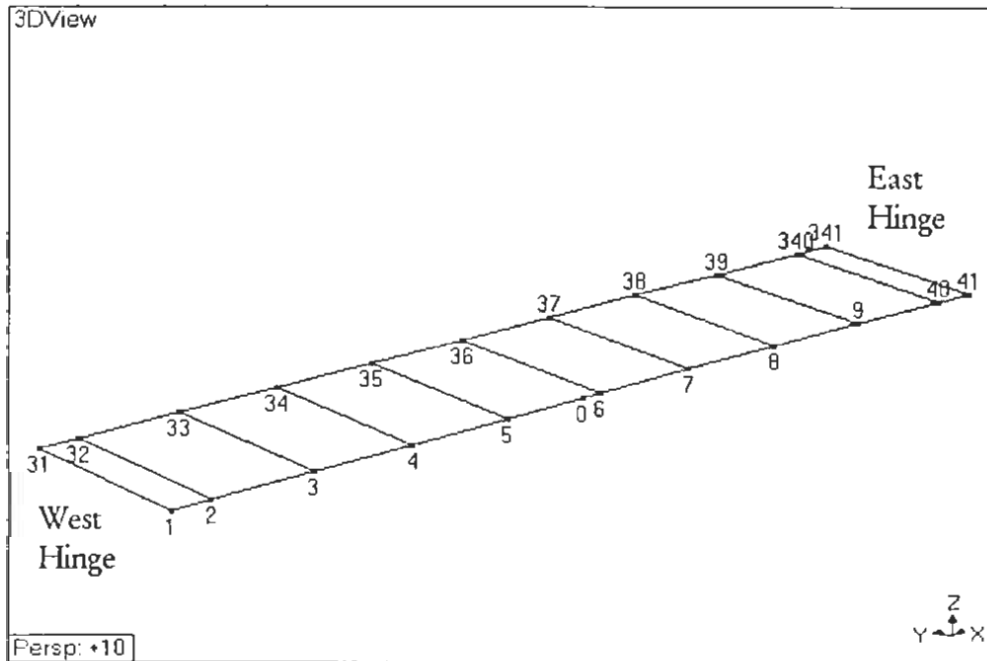
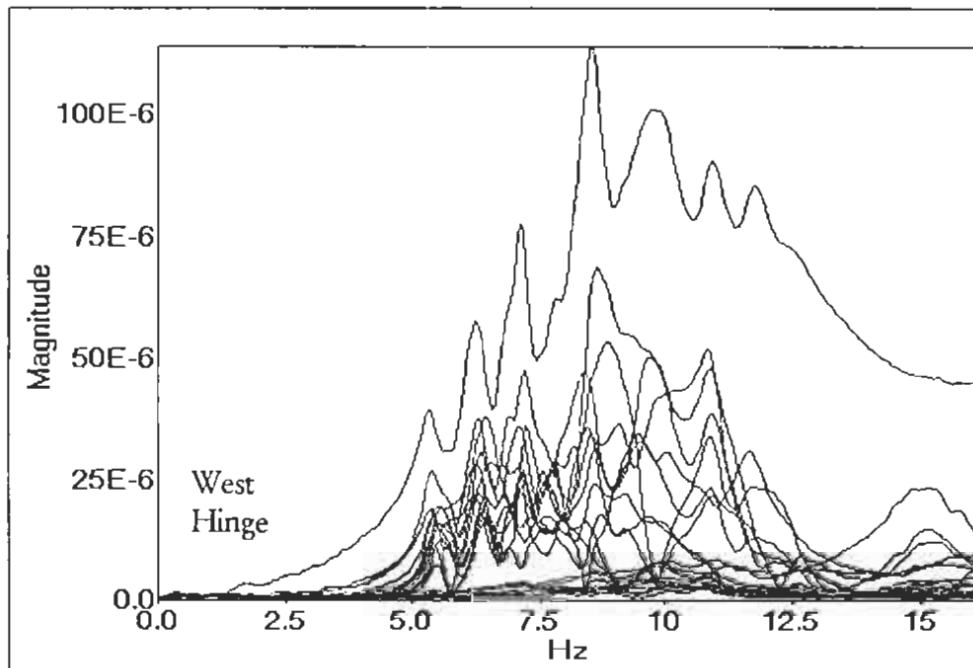


Figure B.34 2<sup>nd</sup> Mode Watson Wash Frame S-2, August 2000 Field Test



**Figure B.35 Wireframe Model of Response Nodes for  
Watson Wash Frame S-3, August 2000 Field Test**



**Figure B.36 Overlay of Vertical FRF Magnitudes for  
Watson Wash Frame S-3, August 2000 Field Test**

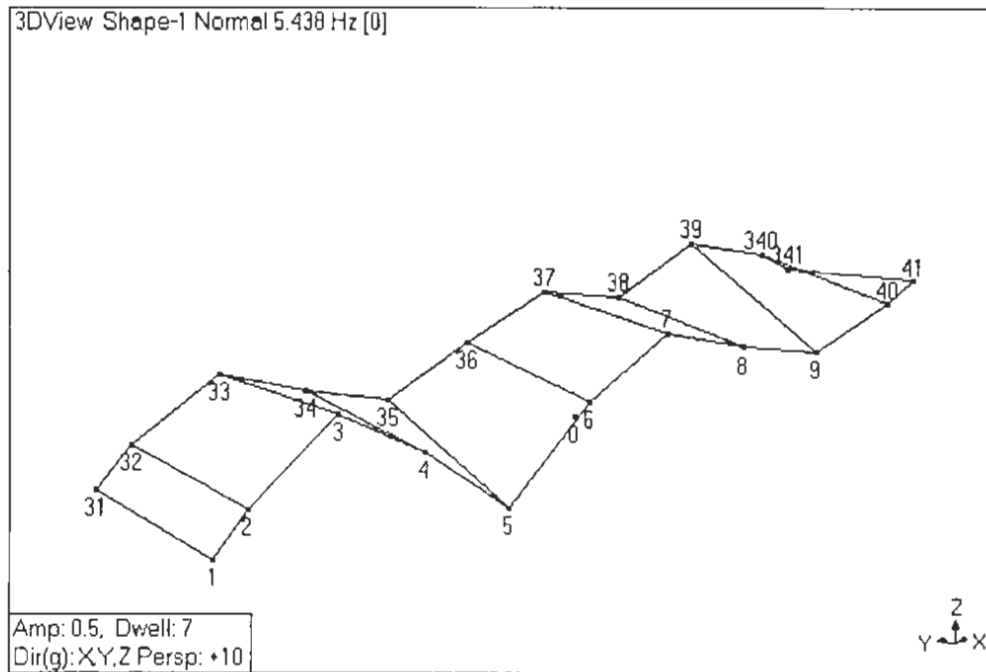


Figure B.37 1<sup>st</sup> Mode Watson Wash Frame S-3, August 2000 Field Test

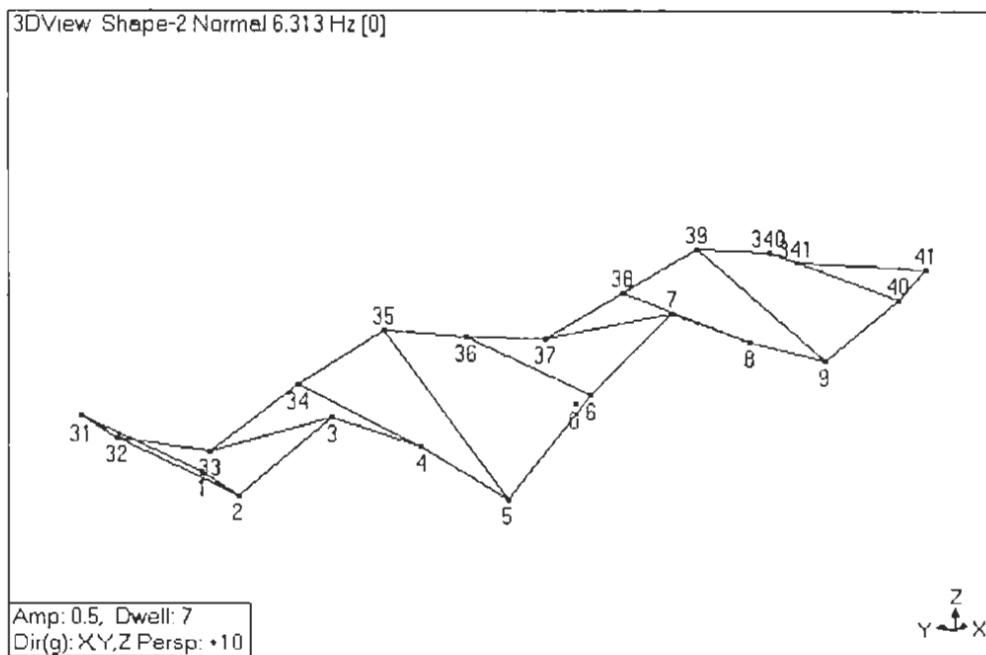
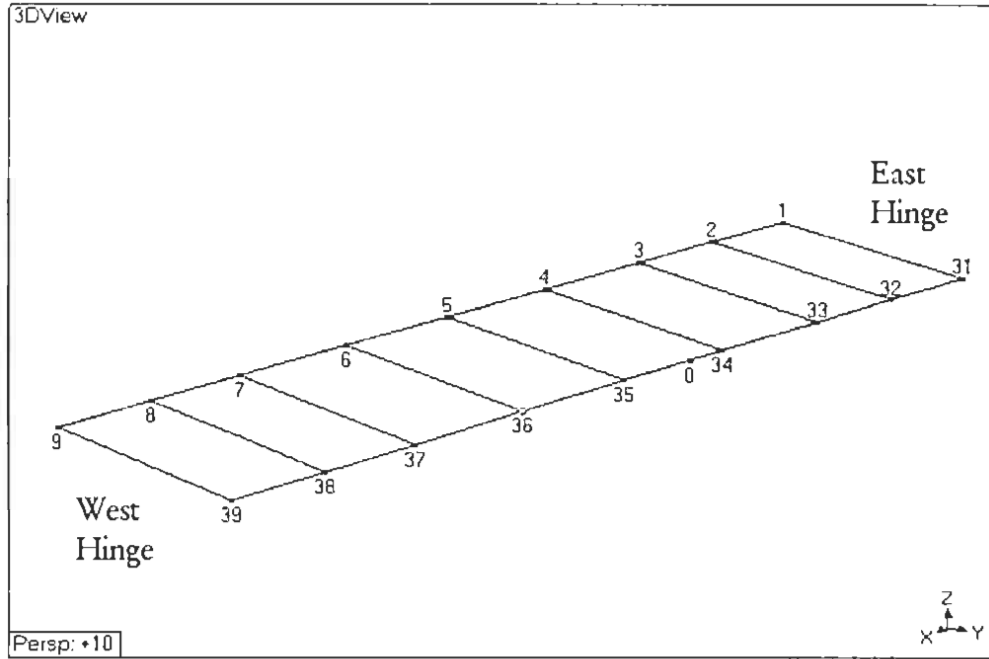
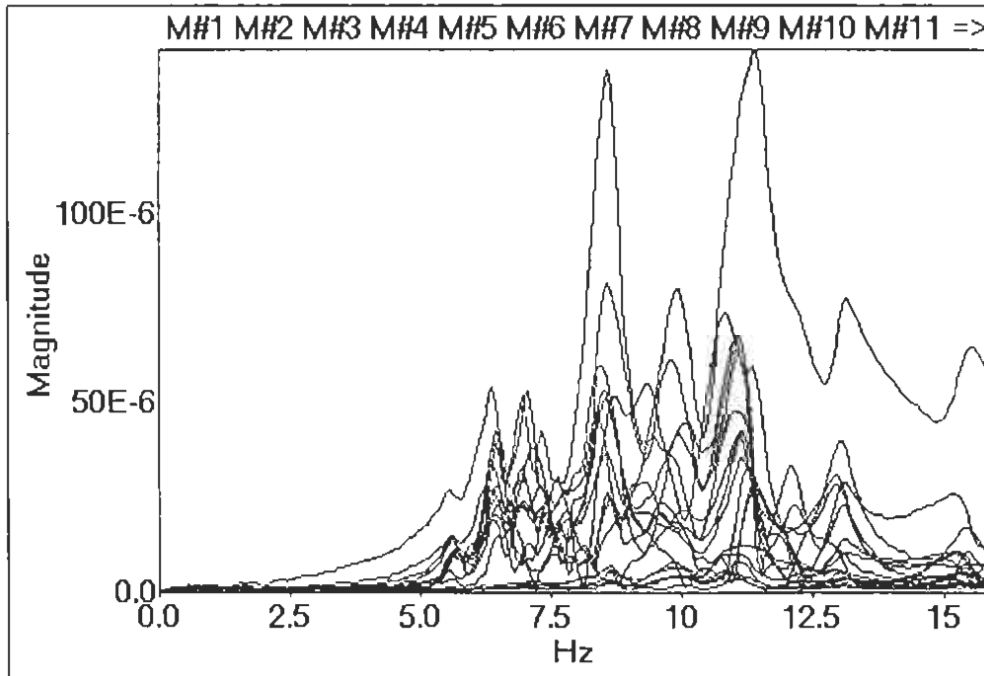


Figure B.38 2<sup>nd</sup> Mode Watson Wash Frame S-3, August 2000 Field Test



**Figure B.39 Wireframe Model of Response Nodes for Watson Wash Frame S-4, August 2000 Field Test**



**Figure B.40 Overlay of Vertical FRF Magnitudes for Watson Wash Frame S-4, August 2000 Field Test**

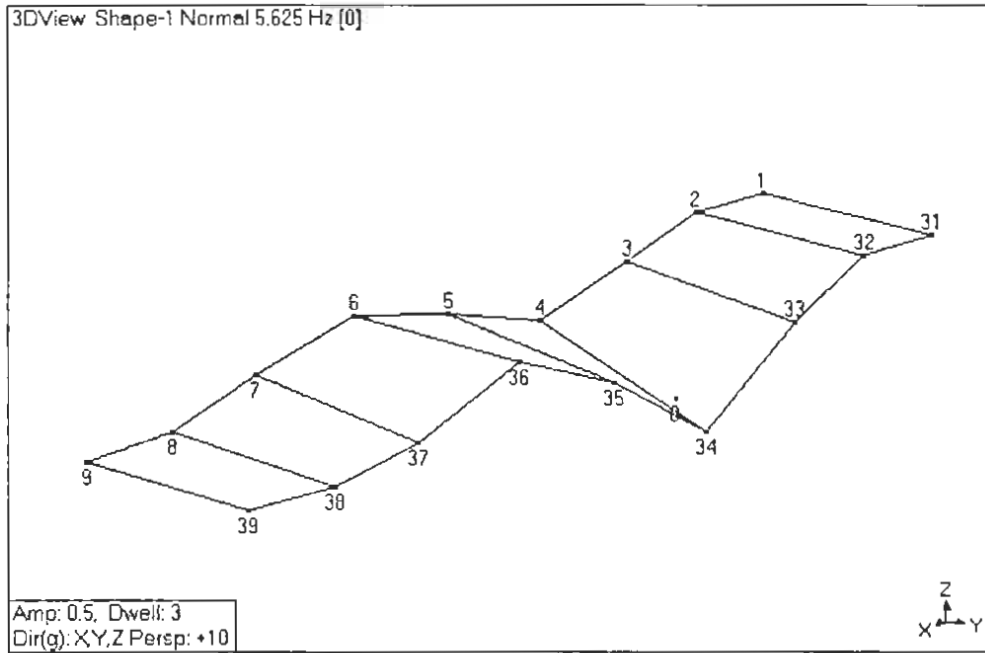


Figure B.41 1<sup>st</sup> Mode Watson Wash Frame S-4, August 2000 Field Test

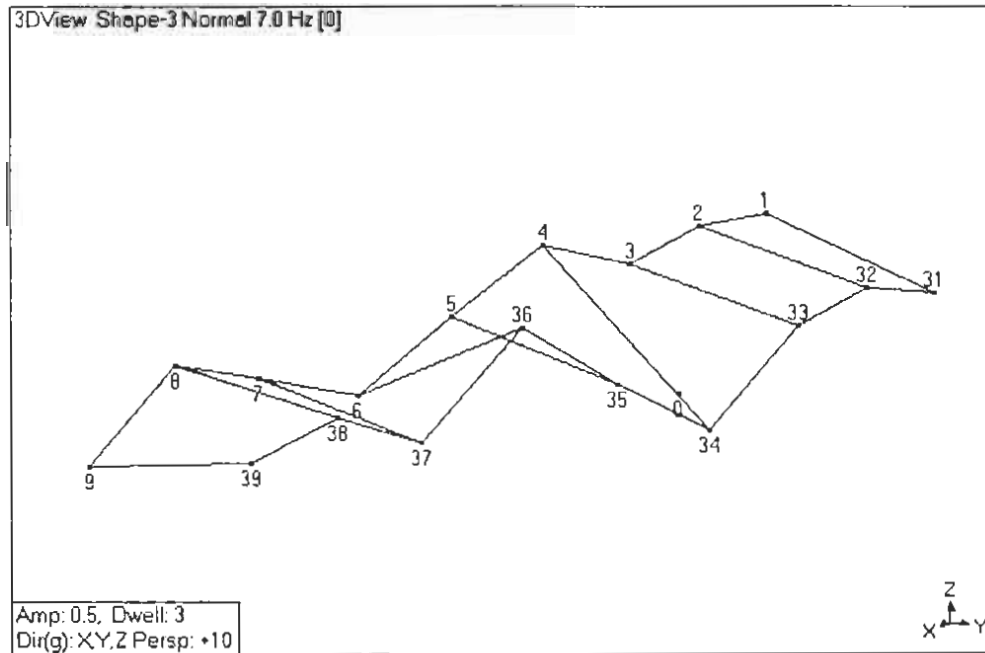
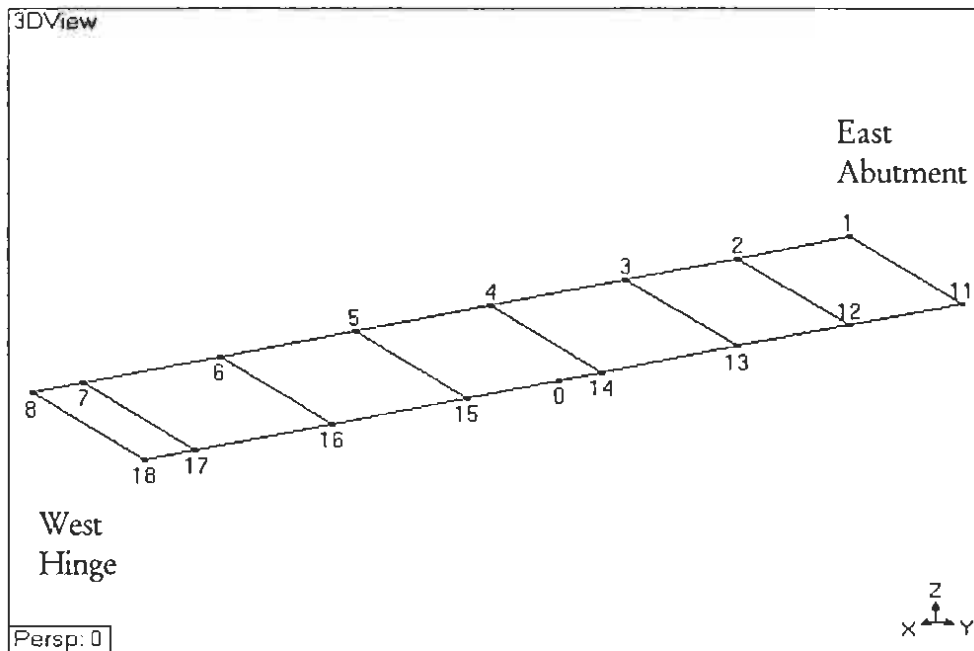
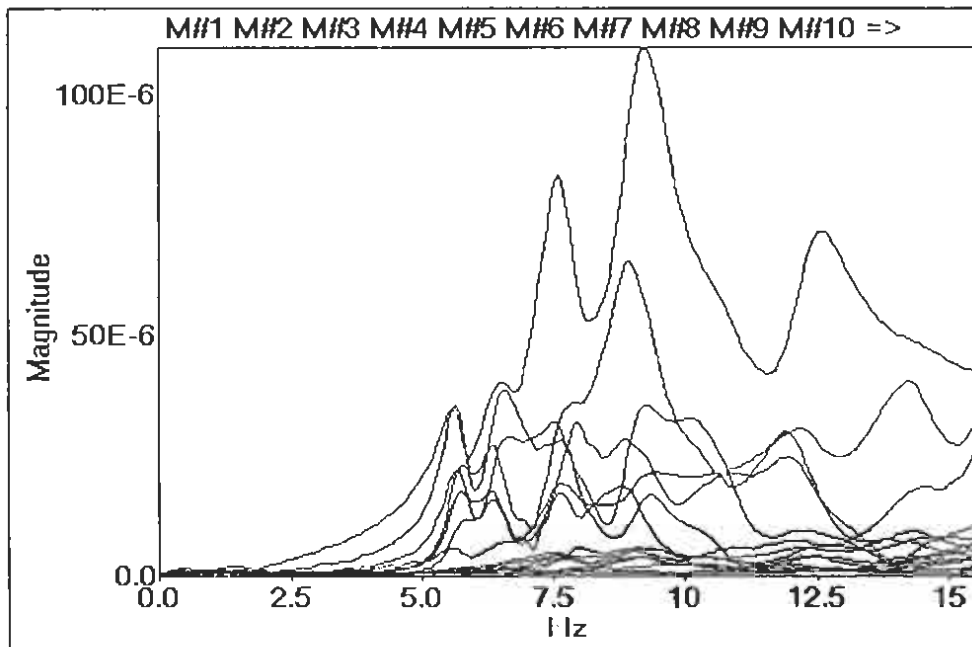


Figure B.42 2<sup>nd</sup> Mode Watson Wash Frame S-4, August 2000 Field Test



**Figure B.43 Wireframe Model of Response Nodes for Watson Wash Frame S-5, August 2000 Field Test**



**Figure B.44 Overlay of Vertical FRF Magnitudes for Watson Wash Frame S-5, August 2000 Field Test**

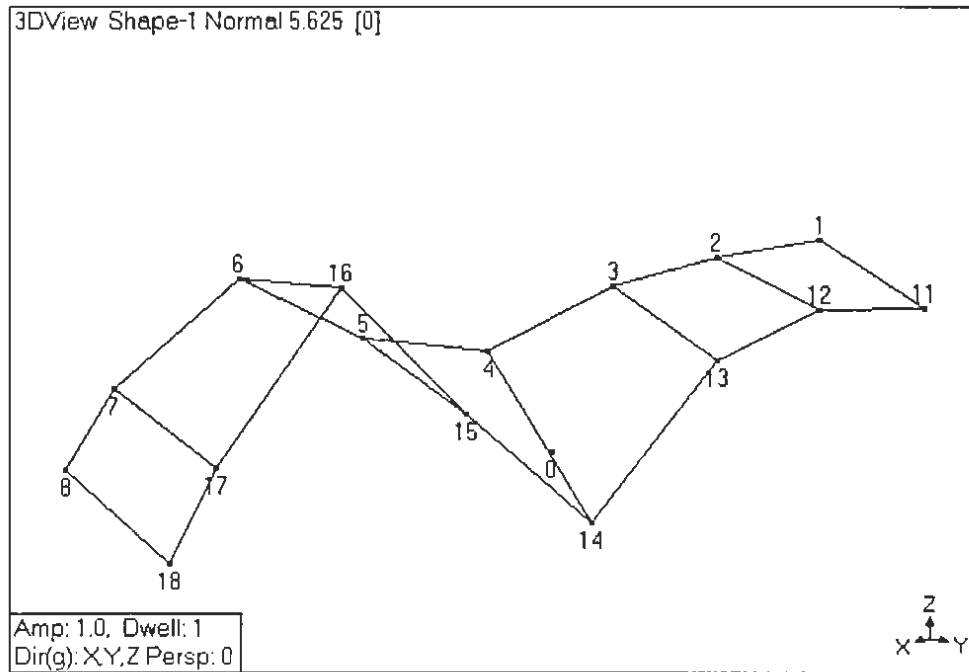


Figure B.45 1<sup>st</sup> Mode Watson Wash Frame S-5, August 2000 Field Test

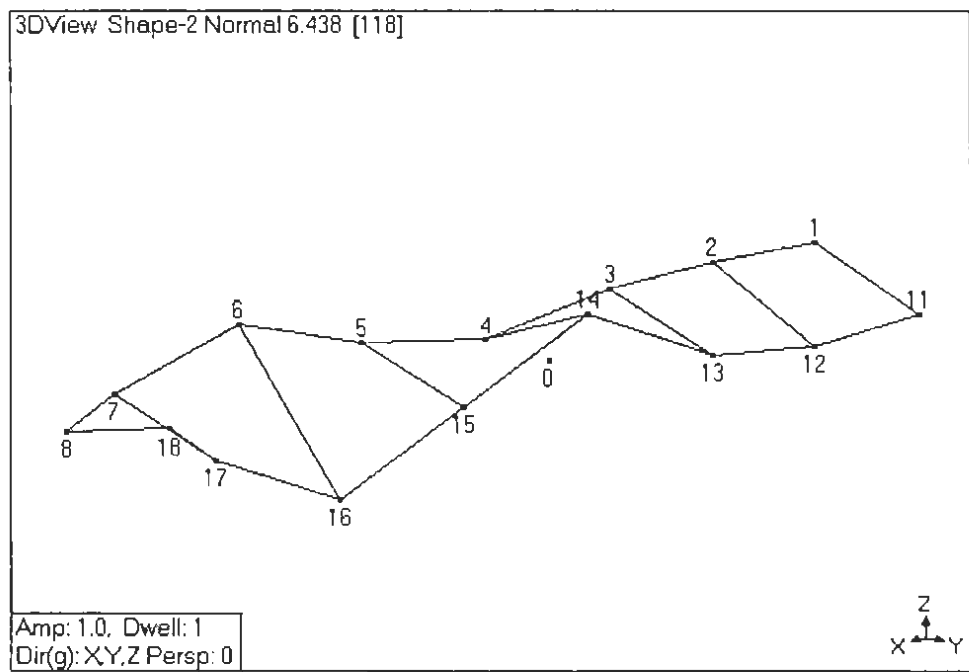


Figure B.46 2<sup>nd</sup> Mode Watson Wash Frame S-5, August 2000 Field Test

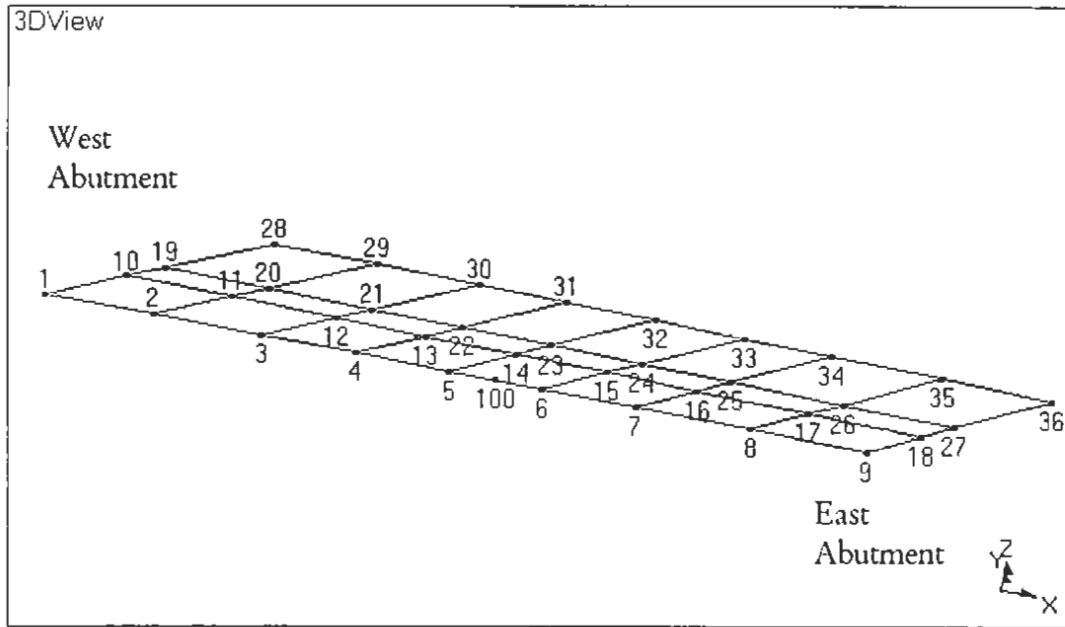


Figure B.47 Wireframe Model of Response Nodes for Fenner Overcrossing, September 1999 Field Test

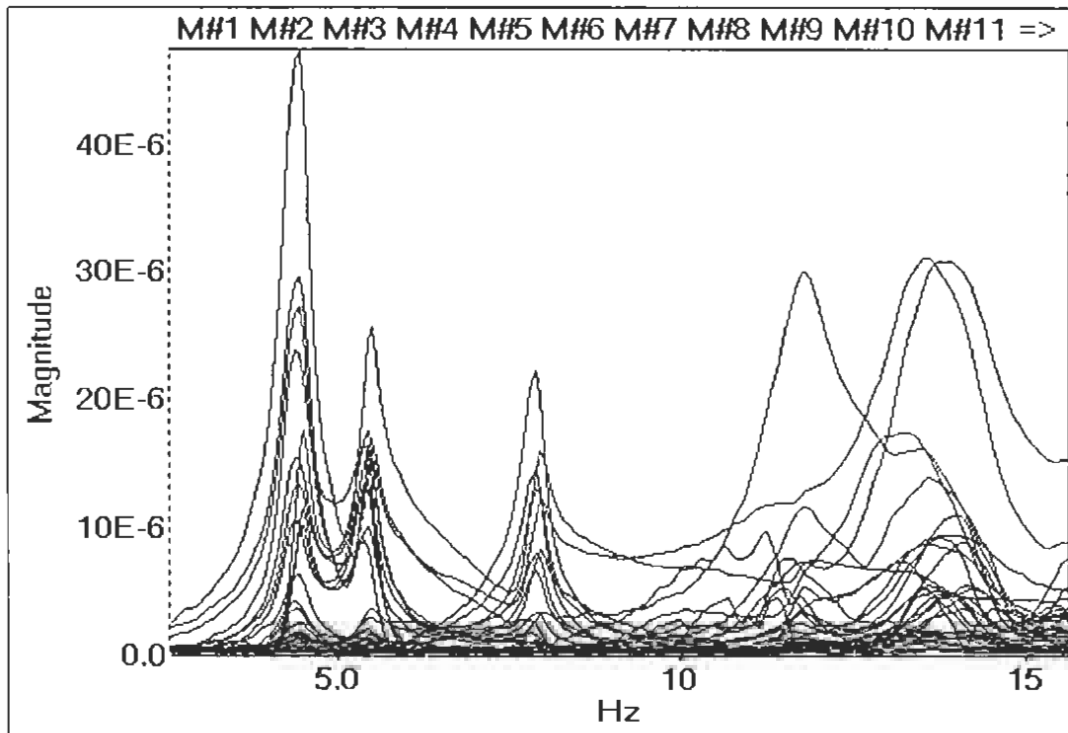


Figure B.48 Overlay of Vertical FRF Magnitudes for Fenner Overcrossing, September 1999 Field Test

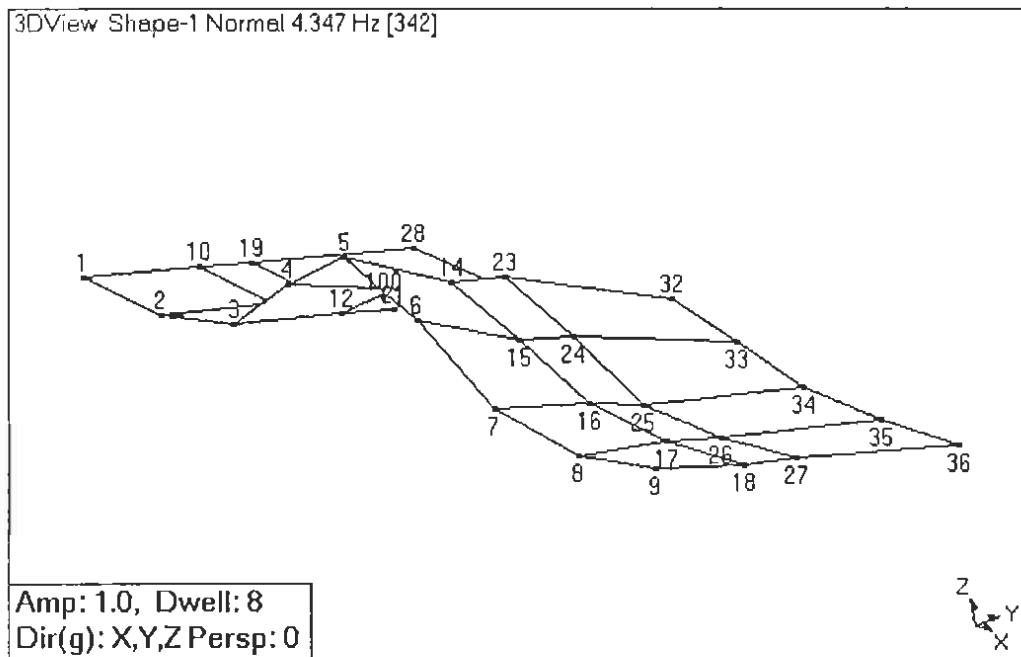


Figure B.49 1<sup>st</sup> Mode Fenner Overcrossing, September 1999 Field Test

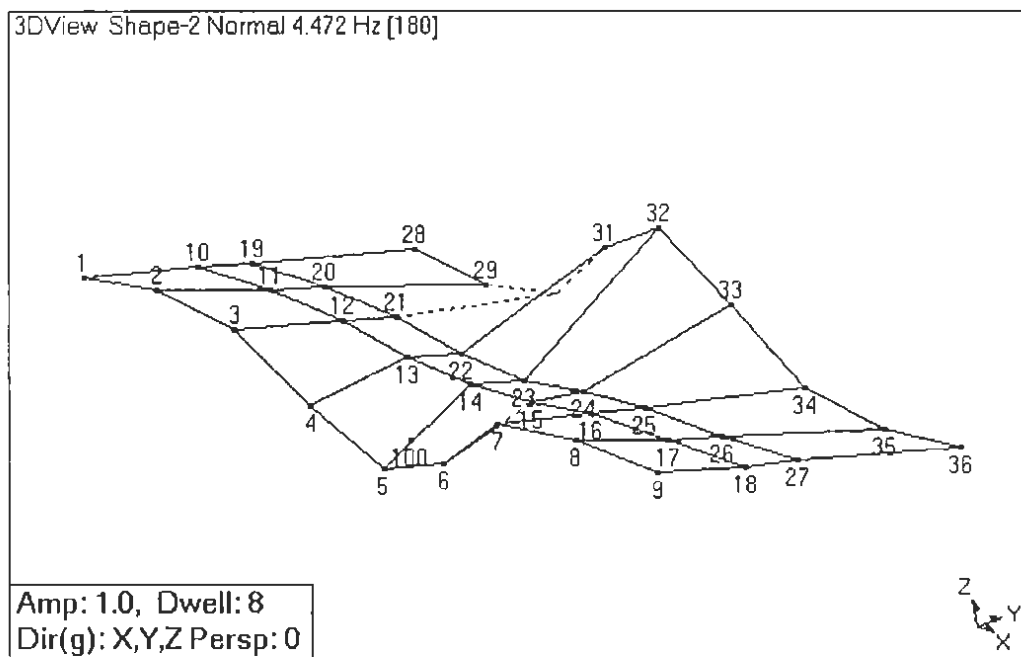


Figure B.50 2<sup>nd</sup> Mode Fenner Overcrossing, September 1999 Field Test

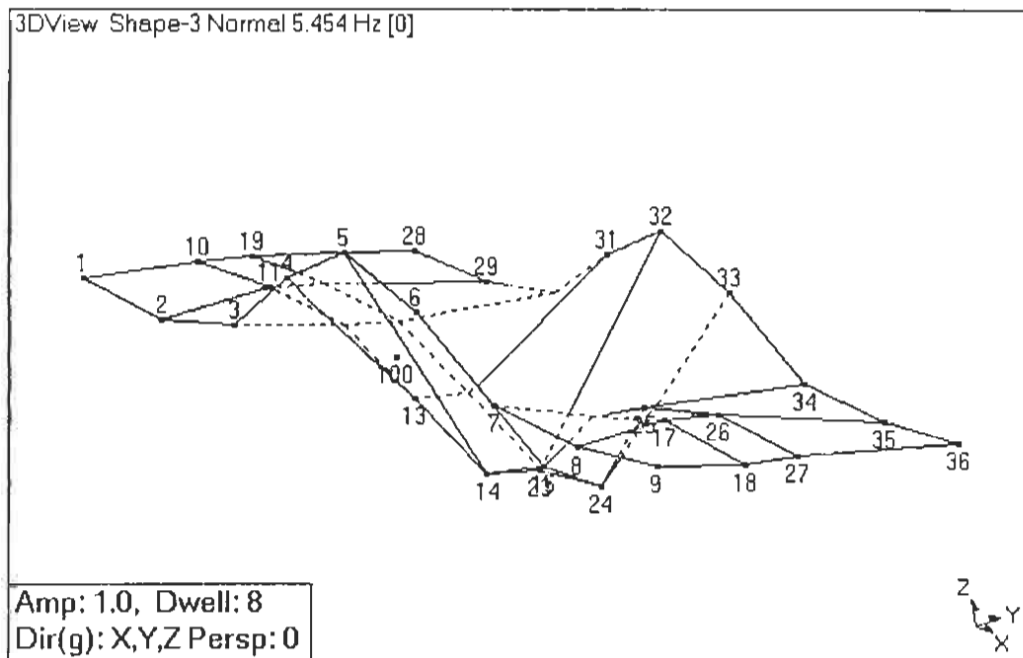


Figure B.51 3<sup>rd</sup> Mode Fenner Overcrossing, September 1999 Field Test

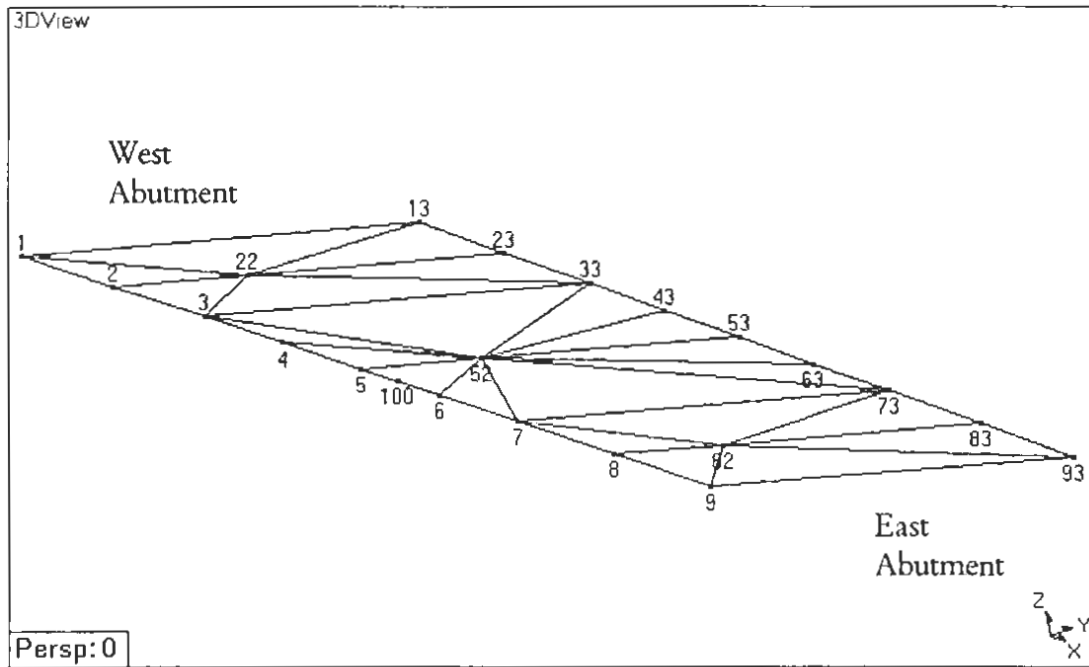


Figure B.52 Wireframe Model of Response Nodes for Fenner Overcrossing, December 2000 Field Test

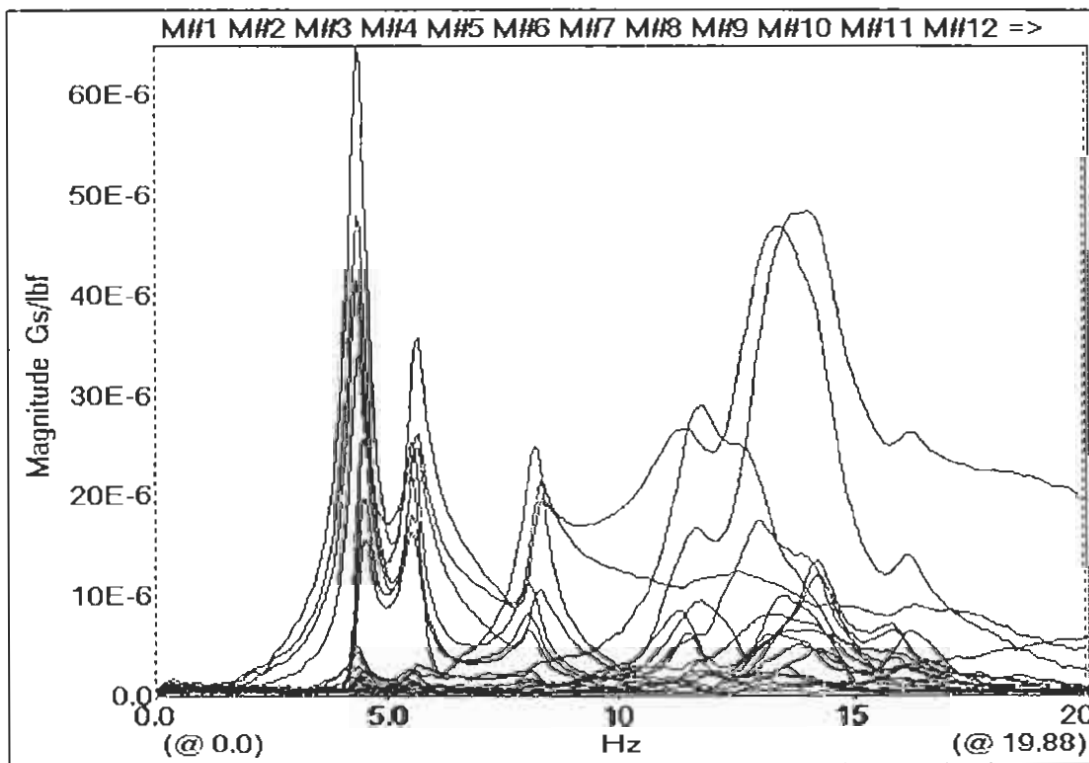


Figure B.53 Overlay of Vertical FRF Magnitudes for Fenner Overcrossing, December 2000 Field Test

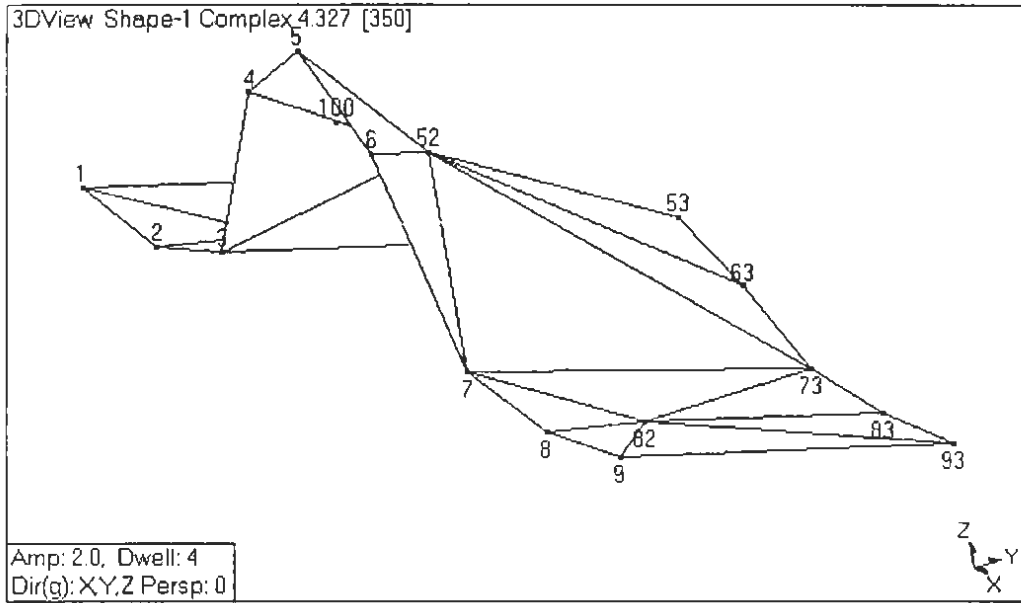


Figure B.54 1<sup>st</sup> Mode Fenner Overcrossing, December 2000 Field Test

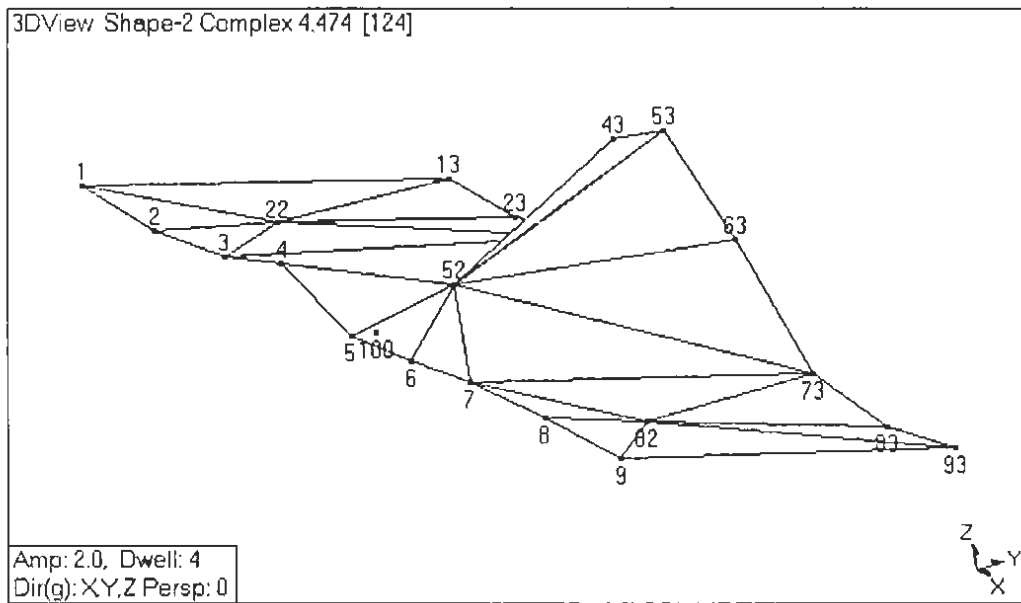


Figure B.55 2<sup>nd</sup> Mode Fenner Overcrossing, December 2000 Field Test

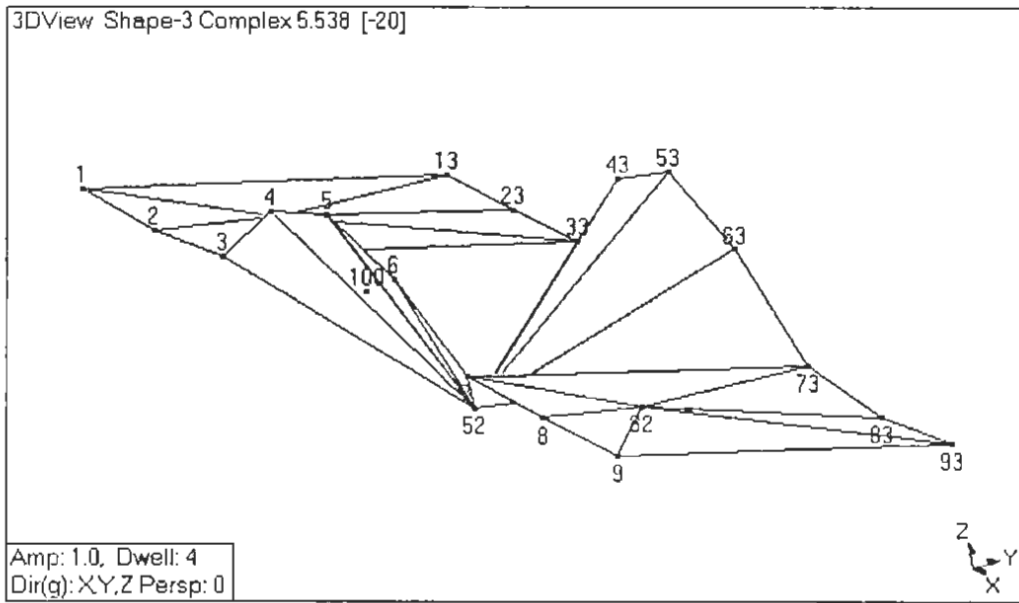


Figure B.56 3<sup>rd</sup> Mode Fenner Overcrossing, December 2000 Field Test

## APPENDIX C

### SYSTEMS IDENTIFICATION AND DAMAGE DETECTION FOR FENNER OVERCROSSING AND WATSON WASH BRIDGE

#### C.1 FENNER OVERCROSSING

##### C.1.1 System Identification, September 1999 Field Test

**Table C.1 Material Properties of the Initial FE Model**

	Girders <sup>a</sup>	Deck, Bent, and Abutments <sup>b</sup>	Modulus of Subgrade Reaction <sup>c</sup>
E (ksi)	3,500	3,000	
k (kef)			800
$\rho$ (lb-s <sup>2</sup> /ft <sup>4</sup> )	4.7	4.7	

- a. See As-Built Plan  
b. Typical Value  
c. See Bowles (1996)

**Table C.2 Comparison of Resonant Frequencies of Initial FE Model and  
Experiment**

Mode Number	Frequency (Hz)	
	Experiment	Initial FE Model
1	4.3471	4.8706
2	4.4718	5.0782
3	5.4536	6.2225

**Table C.3 MAC Values**

	MAC		
	Exp. Mode 1	Exp. Mode 2	Exp. Mode 3
FE mode 1	0.971	0.055	0.019
FE mode 2	0.030	0.946	0.009
FE mode 3	0.002	0.047	0.968

**Table C.4 Sensitivity Matrix F for Fenner Overcrossing, September 1999**

Mode	Girders	Deck, Bent, and Abutments	Stiffness Soil- Structure Interaction
1	0.5738	0.3988	0.0713
2	0.5977	0.3907	0.0519
3	0.6148	0.3738	0.0446

**Table C.5 System Identification for Fenner Overcrossing , September 1999**

Mode (Exp.)	Frequency of Initial FE model*	Updated Frequencies (Hz)			Frequency of Target Structure	Error (%)	
		Iter. 1	Iter. 2			Initial	Final
1	4.8706	4.2601	4.2880	4.2933	4.3471	12.0	1.2
2	5.0782	4.4075	4.4284	4.4331	4.4718	13.6	0.9
3	6.2225	5.3883	5.4083	5.4127	5.4536	14.1	0.7

**Table C.6 Identified Material Properties of Fenner Overcrossing, September 1999**

	Girders	Deck, Bent, and Abutments	Modulus of Subgrade Reaction
E (ksi)	2,430	2,254	12,174*
k (kef)			
$\rho$ (lb-s <sup>2</sup> /ft <sup>4</sup> )	4.7	4.7	

\* The identified results suggest that the supports are essentially rigid. Note also that the relatively large values may be a result of the small frequency-subgrade modulus sensitivity.

C.1.2 System Identification, December 2000 Field Test

**Table C.7 Material Properties of the Initial FE Model**

	Girders	Deck, Bent, and Abutments	Modulus of Subgrade Reaction
E (ksi)	2,430	2,254	
k (kef)			12,174
$\rho$ (lb-s <sup>2</sup> /ft <sup>4</sup> )	4.7	4.7	

**Table C.8 Comparison of Resonant Frequencies of Initial FE Model and Experiment**

Mode Number	Frequency (Hz)	
	Experiment	Initial FE Model
1	4.3269	4.2933
2	4.4738	4.4331
3	5.5378	5.4127

**Table C.9 MAC Values**

	MAC		
	Exp. Mode 1	Exp. Mode 2	Exp. Mode 3
FE mode 1	0.962	0.259	0.392
FE mode 2	0.086	0.585	0.093
FE mode 3	0.303	0.466	0.980

**Table C.10. Sensitivity Matrix F for Fenner Overcrossing, December 2000**

Mode	Girders	Deck, Bent, and Abutments	Stiffness Soil- Structure Interaction
1	0.5738	0.3988	0.0713
2	0.5977	0.3907	0.0519
3	0.6148	0.3738	0.0446

**Table C.11. System Identification for Fenner Overcrossing, December 2000**

Mode (Exp.)	Frequency of Initial FE model*	Updated Frequencies (Hz)			Frequency of Target Structure	Error (%)	
		Iter. 1	Iter. 2			Initial	Final
1	4.2933	4.3507	4.3508		4.3269	0.8	0.5
2	4.4331	4.4924	4.4925		4.4738	0.9	0.4
3	5.4127	5.4853	5.4854		5.5378	2.3	0.9

**Table C.12. Identified Material Properties of Fenner Overcrossing, December 2000**

	Girders	Deck, Bent, and Abutments	Modulus of Subgrade Reaction
E (ksi)	2,497	2,316	
k (kef)			12,174
$\rho$ (lb-s <sup>2</sup> /ft <sup>4</sup> )	4.7	4.7	

### C.1.3 Damage Detection, September 1999 Field Test

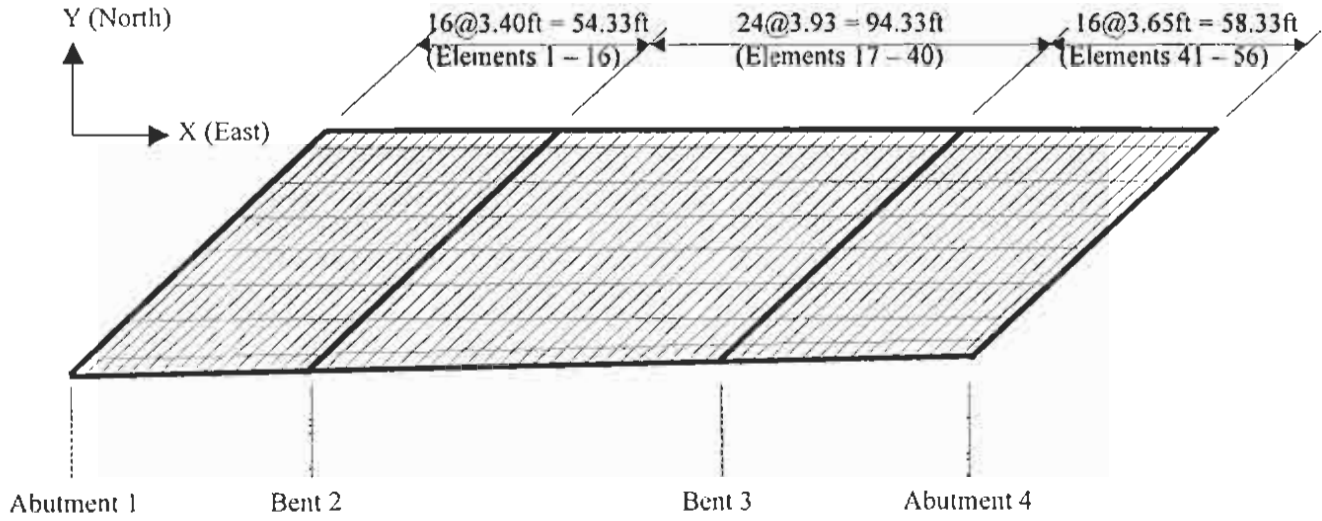


Figure C.1 Damage Detection Model

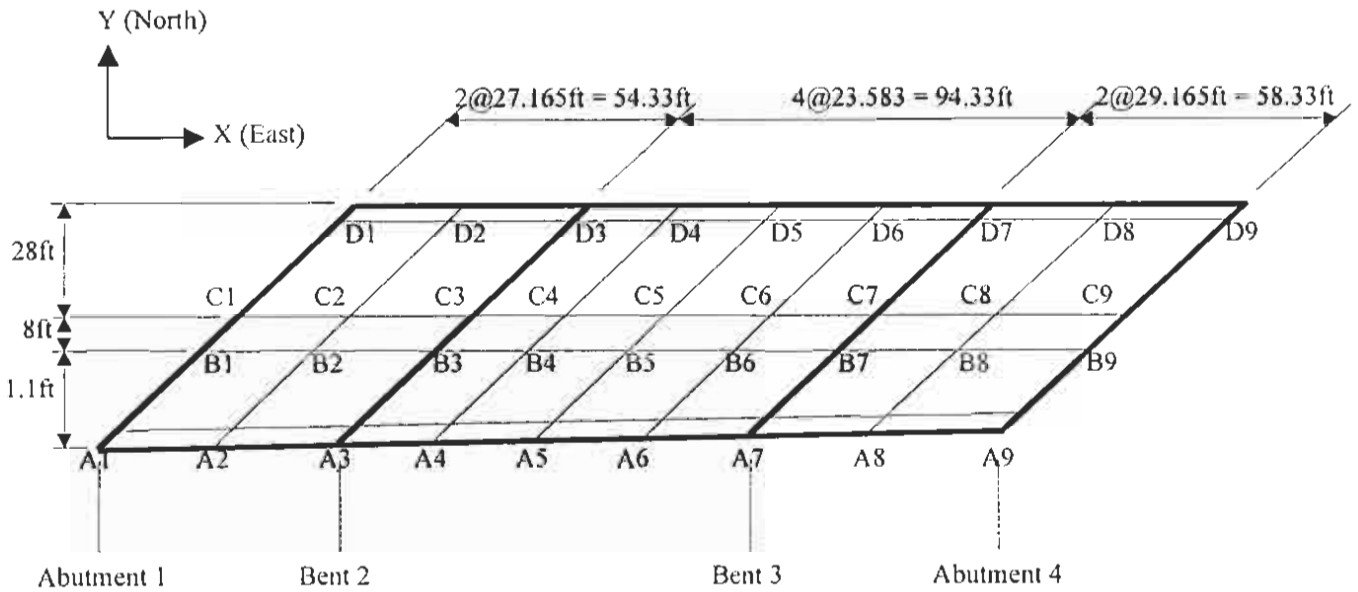
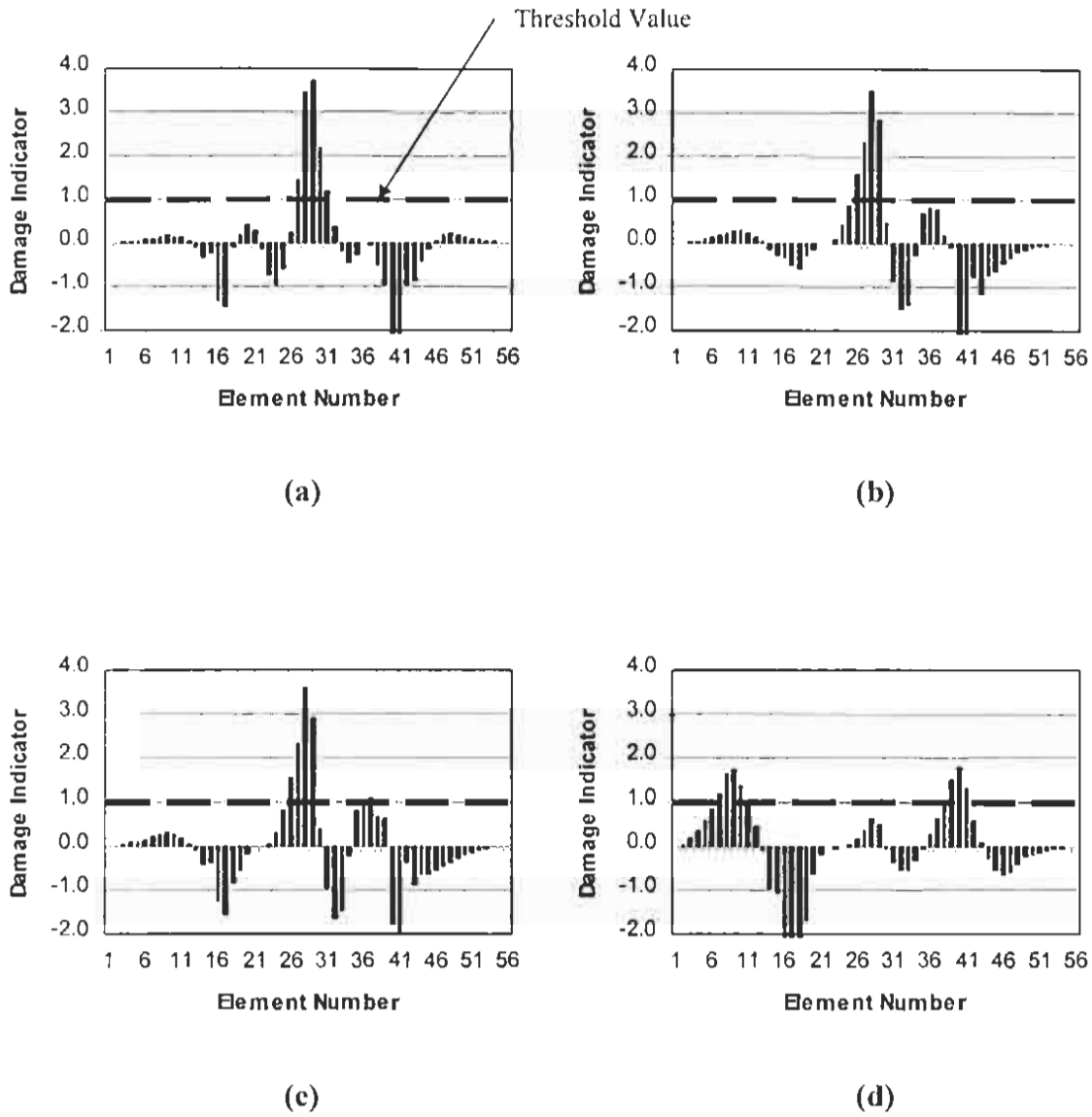
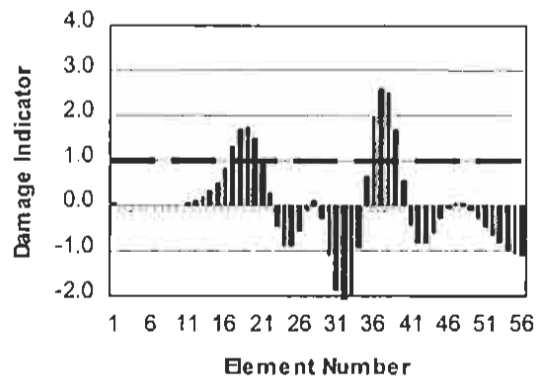


Figure C.2 Sensor Locations



**Figure C.3 Damage Detection Results Using the First Experiment Mode and First Bending Mode of Baseline Model (Note See Appendix A3 for Definition of the Threshold Values):**

- (a) Results using the Measurement along the Sensors A1 – A9;
- (b) Results using the Measurement along the Sensors B1 – B9;
- (c) Results using the Measurement along the Sensors C1 – C9;
- (d) Results using the Measurement along the Sensors D1 – D9



**Figure C.4 Damage Localization Results Using First Torsional Mode of Experimental Data and Baseline Model**

C.1.4 Damage Localization, December 2000 Field Test

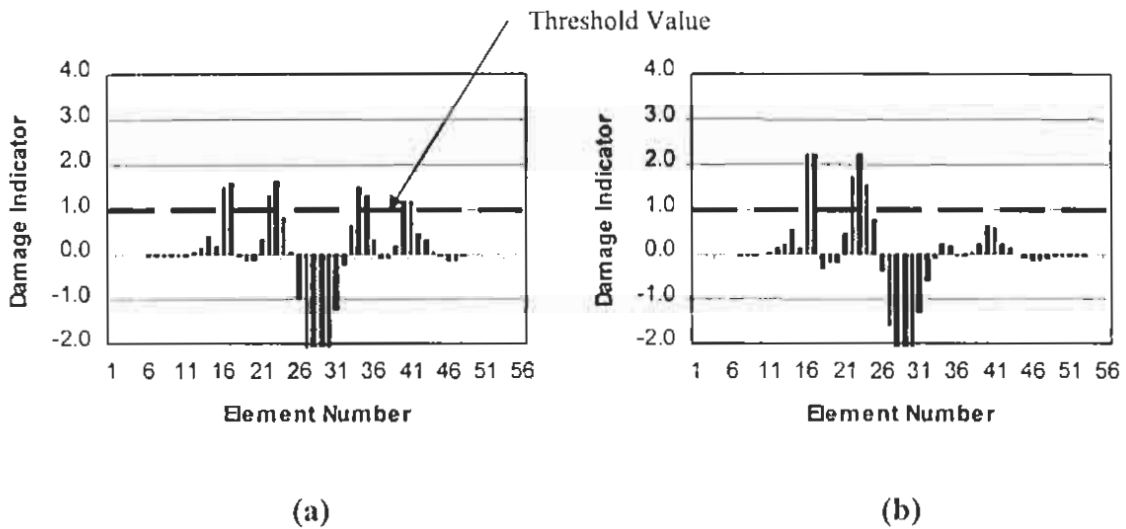
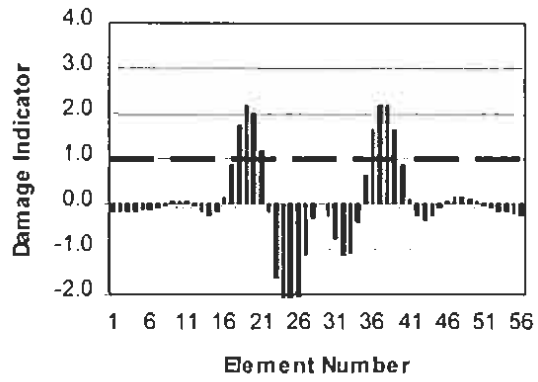


Figure C.5 Damage Detection Results Using the First Experiment Mode and First Bending Mode of Baseline Model: (a) Result using the Measurement along the Sensors A1 – A9; (b) Result using the Measurement along the Sensors D1 – D9



**Figure C.6 Damage Localization Results Using First Torsional Mode of Experimental Data and Baseline Model**

## C.2 WATSON WASH BRIDGE

### C.2.1 System Identification, May 1999 Field Test

#### C.2.1.1 Frame S-1

**Table C.13 Initial Values of Material Properties of the Initial FE Model**

Deck and Bent	
E (lb/ft <sup>2</sup> )	451.12 x 10 <sup>6</sup> (3133 ksi)
$\rho$ (lb·s <sup>2</sup> /ft <sup>4</sup> )	4.7

**Table C.14 Sensitivity Matrices F and G for Watson Wash Frame S-1, May 1999**

Mode	Deck and Bent	
	F	G
1	0.9655	-0.9091
2	0.9147	-0.9089

**Table C.15 System Identification for Watson Wash Frame S-1, May 1999**

Mode	Frequency of Initial FE model	Updated Frequencies (Hz)			Frequency of Target Structure	Error (%)	
		Iter. 1	Iter. 3	Iter. 5		Initial	Final
1	6.406	5.770	5.769	5.769	5.884	8.9	2.0
2	7.781	7.024	7.022	7.022	6.871	13.2	2.2

**Table C.16 Identified Material Properties of Watson Wash Frame S-1, May 1999**

Deck and Bent	
E (lb/ft <sup>2</sup> )	362.18 x 10 <sup>6</sup> (2515 ksi)
$\rho$ (lb·s <sup>2</sup> /ft <sup>4</sup> )	4.71

C.2.1.2 Frame S-2

**Table C.17 Initial Values of Material Properties of Initial FE Model**

Deck and Bent	
E (lb/ft <sup>2</sup> )	451.12 x 10 <sup>6</sup> (3133 ksi)
$\rho$ (lb-s <sup>2</sup> /ft <sup>4</sup> )	4.7

**Table C.18 Sensitivity Matrices F and G for Watson Wash Frame S-2, May 1999**

Mode	Deck and Bent	
	F	G
1	0.8842	-0.9093
2	0.8206	-0.9092

**Table C.19 System Identification for Watson Wash Frame S-2, May 1999**

Mode	Frequency of Initial FE model	Updated Frequencies (Hz)			Frequency of Target Structure	Error (%)	
		Iter. 1	Iter. 3	Iter. 5		Initial	Final
1	6.586	6.110	6.115	6.115	5.981	10.1	2.2
2	7.495	6.987	6.993	6.993	7.154	4.8	2.2

**Table C.20 Identified Material Properties of Watson Wash Frame S-2, May 1999**

Deck and Bent	
E (lb/ft <sup>2</sup> )	378.76 x 10 <sup>6</sup> (2630 ksi)
$\rho$ (lb-s <sup>2</sup> /ft <sup>4</sup> )	4.67

C.2.1.3 Frame S-3

**Table C.21 Initial Values of Material Properties of Initial FE Model**

	Deck and Bent
E (lb/ft <sup>2</sup> )	451.12 x 10 <sup>6</sup> (3133 ksi)
ρ (lb·s <sup>2</sup> /ft <sup>4</sup> )	4.7

**Table C.22 Sensitivity Matrices F and G for Watson Wash Frame S-3, May 1999**

Mode	Deck and Bent	
	F	G
1	0.9582	-0.9092
2	0.9720	-0.9092

**Table C.23 System Identification for Watson Wash Frame S-3, May 1999**

Mode	Frequency of Initial FE model	Updated Frequencies (Hz)			Frequency of Target Structure	Error (%)	
		Iter. 1	Iter. 3	Iter. 5		Initial	Final
1	6.128	5.588	5.590	5.590	5.594	9.5	0.1
2	7.656	6.972	6.974	6.974	6.968	9.9	0.1

**Table C.24 Identified Material Properties of Watson Wash Frame S-3, May 1999**

	Deck and Bent
E (lb/ft <sup>2</sup> )	372.01 x 10 <sup>6</sup> (2583 ksi)
ρ (lb·s <sup>2</sup> /ft <sup>4</sup> )	4.7

C.2.1.4 Frame S-4

**Table C.25 Initial Values of Material Properties of Initial FE Model**

	Deck and Bent
E (lb/ft <sup>2</sup> )	451.12 x 10 <sup>6</sup> (3133 ksi)
ρ (lb·s <sup>2</sup> /ft <sup>4</sup> )	4.7

**Table C.26 Sensitivity Matrices F and G for Watson Wash Frame S-4, May 1999**

Mode	Deck and Bent	
	F	G
1	0.8842	-0.9089
2	0.8206	-0.9092

**Table C.27 System Identification for Watson Wash Frame S-4, May 1999**

Mode	Frequency of Initial FE model	Updated Frequencies (Hz)			Frequency of Target Structure	Error (%)	
		Iter. 1	Iter. 3	Iter. 5		Initial	Final
1	6.586	5.994	6.009	6.009	5.975	10.2	0.6
2	7.495	6.871	6.888	6.888	6.930	8.1	0.6

**Table C.28 Identified Material Properties of Watson Wash Frame S-4, May 1999**

	Deck and Bent
E (lb/ft <sup>2</sup> )	365.09 x 10 <sup>6</sup> (2535 ksi)
ρ (lb·s <sup>2</sup> /ft <sup>4</sup> )	4.67

C.2.1.5 Frame S-5

**Table C.29 Initial Values of Material Properties of Initial FE Model**

	Deck and Bent
E (lb/ft <sup>2</sup> )	451.12 x 10 <sup>6</sup> (3133 ksi)
ρ (lb·s <sup>2</sup> /ft <sup>4</sup> )	4.7

**Table C.30 Sensitivity Matrices F and G for Watson Wash Frame S-5, May 1999**

Mode	Deck and Bent	
	F	G
1	0.9655	-0.9090
2	0.9147	-0.9092

**Table C.31 System Identification for Watson Wash Frame S-5, May 1999**

Mode	Frequency of Initial FE model	Updated Frequencies (Hz)			Frequency of Target Structure	Error (%)	
		Iter. 1	Iter. 3	Iter. 5		Initial	Final
1	6.406	5.859	5.854	5.854	5.937	7.9	1.4
2	7.781	7.129	7.127	7.127	7.019	10.9	1.5

**Table C.32 Identified Material Properties of Watson Wash Frame S-5, May 1999**

	Deck and Bent
E (lb/ft <sup>2</sup> )	373.62 x 10 <sup>6</sup> (2595 ksi)
ρ (lb·s <sup>2</sup> /ft <sup>4</sup> )	4.71

C.2.2 System Identification, August 2000 Field Test

C.2.2.1 Frame S-1

**Table C.33 Initial Values of Material Properties of Initial FE Model**

	Deck and Bent
E (lb/ft <sup>2</sup> )	362.18 x 10 <sup>6</sup> (2515 ksi)
ρ (lb·s <sup>2</sup> /ft <sup>4</sup> )	4.71

**Table C.34 Sensitivity Matrices F and G for Watson Wash Frame S-1, August 2000**

Mode	Deck and Bent	
	F	G
1	0.9399	-0.8162
2	0.9352	-0.8522
3	0.8750	-0.8230

**Table C.35 System Identification for Watson Wash Frame S-1, August 2000**

Mode	Frequency of Initial FE model	Updated Frequencies (Hz)			Frequency of Target Structure	Error (%)	
		Iter. 1	Iter. 3	Iter. 5		Initial	Final
1	5.514	5.352	5.356	5.356	5.500	0.3	2.6
2	6.830	6.621	6.625	6.625	6.250	9.3	6.0
3	8.127	7.887	7.892	7.892	8.125	0.0	2.9

**Table C.36 Identified Material Properties of Watson Wash Frame S-1, August 2000**

	Deck and Bent
E (lb/ft <sup>2</sup> )	362.95 x 10 <sup>6</sup> (2520 ksi)
ρ (lb·s <sup>2</sup> /ft <sup>4</sup> )	5.04

C.2.2.2 Frame S-2

**Table C.37 Initial Values of Material Properties of Initial FE Model**

Deck and Bent	
E (lb/ft <sup>2</sup> )	378.76 x 10 <sup>6</sup> (2630 ksi)
ρ (lb·s <sup>2</sup> /ft <sup>4</sup> )	4.67

**Table C.38 Sensitivity Matrices F and G for Watson Wash Frame S-2, August 2000**

Mode	Deck and Bent	
	F	G
1	0.7224	-0.9055
2	0.8437	-0.9007

**Table C.39 System Identification for Watson Wash Frame S-2, August 2000**

Mode	Frequency of Initial FE model	Updated Frequencies (Hz)			Frequency of Target Structure	Error (%)	
		Iter. 1	Iter. 3	Iter. 5		Initial	Final
1	6.104	5.724	5.709	5.710	5.500	11.0	3.82
3	6.963	6.533	6.515	6.515	6.750	3.16	3.48

**Table C.40 Identified Material Properties of Watson Wash Frame S-2, August 2000**

Deck and Bent	
E (lb/ft <sup>2</sup> )	382.32 x 10 <sup>6</sup> (2655 ksi)
ρ (lb·s <sup>2</sup> /ft <sup>4</sup> )	5.38

C.2.2.3 Frame S-3

**Table C.41 Initial Values of Material Properties of Initial FE Model**

Deck and Bent	
E (lb/ft <sup>2</sup> )	372.01 x 10 <sup>6</sup> (2583 ksi)
ρ (lb·s <sup>2</sup> /ft <sup>4</sup> )	4.70

**Table C.42 Sensitivity Matrices F and G for Watson Wash Frame S-3, August 2000**

Mode	Deck and Bent	
	F	G
1	0.9591	-0.8405
2	0.9777	-0.8750
3	0.9033	-0.8207

**Table C.43 System Identification for Watson Wash Frame S-3, August 2000**

Mode	Frequency of Initial FE model	Updated Frequencies (Hz)			Frequency of Target Structure	Error (%)	
		Iter. 1	Iter. 3	Iter. 4		Initial	Final
	1	5.409	5.141	5.136	5.139	5.438	0.53
2	6.867	6.512	6.506	6.510	6.313	8.78	3.12
3	7.802	7.425	7.419	7.423	7.188	8.54	3.27

**Table C.44 Identified Material Properties of Watson Wash Frame S-3, August 2000**

Deck and Bent	
E (lb/ft <sup>2</sup> )	372.32 x 10 <sup>6</sup> (2586 ksi)
ρ (lb·s <sup>2</sup> /ft <sup>4</sup> )	5.26

C.2.2.4 Frame S-4

**Table C.45 Initial Values of Material Properties of Initial FE Model**

	Deck and Bent
E (lb/ft <sup>2</sup> )	365.09 x 10 <sup>6</sup> (2535 ksi)
ρ (lb·s <sup>2</sup> /ft <sup>4</sup> )	4.67

**Table C.46 Sensitivity Matrices F and G for Watson Wash Frame S-4, August 2000**

Mode	Deck and Bent	
	F	G
1	0.4826	-0.9051
2	0.8469	-0.9012

**Table C.47 System Identification for Watson Wash Frame S-4, August 2000**

Mode	Frequency of Initial FE model	Updated Frequencies (Hz)		Frequency of Target Structure	Error (%)	
		Iter. 1	Iter. 3		Initial	Final
		1	6.005		5.875	5.879
3	6.858	6.710	6.709	7.000	2.03	4.16

**Table C.48 Identified Material Properties of Watson Wash Frame S-4, August 2000**

	Deck and Bent
E (lb/ft <sup>2</sup> )	378.37 x 10 <sup>6</sup> (2628 ksi)
ρ (lb·s <sup>2</sup> /ft <sup>4</sup> )	5.03

C.2.2.5 Frame S-5

**Table C.49 Initial Values of Material Properties of Initial FE Model**

	Deck and Bent
E (lb/ft <sup>2</sup> )	373.62 x 10 <sup>6</sup> (2595 ksi)
ρ (lb·s <sup>2</sup> /ft <sup>4</sup> )	4.71

**Table C.50 Sensitivity Matrices F and G for Watson Wash Frame S-5, August 2000**

Mode	Deck and Bent	
	F	G
1	0.9383	-0.8153
2	0.8330	-0.8716

**Table C.51 System Identification for Watson Wash Frame S-5, August 2000**

Mode	Frequency of Initial FE model	Updated Frequencies (Hz)		Frequency of Target Structure	Error (%)	
		Iter. 1	Iter. 3		Initial	Final
2	7.480	7.591	7.581	7.625	1.90	0.58

**Table C.52 Identified Material Properties of Watson Wash Frame S-5, August 2000**

	Deck and Bent
E (lb/ft <sup>2</sup> )	371.85 x 10 <sup>6</sup> (2582 ksi)
ρ (lb·s <sup>2</sup> /ft <sup>4</sup> )	4.561

**C.2.3 Damage Detection, May 1999 Field Test**

**C.2.3.1 Frame S-1**

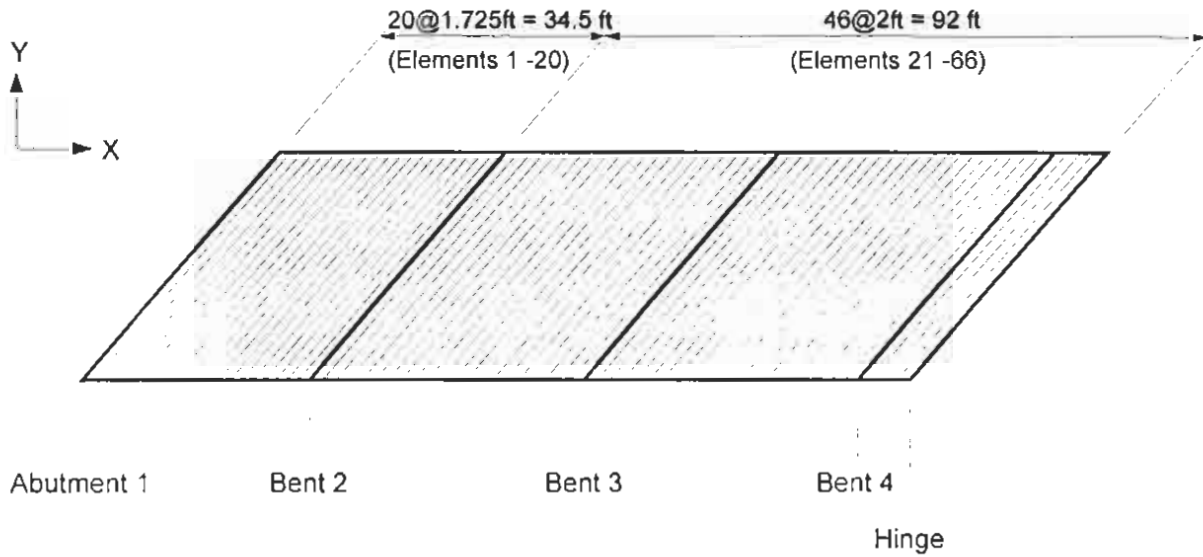


**Figure C.7 Damage Detection Model for Watson Wash Frame S-1, May 1999**

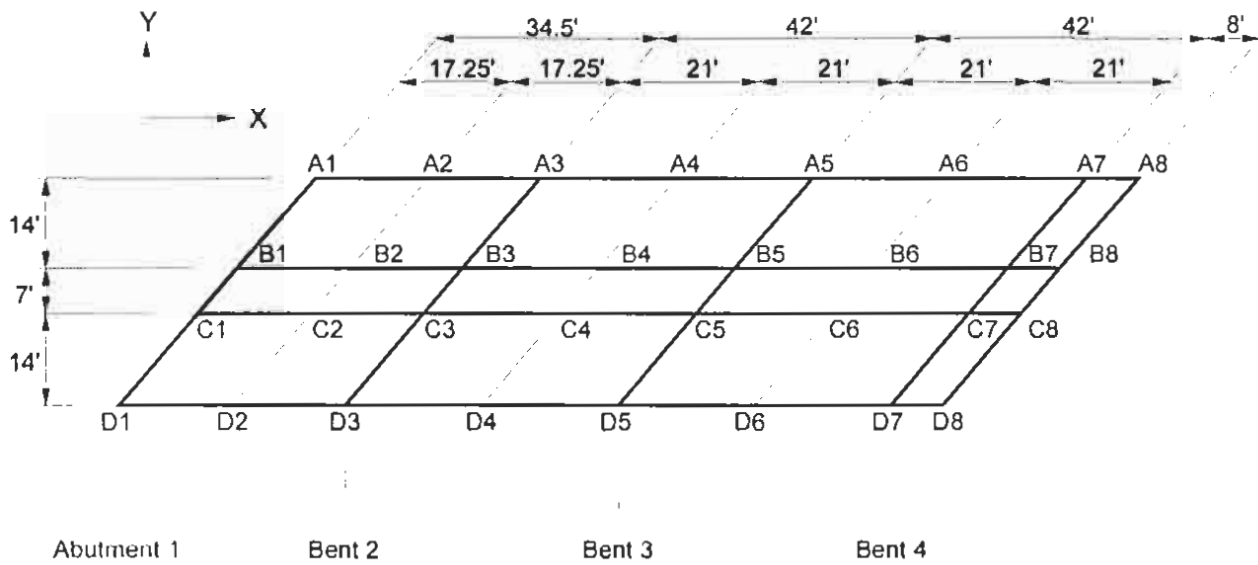
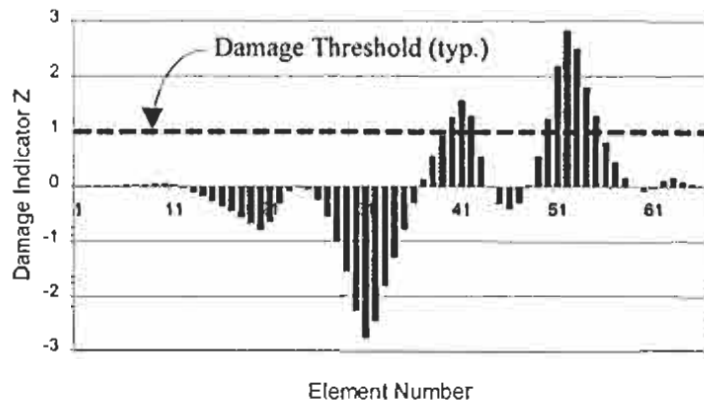
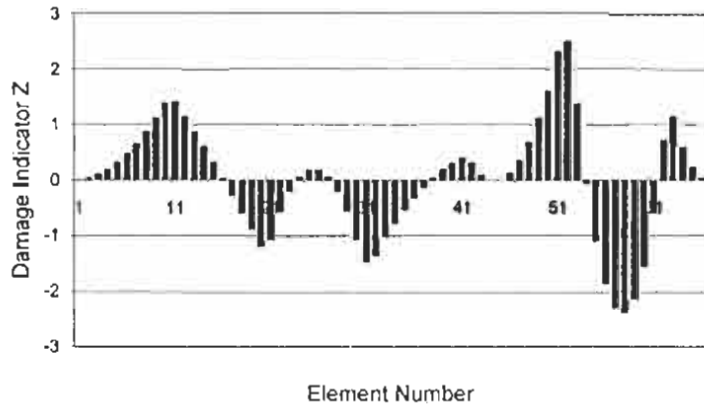


**Figure C.8 Sensor Locations for Watson Wash Frame S-1, May 1999**

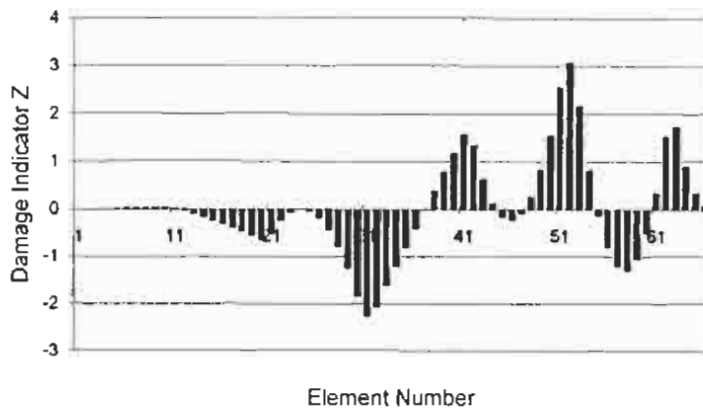


(a)

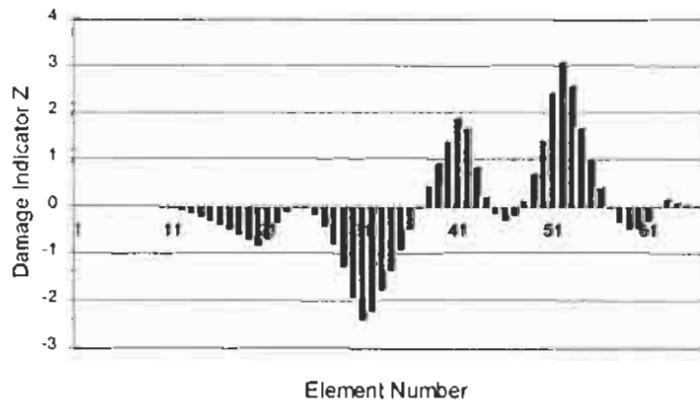


(b)

**Figure C.9 Damage Detection Results Using the First Bending Mode: (a) Result Using the Measurements along the Sensors A1 - A8; ; (b) Result Using the Measurements along the Sensors B1 - B8**



(a)



(b)

**Figure C.10 Damage Detection Results Using the First Bending Mode: (a) Result Using the Measurements along the Sensors C1 - C8; (b) Result Using the Measurements along the Sensors D1 - D8**

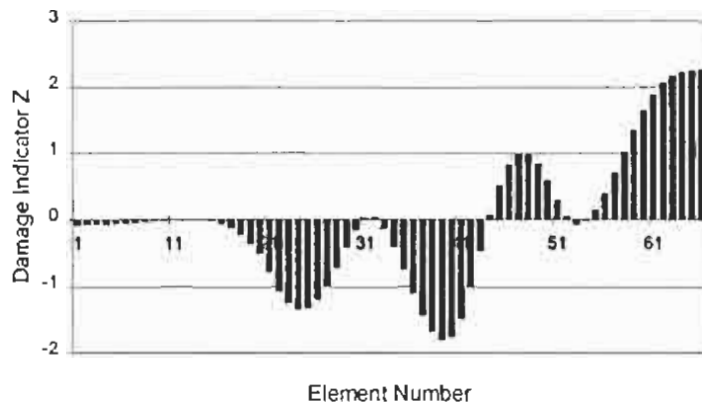


**Figure C.11 Damage Detection Results Using the First Torsional Mode**

C.2.3.2 Frame S-2

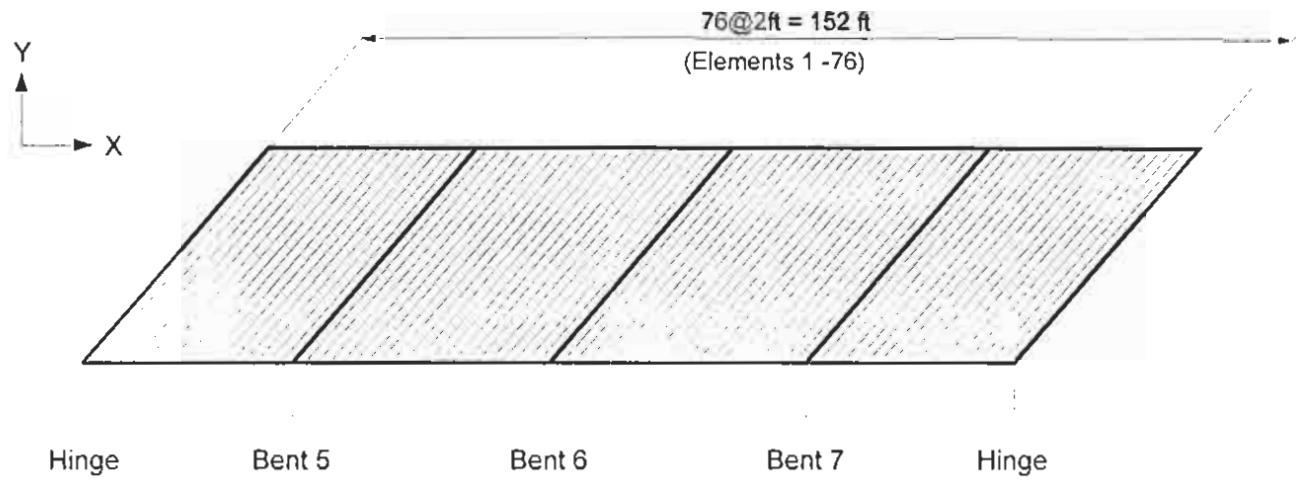


Figure C.12 Damage Detection Model for Watson Wash Frame S-2, May 1999

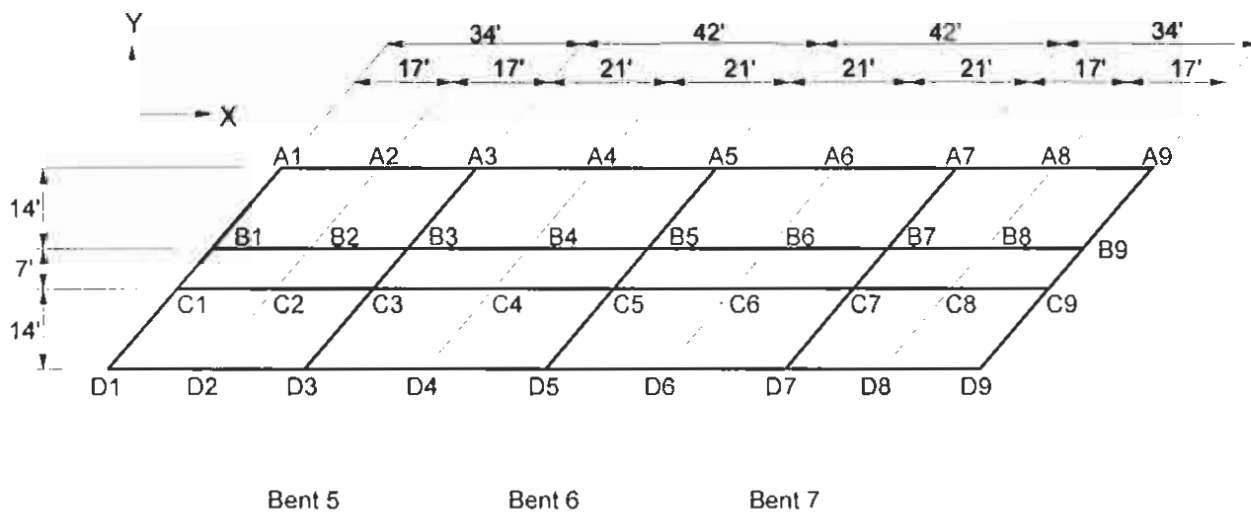
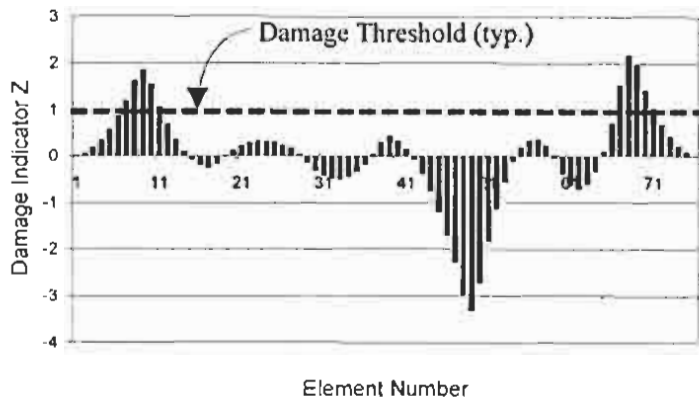
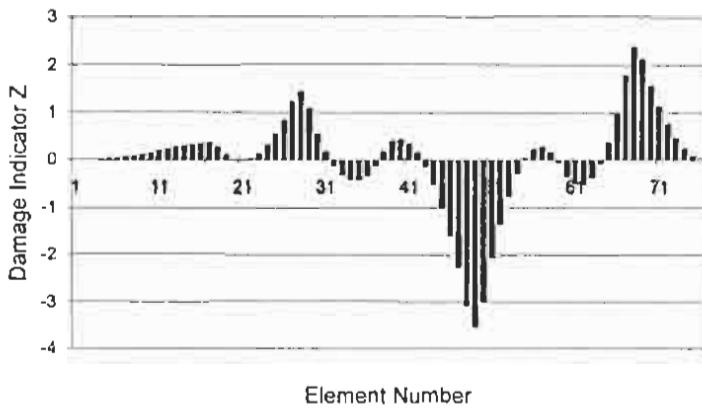


Figure C.13 Sensor Locations for Watson Wash Frame S-2, May 1999

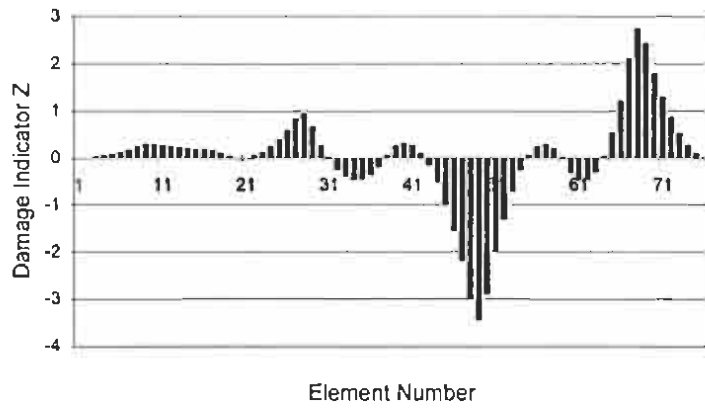


(a)

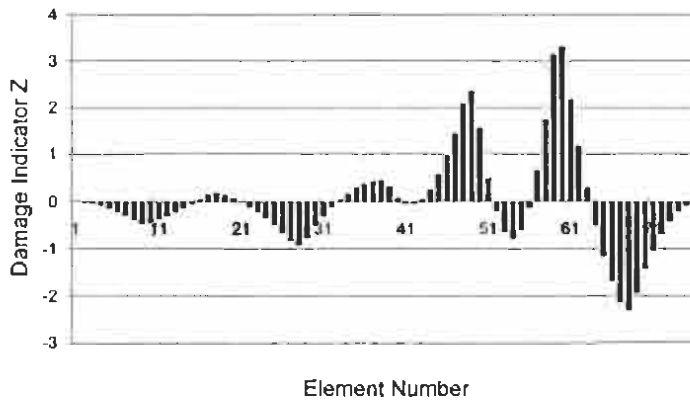


(b)

**Figure C.14 Damage Detection Results Using the First Bending Mode: (a) Result Using the Measurements along the Sensors A1 - A9; (b) Result Using the Measurements along the Sensors B1 - B9**



(a)



(b)

**Figure C.15 Damage Detection Results Using the First Bending Mode: (a) Result Using the Measurements along the Sensors C1 - C9; (b) Result Using the Measurements along the Sensors D1 - D9**

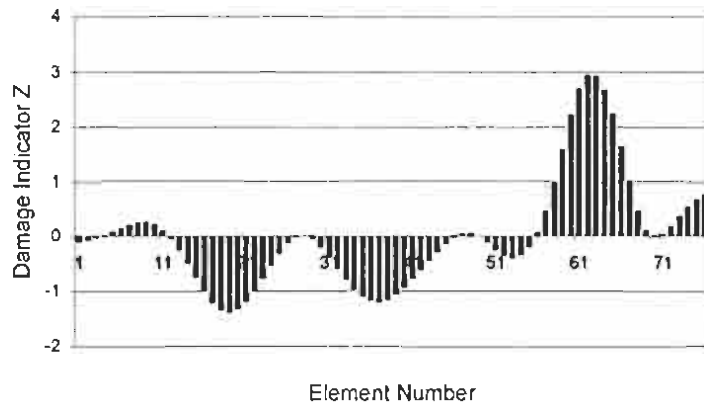


**Figure C.16 Damage Detection Results Using the First Torsional Mode**

### C.2.3.3 Frame S-3

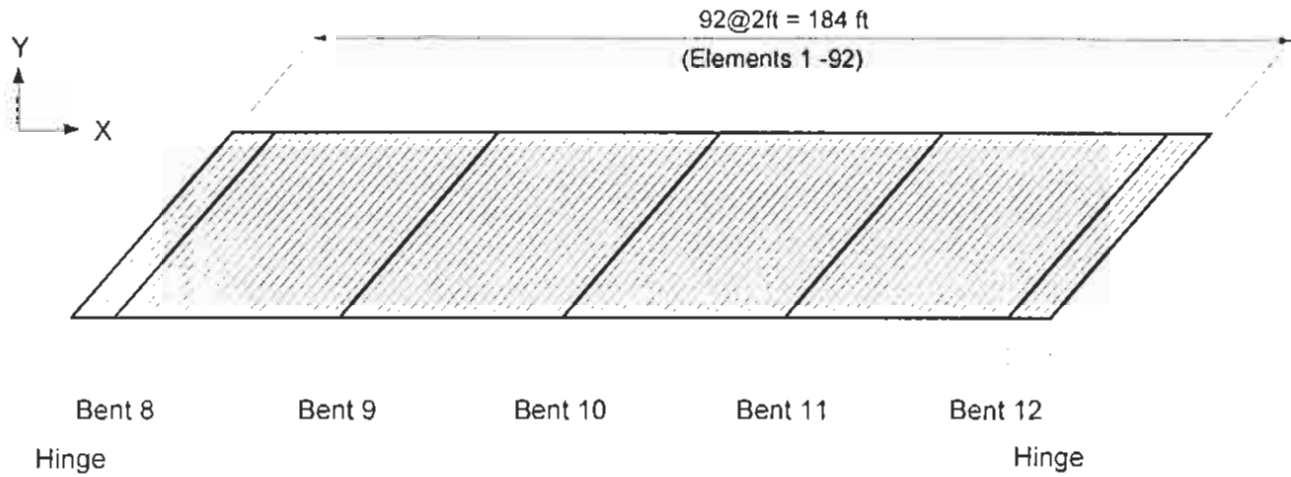


Figure C.17 Damage Detection Model for Watson Wash Frame S-3, May 1999

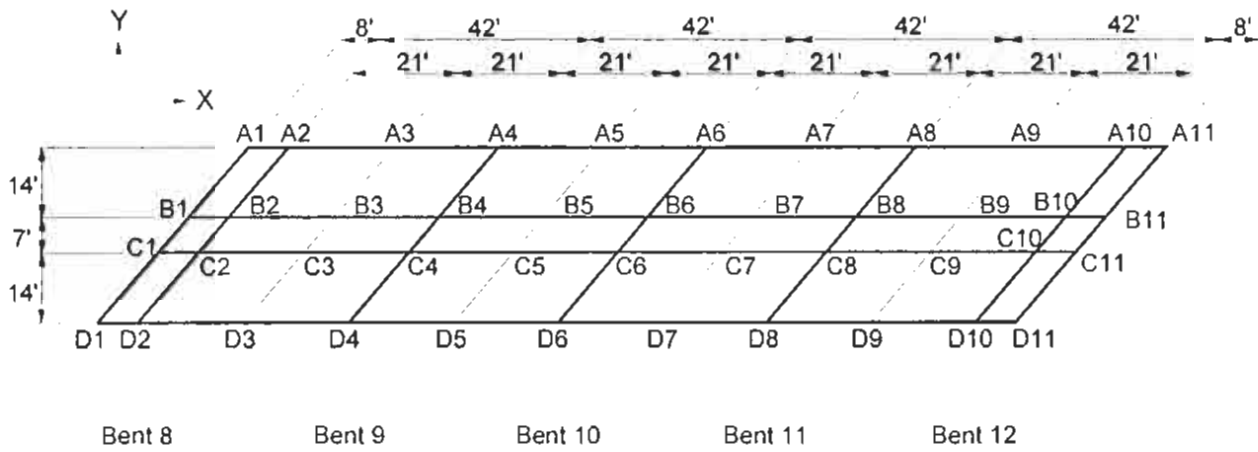
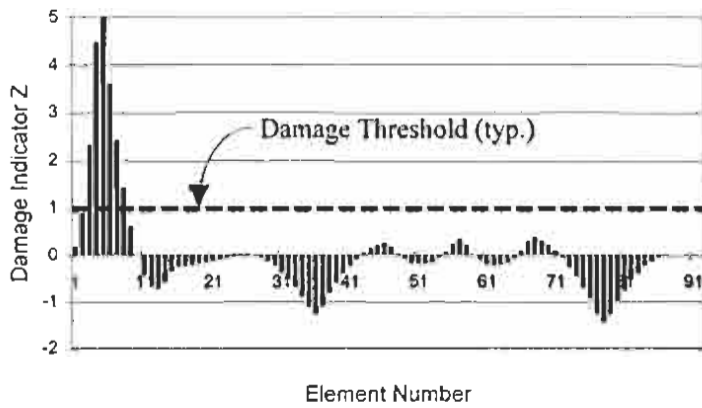
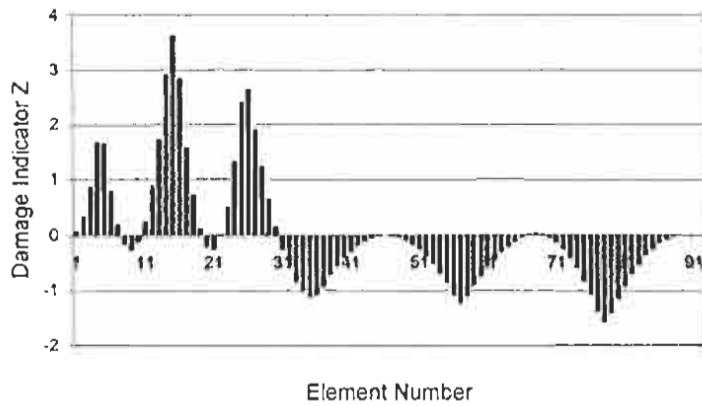


Figure C.18 Sensor Locations for Watson Wash Frame S-3, May 1999

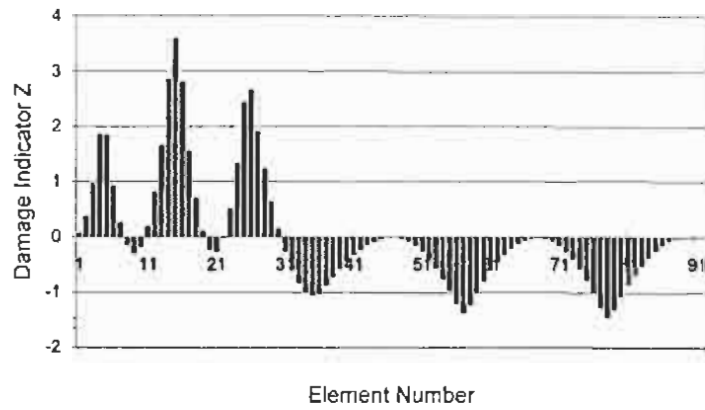


(a)

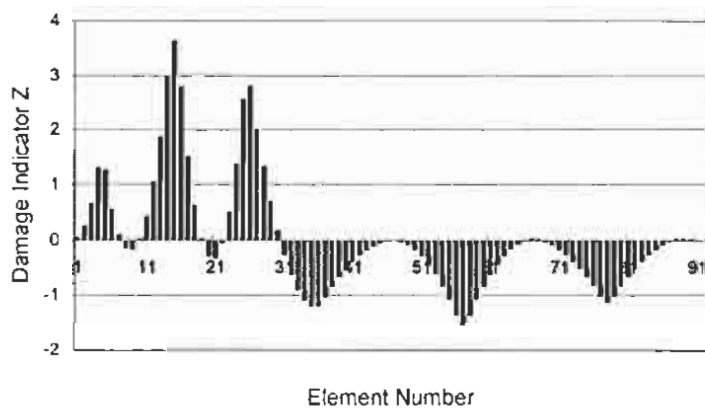


(b)

**Figure C.19 Damage Detection Results Using the First Bending Mode: (a) Result Using the Measurements along the Sensors A1 - A11; ; (b) Result Using the Measurements along the Sensors B1 - B11**



(a)



(b)

**Figure C.20 Damage Detection Results Using the First Bending Mode: (a) Result Using the Measurements along the Sensors C1 - C11; ; (b) Result Using the Measurements along the Sensors D1 - D11**

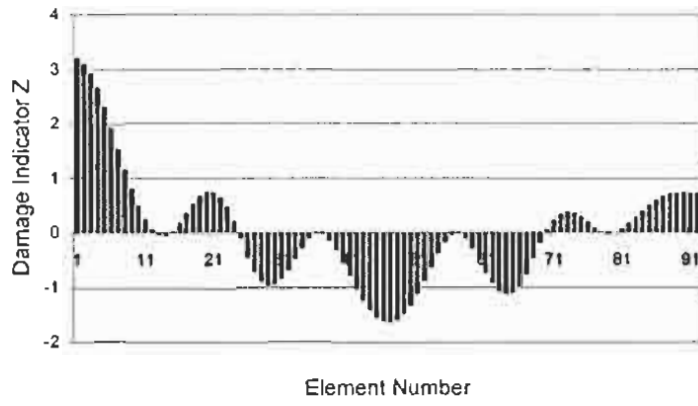


**Figure C.21 Damage Detection Results Using the First Torsional Mode**

C.2.3.4 Frame S-4

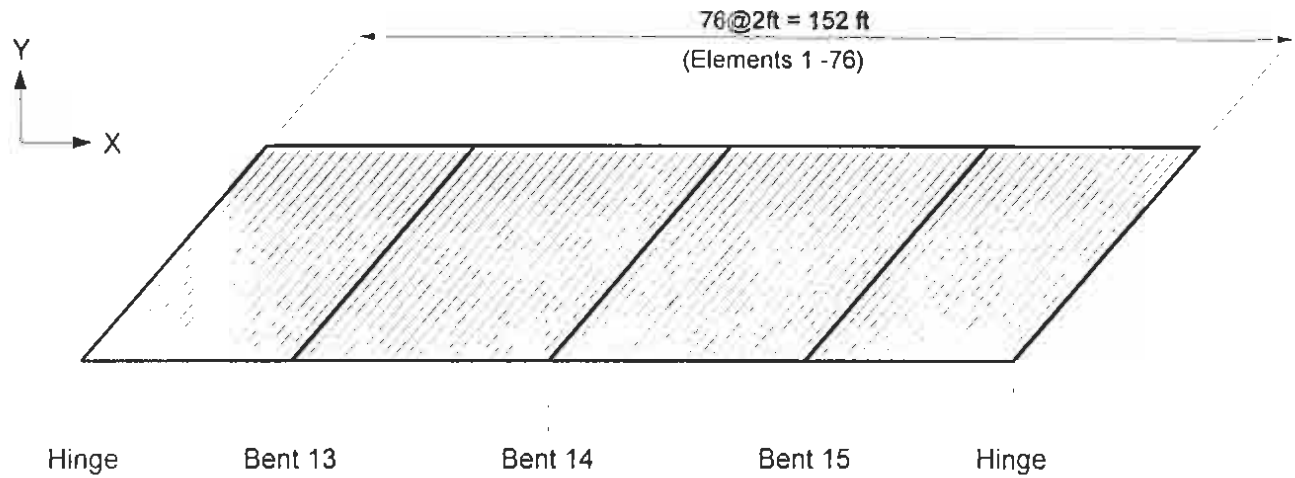


Figure C.22 Damage Detection Model for Watson Wash Frame S-4, May 1999

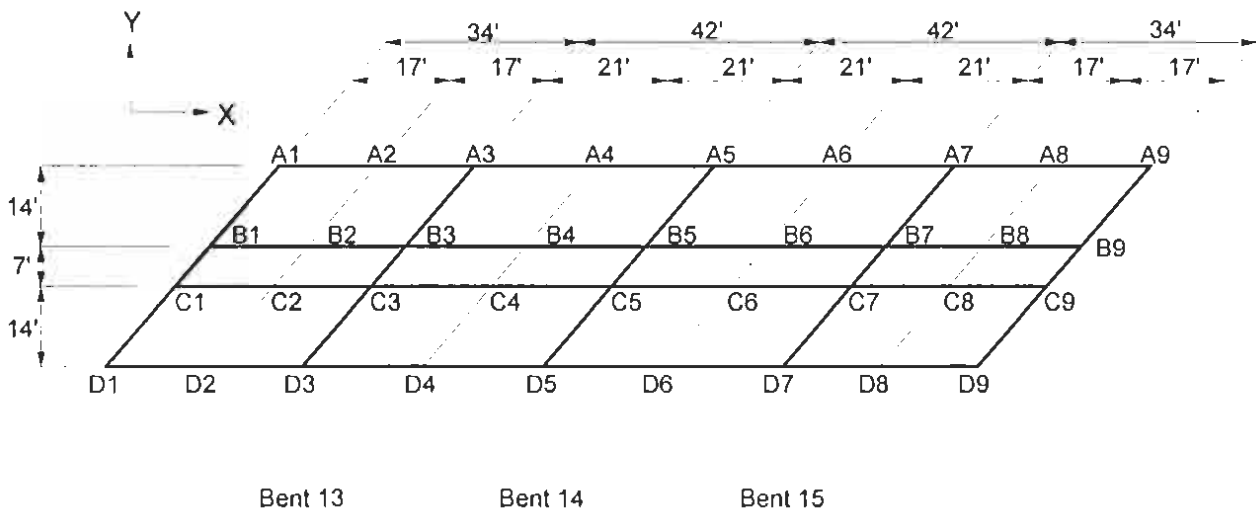
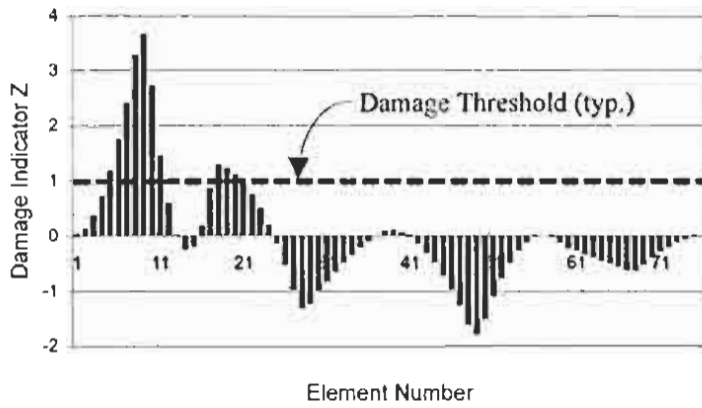
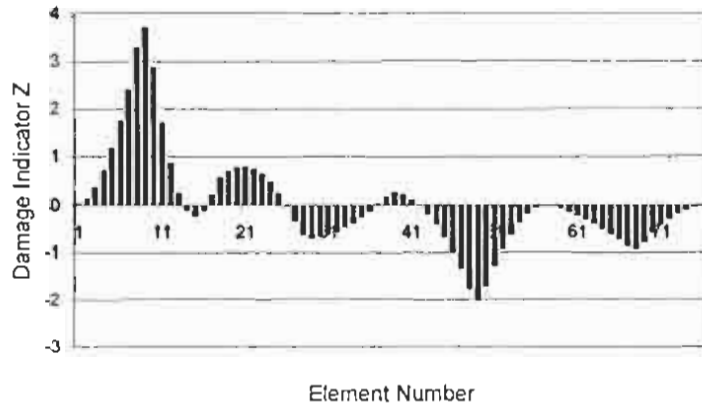


Figure C.23 Sensor Locations for Watson Wash Frame S-4, May 1999

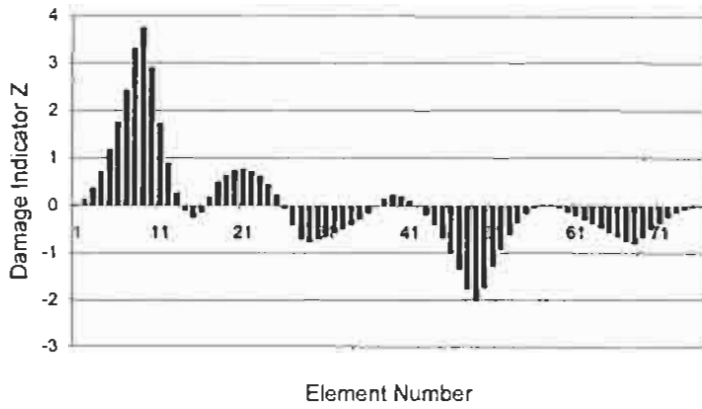


(a)

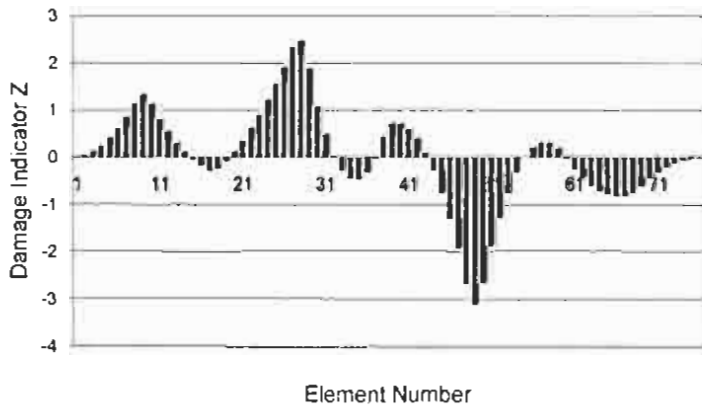


(b)

**Figure C.24 Damage Detection Results Using the First Bending Mode: (a) Result Using the Measurements along the Sensors A1 - A9; (b) Result Using the Measurements along the Sensors B1 - B9**



(a)



(b)

**Figure C.25 Damage Detection Results Using the First Bending Mode: (a) Result Using the Measurements along the Sensors C1 - C9; (b) Result Using the Measurements along the Sensors D1 - D9**

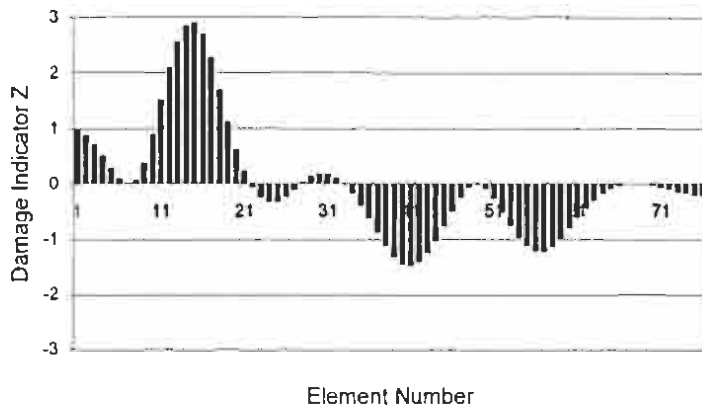


**Figure C.26 Damage Detection Results Using the First Torsional Mode**

### C.2.3.5 Frame S-5

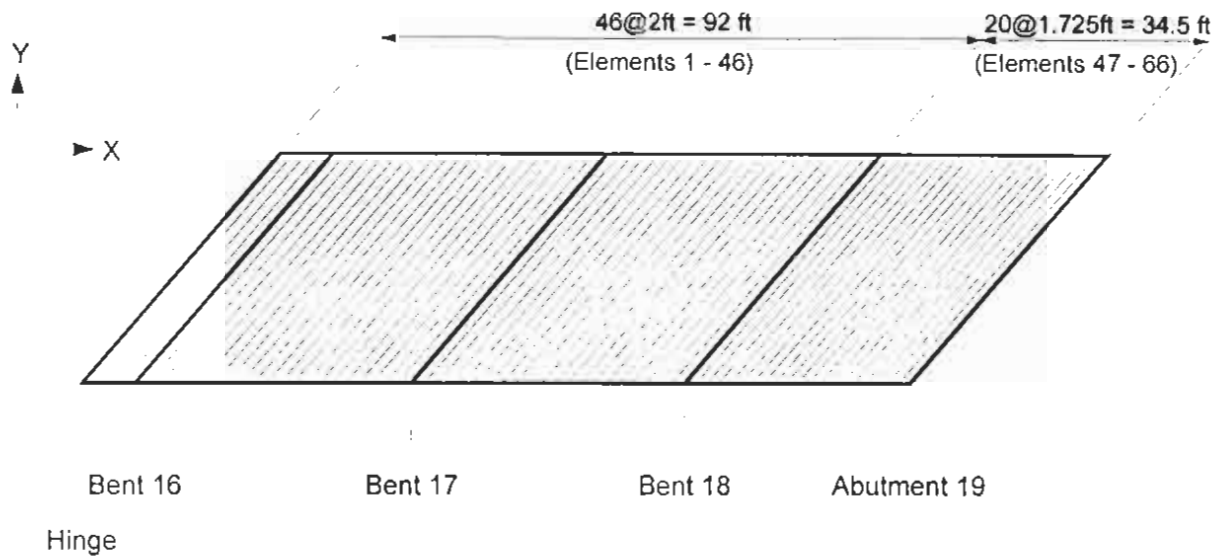


Figure C.27 Damage Detection Model for Watson Wash Frame S-5, May 1999

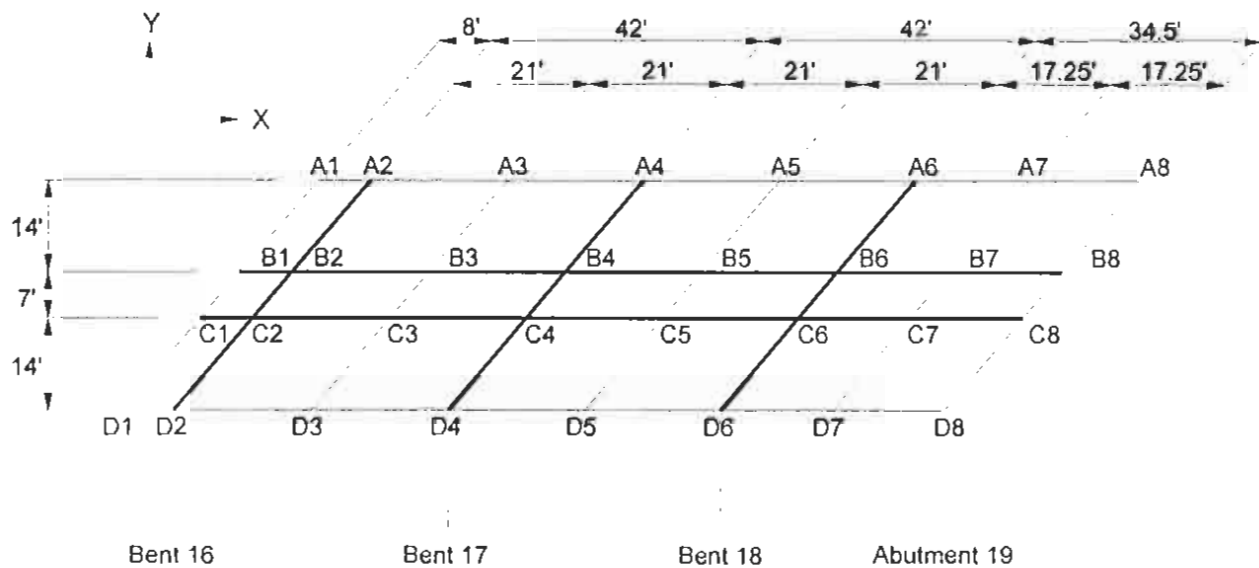
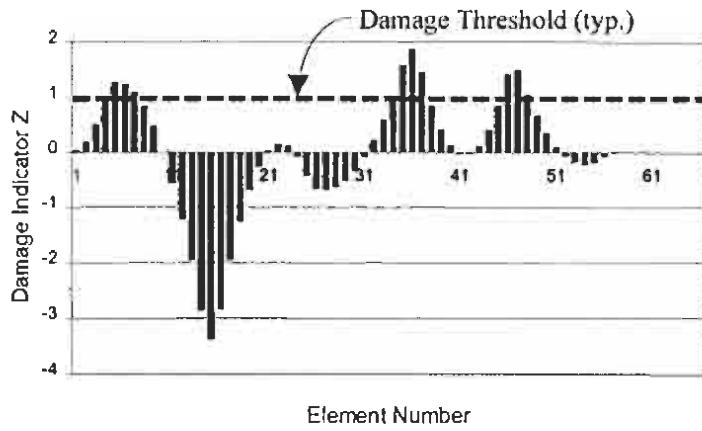
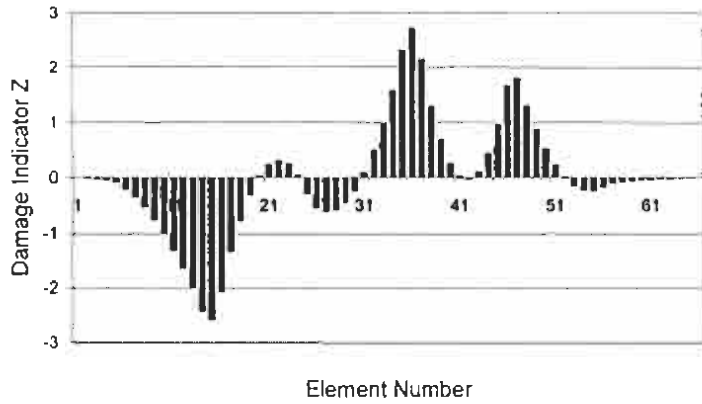


Figure C.28 Sensor Locations for Watson Wash Frame S-5, May 1999

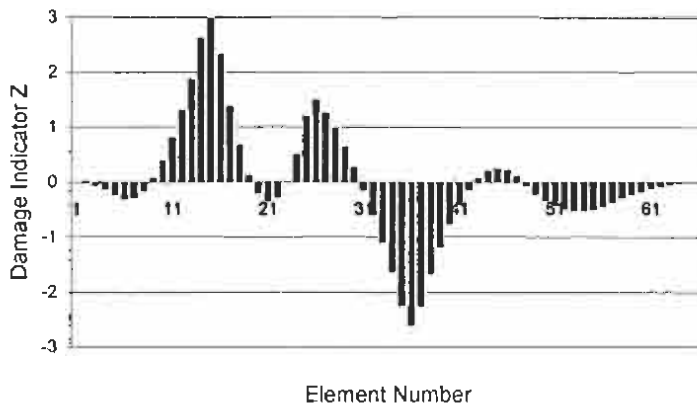


(a)

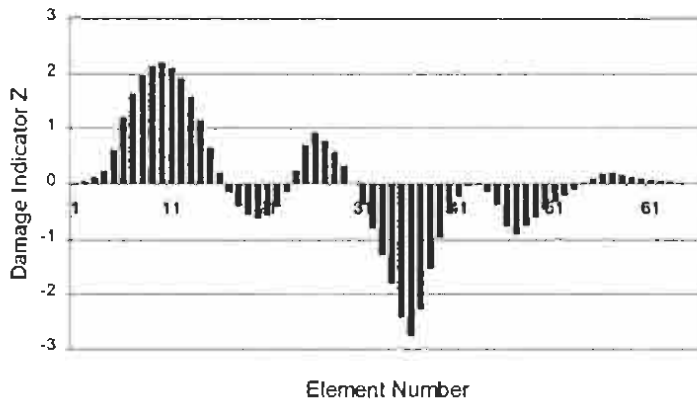


(b)

**Figure C.29 Damage Detection Results Using the First Bending Mode: (a) Result Using the Measurements along the Sensors A1 - A8; (b) Result Using the Measurements along the Sensors B1 - B8**



(a)



(b)

**Figure C.30 Damage Detection Results Using the First Bending Mode: (a) Result Using the Measurements along the Sensors C1 - C8; (b) Result Using the Measurements along the Sensors D1 - D8**

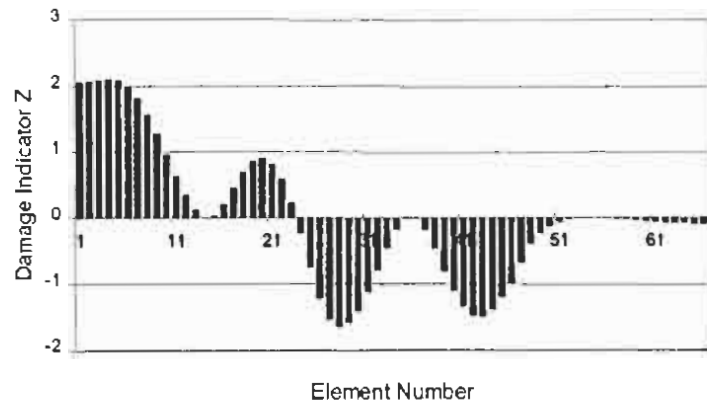


**Figure C.31 Damage Detection Results Using the First Torsional Mode**

**C.2.4 Damage Detection, August 2000 Field Test**

**C.2.4.1 Frame S-1**

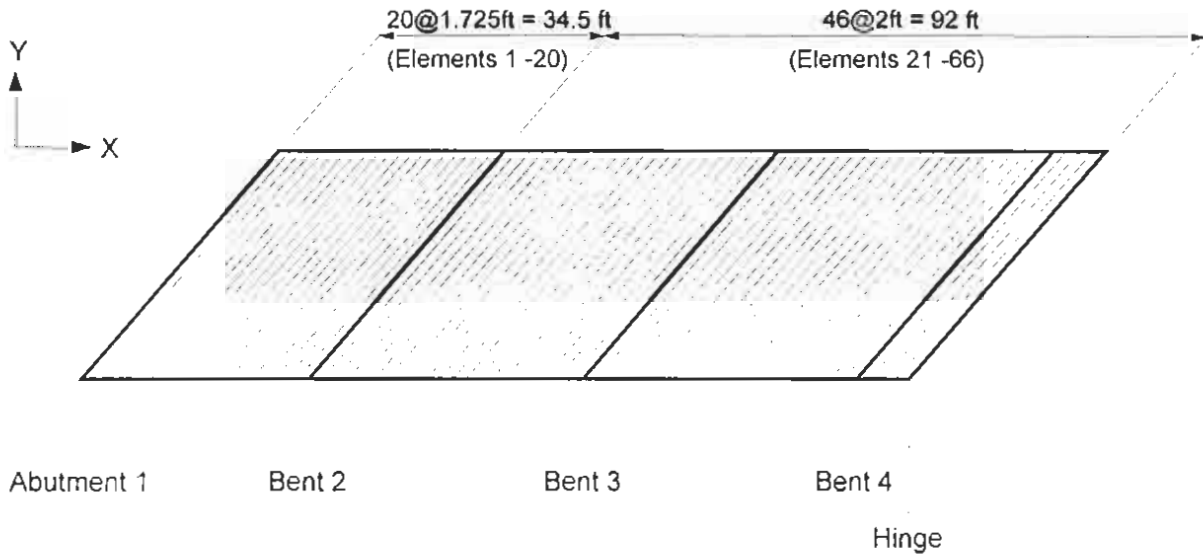


**Figure C.32 Damage Detection Model for Watson Wash Frame S-1, August 2000**

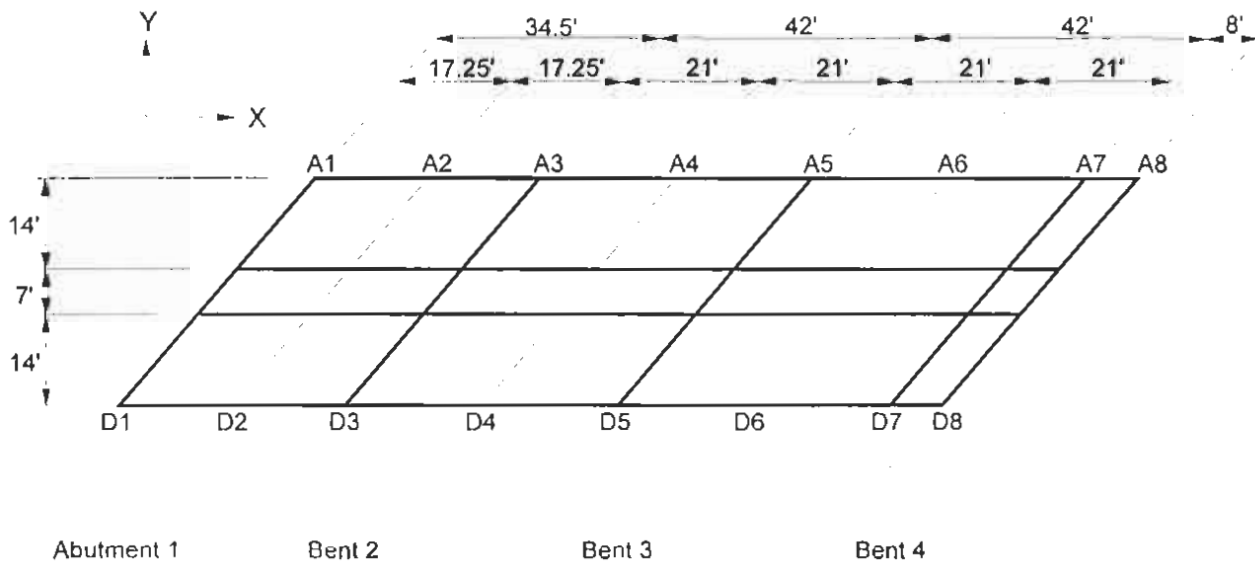
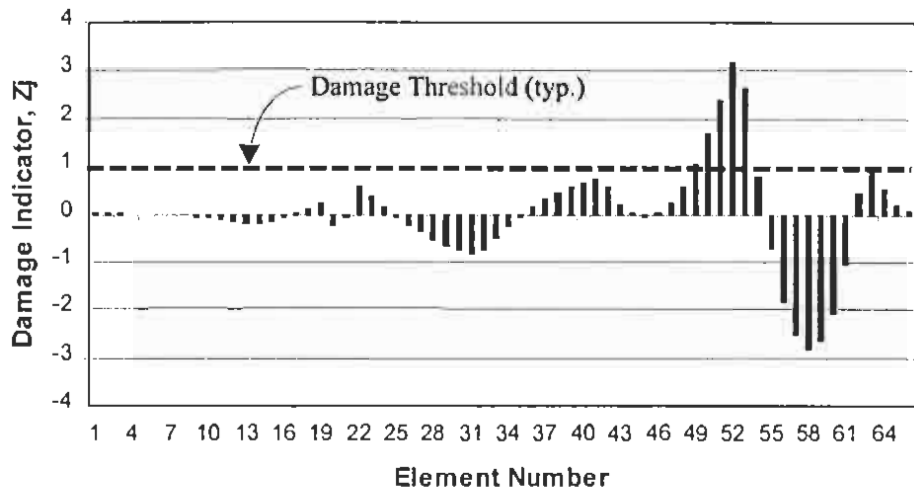
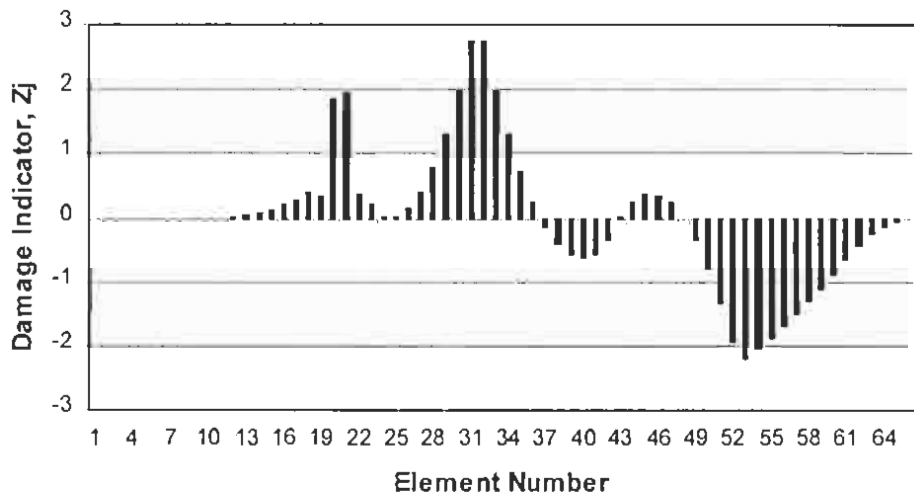


**Figure C.33 Sensor Locations for Watson Wash Frame S-1, August 2000**



(a)



(b)

**Figure C.34 Damage Detection Results Using the First Bending Mode: (a) Result Using the Measurements along the Sensors A1 - A8; ; (b) Result Using the Measurements along the Sensors D1 - D8**

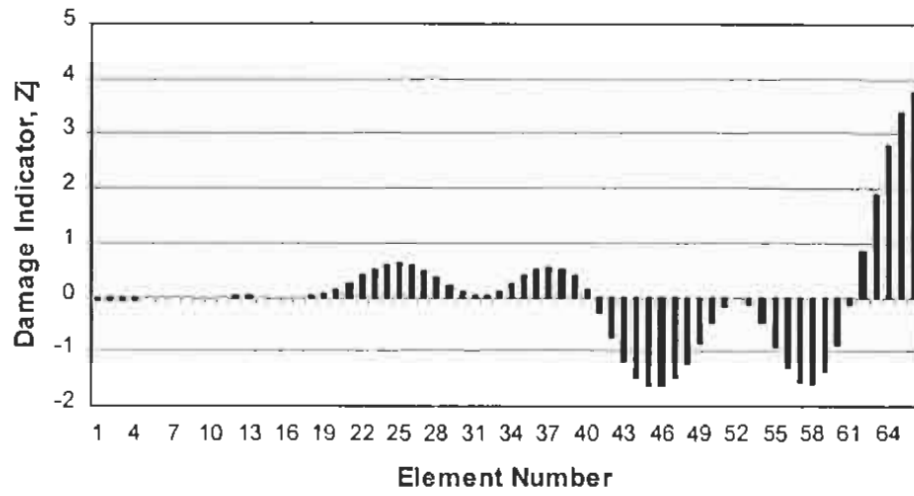


**Figure C.35 Damage Detection Results Using the First Torsional Mode**

C.2.4.2 Frame S-2

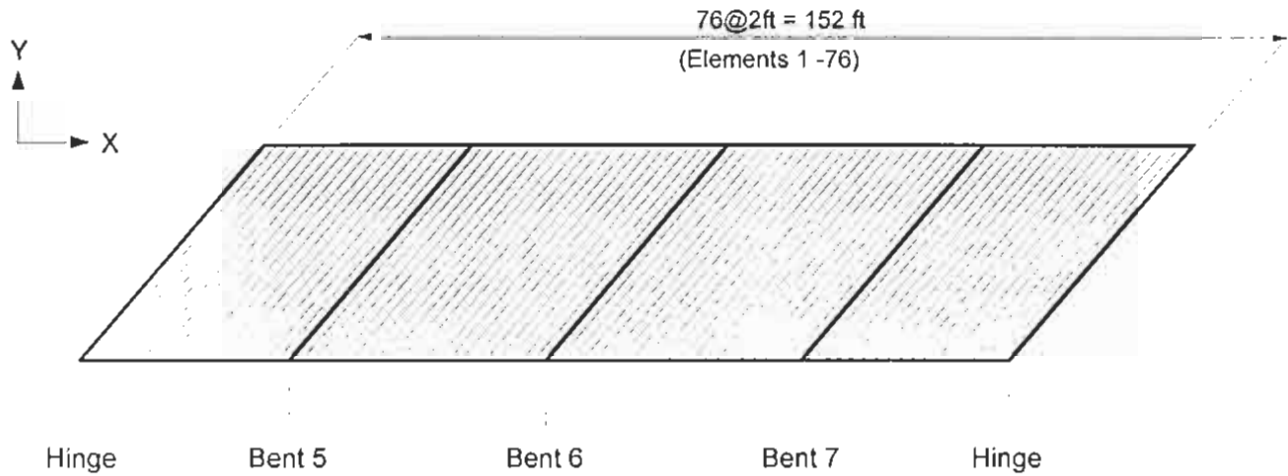


Figure C.36 Damage Detection Model for Watson Wash Frame S-2, August 2000

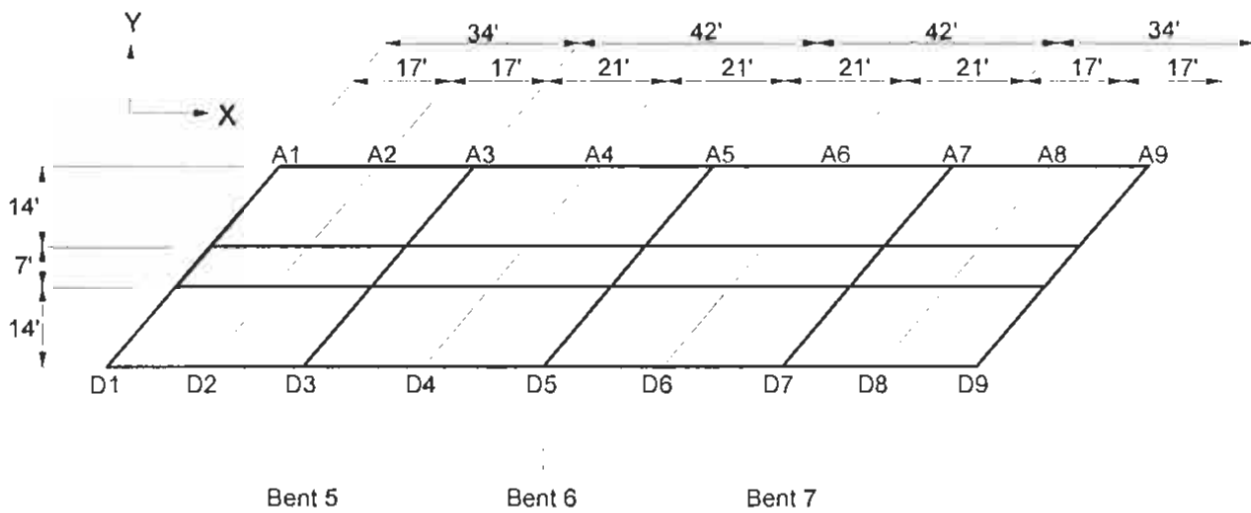
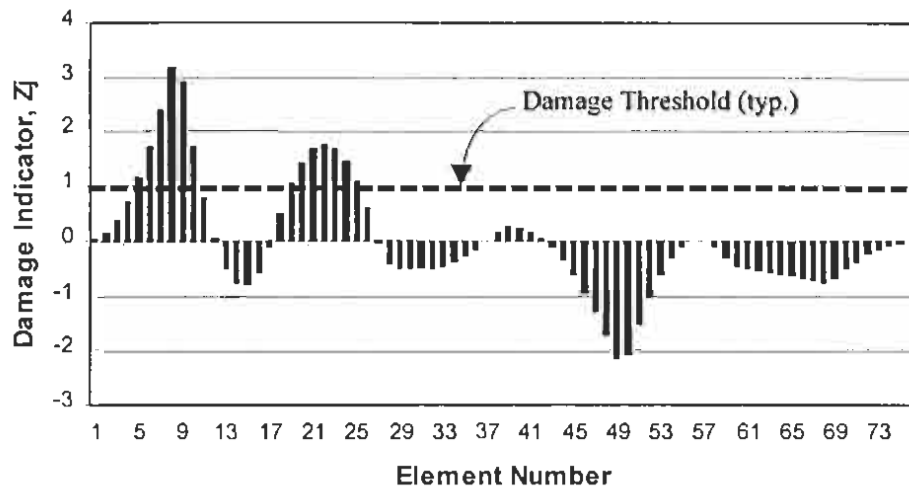
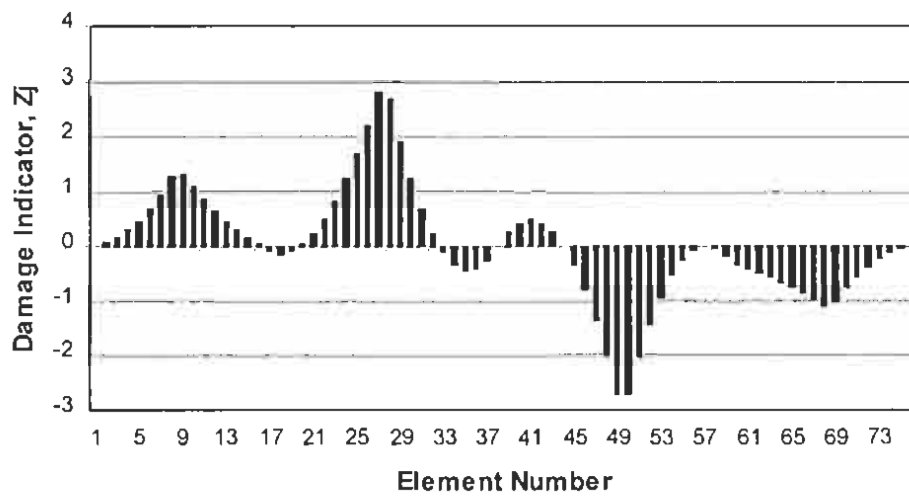


Figure C.37 Sensor Locations for Watson Wash Frame S-2, August 2000



(a)



(b)

**Figure C.38 Damage Detection Results Using the First Bending Mode: (a) Result Using the Measurements along the Sensors A1 - A9; (b) Result Using the Measurements along the Sensors D1 - D9**

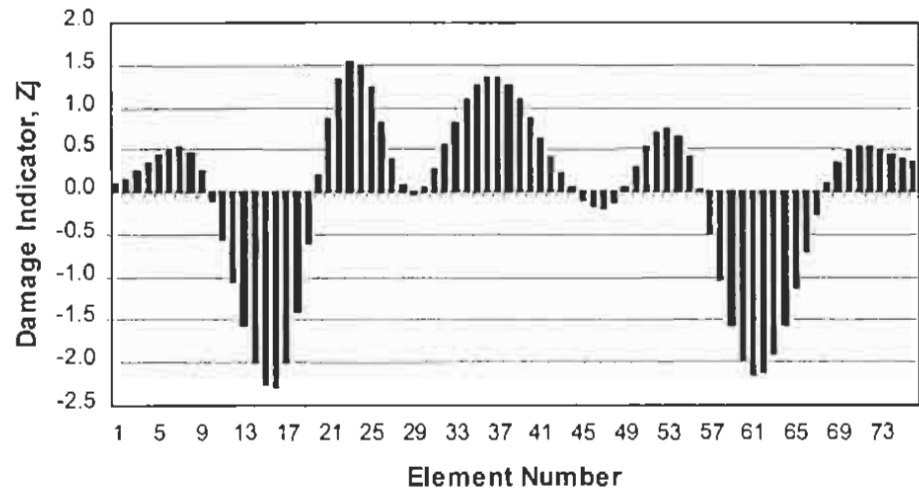


**Figure C.39 Damage Detection Results Using the First Torsional Mode**

C.2.4.3 Frame S-3

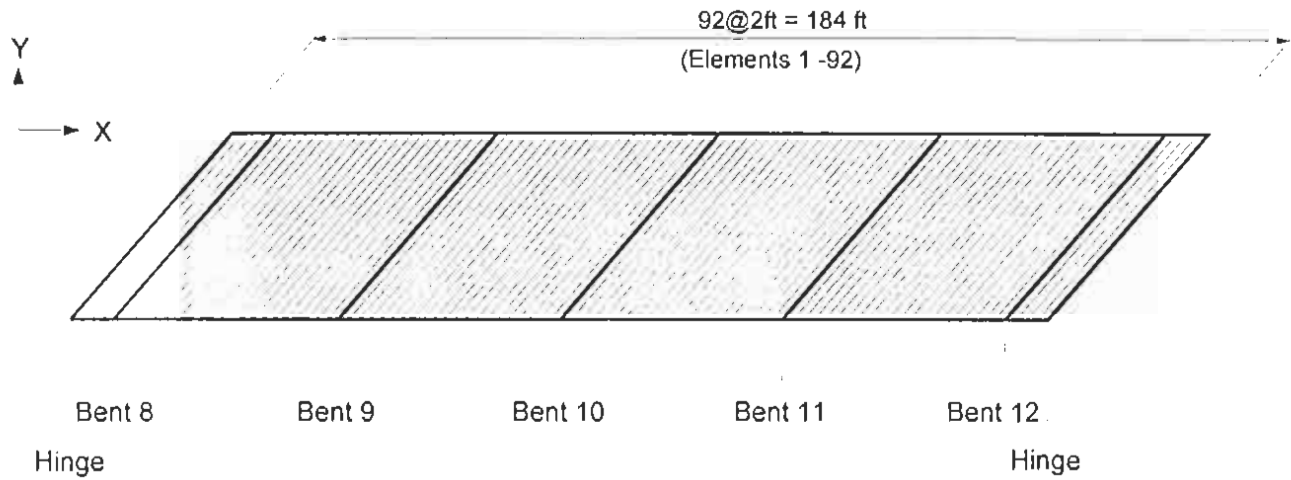


Figure C.40 Damage Detection Model for Watson Wash Frame S-3, August 2000

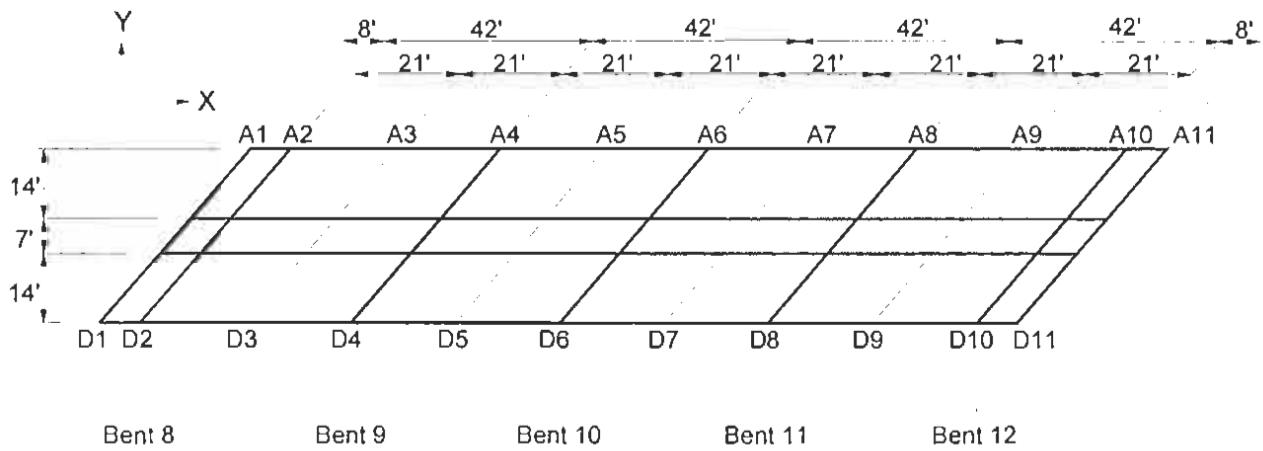
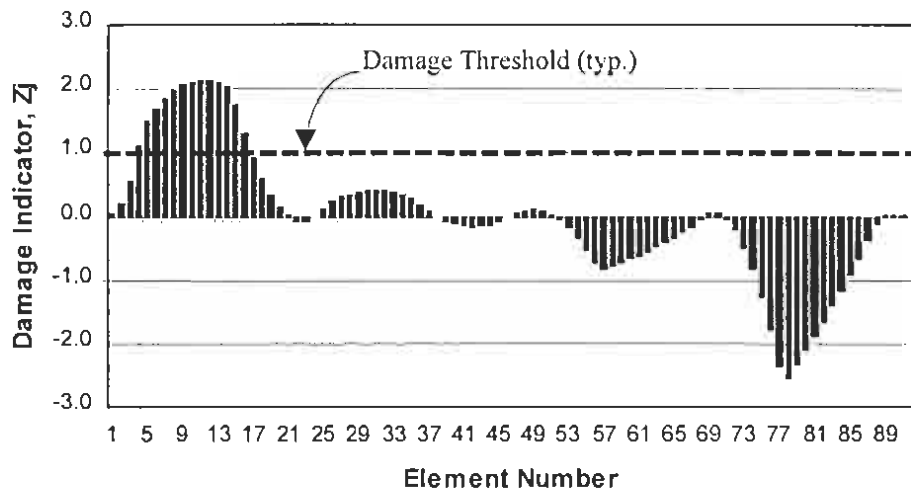
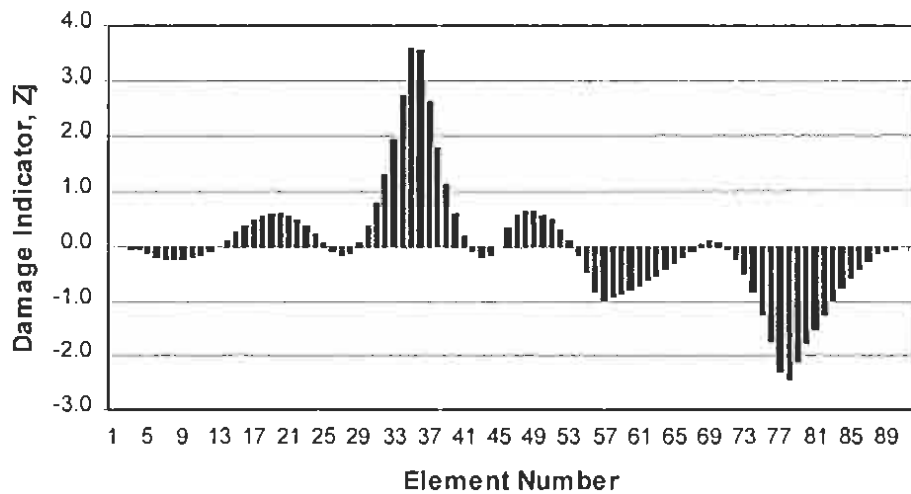


Figure C.41 Sensor Locations for Watson Wash Frame S-3, August 2000



(a)



(b)

**Figure C.42 Damage Detection Results Using the First Bending Mode: (a) Result Using the Measurements along the Sensors A1 - A11; ; (b) Result Using the Measurements along the Sensors D1 - D11**

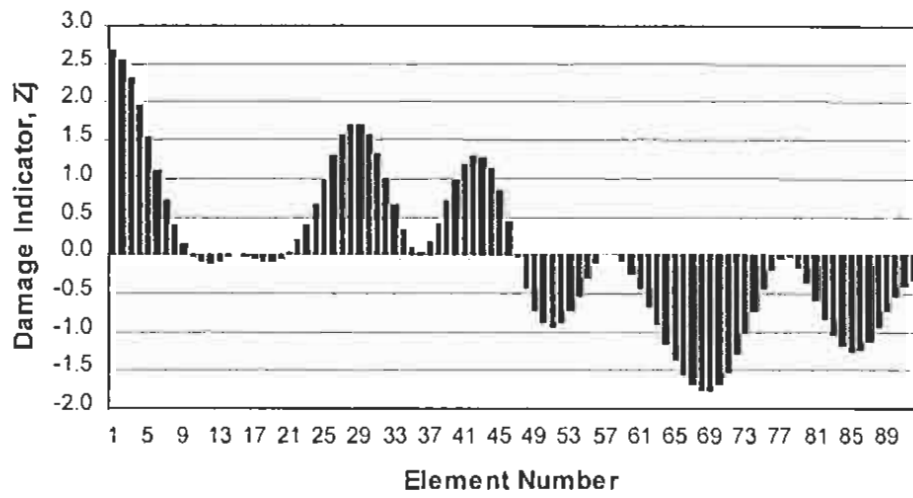


Figure C.43 Damage Detection Results Using the First Torsional Mode

C.2.4.4 Frame S-4

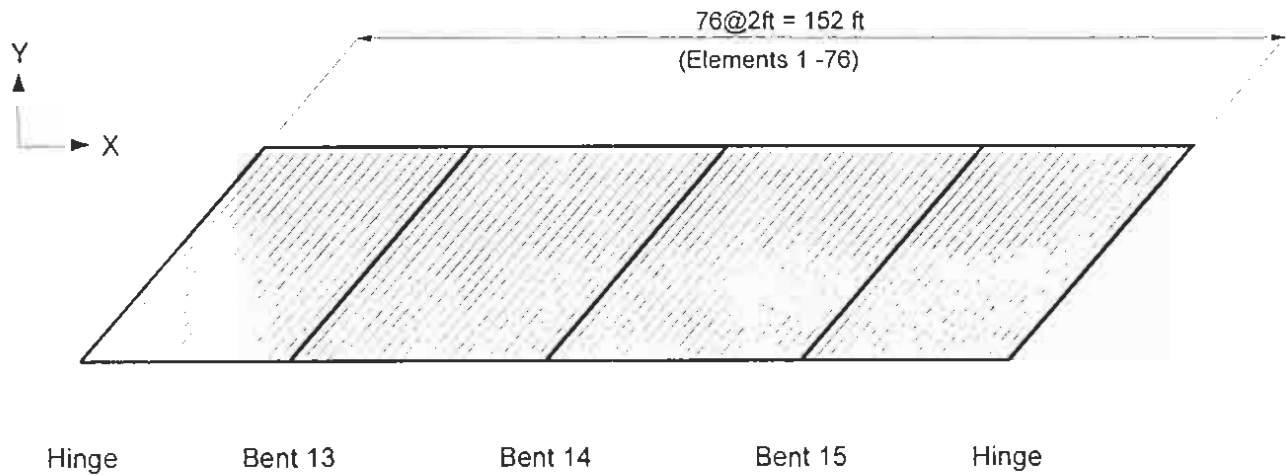


Figure C.44 Damage Detection Model for Watson Wash Frame S-4, August 2000

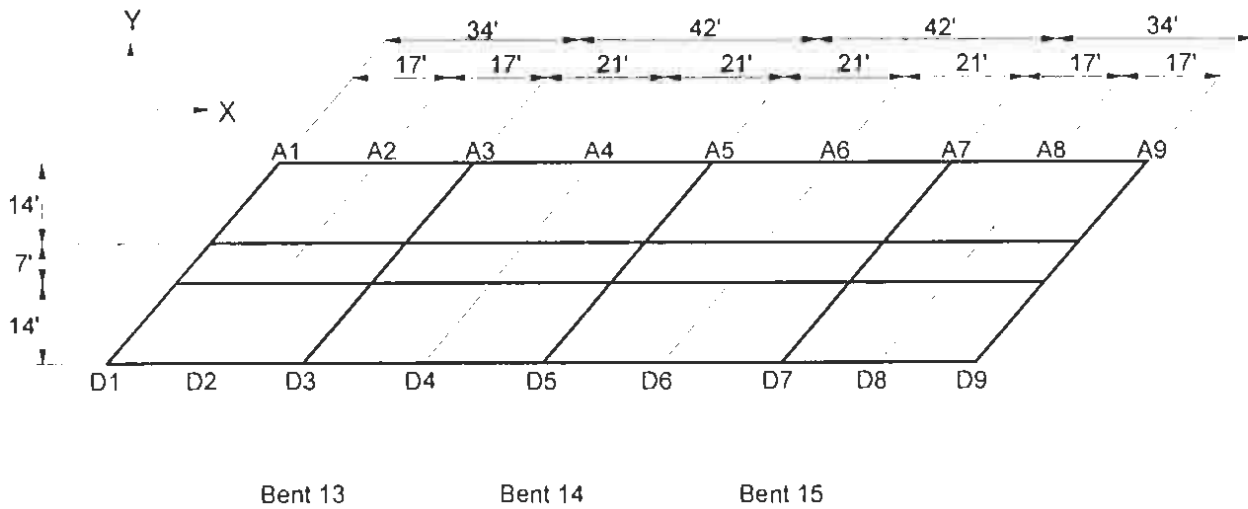
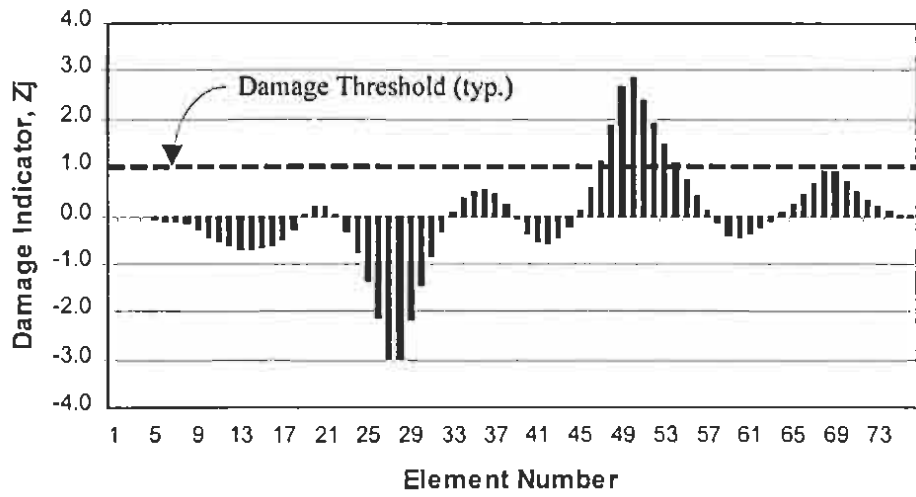
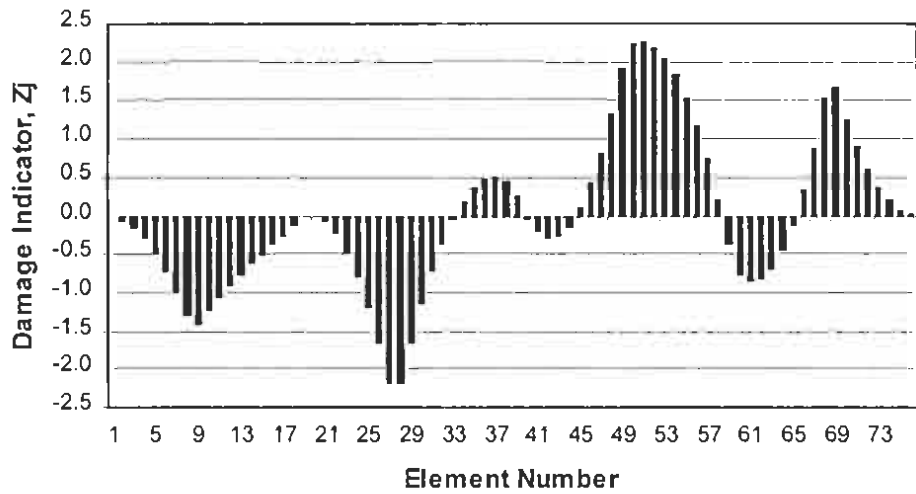


Figure C.45 Sensor Locations for Watson Wash Frame S-4, August 2000



(a)



(b)

**Figure C.46 Damage Detection Results Using the First Bending Mode: (a) Result Using the Measurements along the Sensors A1 - A9; (b) Result Using the Measurements along the Sensors D1 - D9**

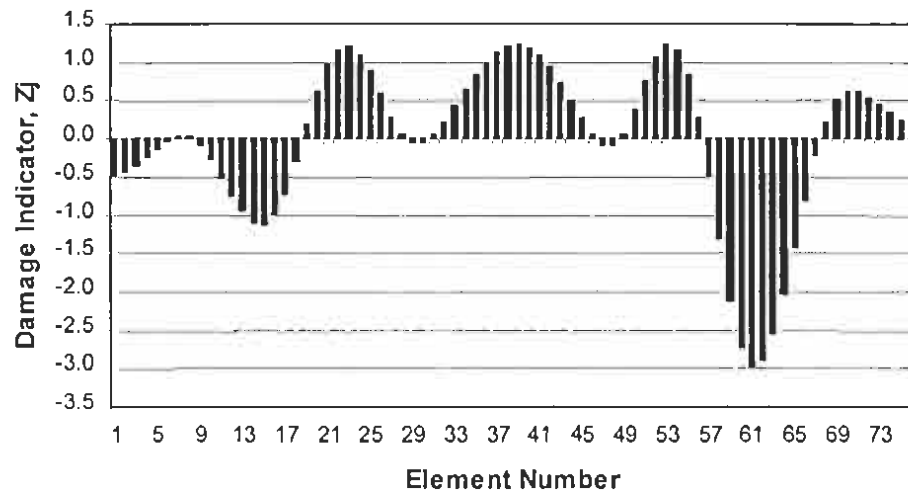


**Figure C.47 Damage Detection Results Using the First Torsional Mode**

C.2.4.5 Frame S-5

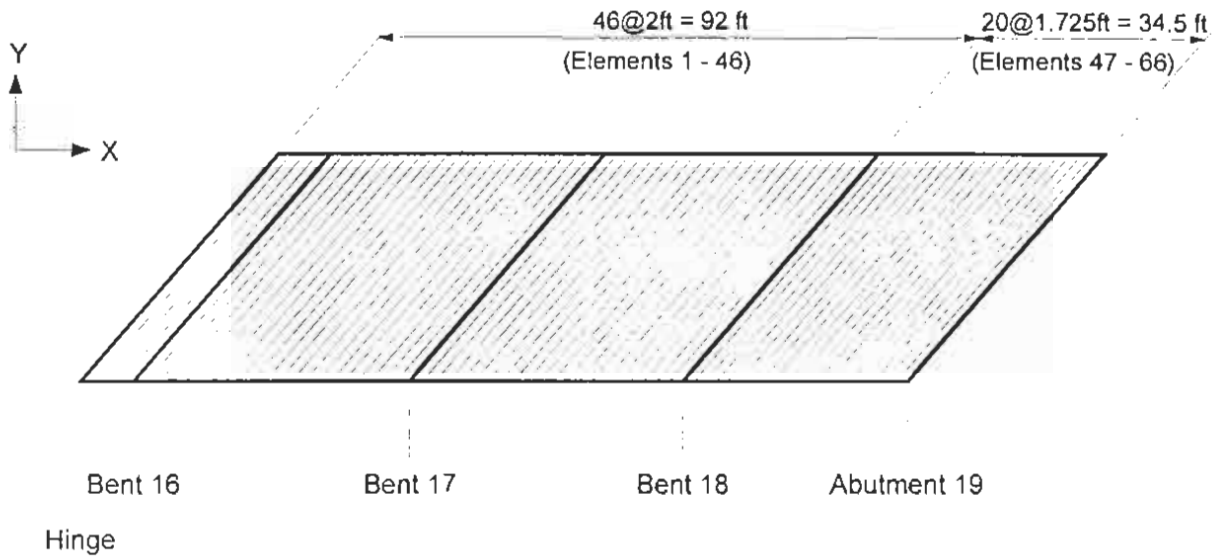


Figure C.48 Damage Detection Model for Watson Wash Frame S-5, August 2000

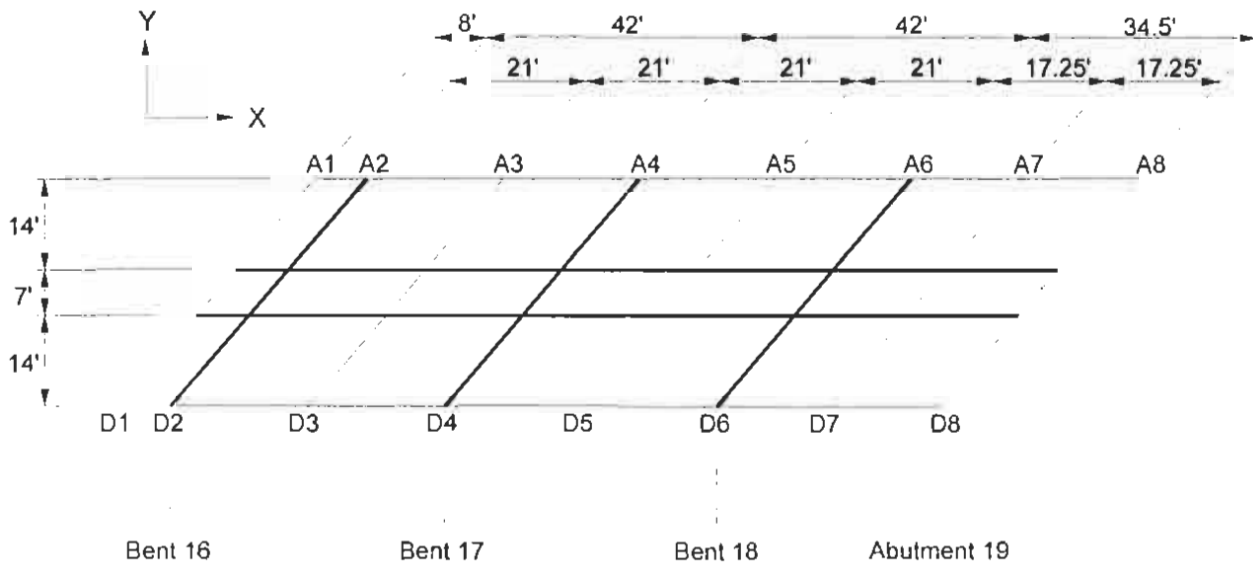
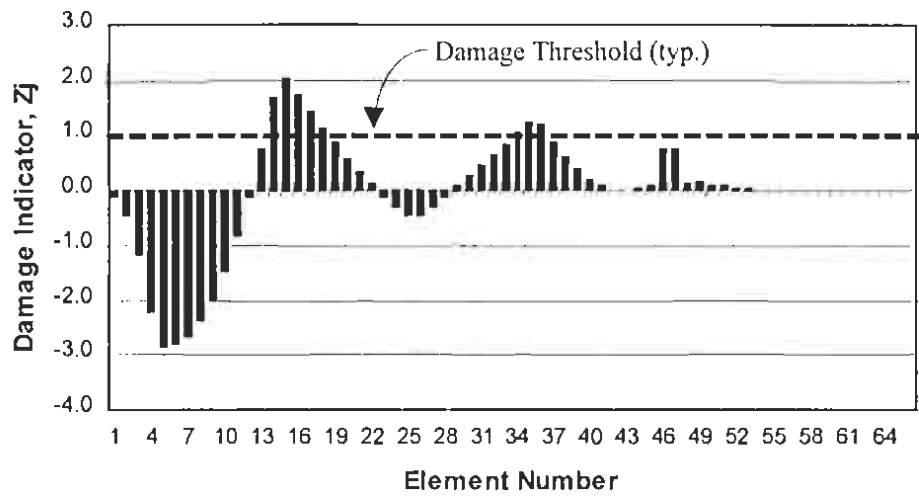
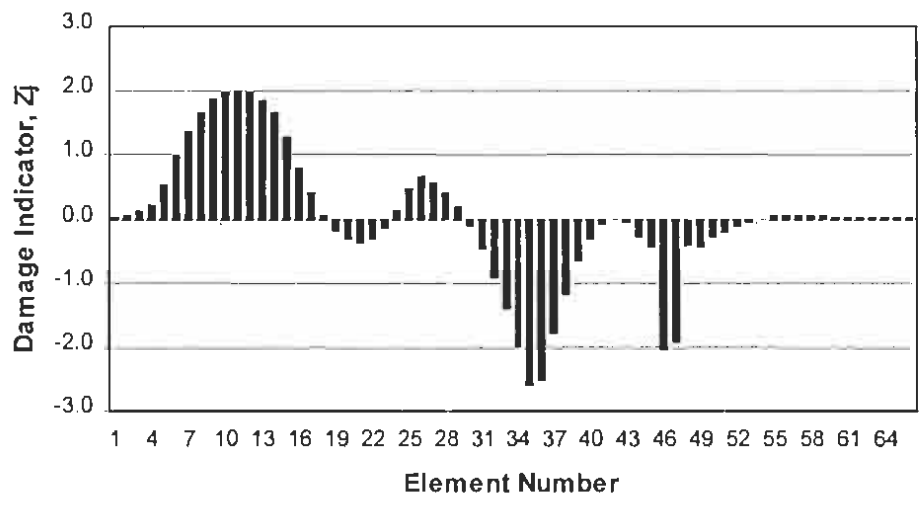


Figure C.49 Sensor Locations for Watson Wash Frame S-5, August 2000



(a)



(b)

**Figure C.50 Damage Detection Results Using the First Bending Mode: (a) Result Using the Measurements along the Sensors A1 - A8; (b) Result Using the Measurements along the Sensors D1 - D8**

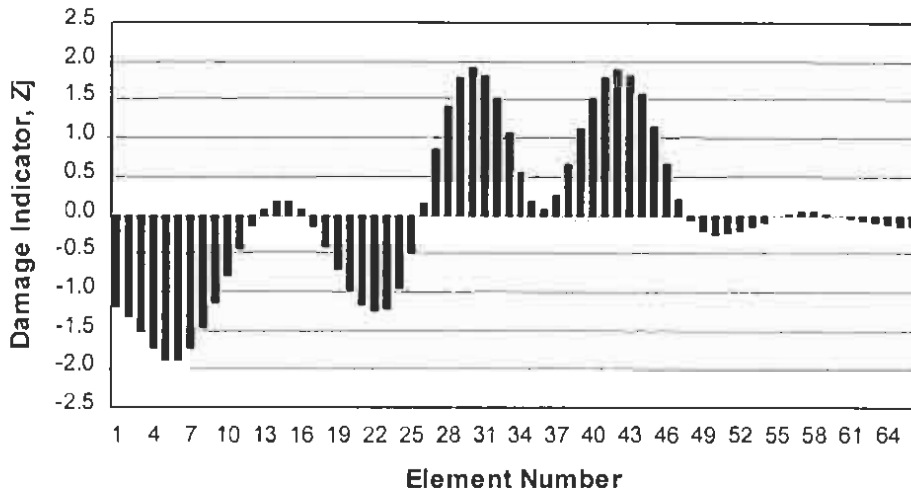


**Figure C.51 Damage Detection Results Using the First Torsional Mode**